ABSTRACT

Wei Xie. Characterization of Reclaimed Asphalt Pavement (RAP) Binders and Implications on Recycled Binder Replacement Specifications. (Under the direction of Dr. Cassie Castorena.)

Asphalt pavement is the largest infrastructure network in the United States, serving as a foundation for economic activity and daily transportation needs. Annual road maintenance and rehabilitation operations generate substantial quantities of recycled asphalt material (RAM), including reclaimed asphalt pavement (RAP) and recycled asphalt shingles (RAS). The construction industry incorporates this RAM into new pavement projects, creating RAM mixtures that provide significant economic and environmental benefits. RAM use reduces costs by decreasing demand for expensive virgin asphalt binder, conserves natural resources including aggregates and binder materials, and minimizes landfill requirements for waste pavement materials. These advantages have led to widespread RAM adoption throughout the United States pavement construction industry.

State transportation agencies establish recycled binder replacement (RBR) percentage limits to control RAM incorporation and maintain pavement performance standards. North Carolina's approach involved characterizing high-temperature performance graded properties and intermediate-temperature properties using Dynamic Shear Rheometer (DSR) test following AASHTO M 320 specifications. Low-temperature performance graded properties require Bending Beam Rheometer (BBR) test following AASHTO T 313 procedures for both virgin and RAM binders. Researchers compared measured properties against established thresholds to determine appropriate RBR limits.

However, previous studies establish RBR limits using deterministic analysis methods that evaluate limited selections of virgin binders, RAM binders, and their blends. This approach cannot assess the risk of blended binders failing to meet performance-graded criteria at different RBR levels because it does not account for combined variability effects in virgin and RAM binder properties. This method also fails to use Quality Assurance (QA) datasets containing extensive virgin binder property information. Additionally, BBR test requires significantly more long-term aged binder compared to DSR test, while the extraction and recovery processes needed to obtain recovered RAM binder samples are time-consuming and require hazardous, expensive solvents.

This thesis evaluates variability within and across RAP stockpiles by characterizing 44 RAP binders and 342 virgin binders. The research employs QA data for PG 64-22 and PG 58-28

virgin binder performance properties collected from 2022 to 2024, combined with characterization of 44 RAP binders extracted and recovered from various North Carolina stockpiles. RAP binder property measured at critical climate temperatures of North Carolina. The study uses blending chart equations to virtually blend virgin binders with RAP binders at different RBR levels, enabling prediction of blended binder performance characteristics. Frequency distributions for blended binder properties at various RBR levels are plotted and compared against threshold requirements to determine the percentage of blended binder that meets the threshold and inform appropriate RAP RBR limits. This thesis also addresses low-temperature testing limitations by applying an existing DSR method to conduct temperature frequency sweep tests and uses time-temperature superposition and linear viscoelastic interconversion principles to predict low-temperature performance grades for both virgin asphalt binder and recovered RAM binder. The previous study that developed the approach only evaluated virgin binder and thus, this thesis adds knowledge by evaluating and improving its accuracy for the prediction of RAM binder properties.

Characterization of Reclaimed Asphalt Pavement (RAP) Binders and Implications on Recycled Binder Replacement Specifications

by
Wei Xie

A thesis submitted to the Graduate Faculty of
North Carolina State University
in partial fulfillment of the
requirements for the degree of
Master of Science

Civil Engineering

Raleigh, North Carolina
2025

APPROVED BY:

Dr. Cassie Castorena Committee Chair	Dr. Y. Richard Kim
Dr. Shane Underwood	

BIOGRAPHY

Wei Xie was born and raised in Ludian, Yunnan, China, where she enjoyed her childhood and teenage years with her family. After graduating from Zhaotong No.1 High School, she moved to Beijing. She received her bachelor's degree from Beijing University of Technology in 2018. After graduation, she worked in Kunming. In 2023, she started her graduate program at NC State University under the direction of Dr. Cassie Castorena.

ACKNOWLEDGMENTS

I would like to express my gratitude to my advisor, Dr. Cassie Castorena, for her valuable guidance, support, and encouragement. A sincere thank you to my committee members, Dr. Richard Kim and Dr. Shane Underwood, for their valuable suggestions. I would like to thank Gabriel Macedo Duarte and all the group members for their help with sampling materials. I am grateful to Dr. Zhe Zeng for his help with adjusting the software, and to Maria Carolina Aparicio Alvis for conducting the preliminary probabilistic analysis. Thank you to Emilio for his help with classes. Finally, I would like to thank Lei Xue for his unconditional encouragement and support.

TABLE OF CONTENTS

LIST OF TABLES

LIST OF FIGURES

1. Introduction

1.1. Background

Asphalt pavement is the largest infrastructure network in the United States, serving as a foundation for economic activity and daily transportation needs. Annual road maintenance and rehabilitation operations generate substantial quantities of recycled asphalt material (RAM), including reclaimed asphalt pavement (RAP) and recycled asphalt shingles (RAS). The construction industry incorporates this RAM into new pavement projects, creating RAM mixtures that provide significant economic and environmental benefits. RAM use reduces costs by decreasing demand for expensive virgin asphalt binder, conserves natural resources including aggregates and binder materials, and minimizes landfill requirements for waste pavement materials. These advantages have led to widespread RAM adoption throughout the United States pavement construction industry.

Many state transportation agencies have established recycled binder replacement (RBR) percentage limits to control RAM incorporation and maintain pavement performance standards. For example, North Carolina Department of Transportation (NCDOT) sponsored research that characterized high-temperature and intermediate-temperature performance graded (PG) properties using Dynamic Shear Rheometer (DSR) test following AASHTO M 320 specifications to inform their RBR limits (*1*).

Other state agencies have developed different approaches for evaluating RBR limits. Tavakol et al. (*2*) conducted research for Kansas DOT to identify maximum RAM content by evaluating mixture performance. Mogawer et al. (*3*) studied higher RAP percentages for MassDOT and confirmed softer binder benefits by evaluating both binder and mixture performance. These studies assumed complete blending of virgin and RAM binder. Stephens et al. (*4*) developed a simple physical testing procedure for Connecticut DOT to determine effective blended binder grade in asphalt mixtures with RAP. Roque et al. (*5*) investigated the relationship between RAP content and mixture cracking performance for Florida DOT by testing the fine mortar fraction of the mix.

However, previous studies on RBR limits used deterministic analysis methods that evaluated a limited combination of virgin and RAM binders. This approach cannot assess the risk of blended binders failing to meet performance-graded criteria at different RBR levels because it does not account for combined variability of virgin and RAM binder properties. This method also fails to leverage Quality Assurance (QA) datasets containing extensive virgin binder property information.

Additionally, the past research that informed the NCDOT RBR limits did not consider low-temperature PG properties. Low-temperature performance graded properties require Bending Beam Rheometer (BBR) test following AASHTO T 313. BBR testing requires significantly more binder compared to the DSR test, which poses challenges due to the extensive solvent extraction and recovery needed to obtain the recovered RAM binder samples. Extraction and recovery is time-consuming and require hazardous, expensive solvents. Smaller DSR samples are more readily extracted and recovered. Researchers have attempted to use DSR testing to evaluate low-temperature properties as an alternative to BBR testing. Different geometries including the torsion bar (*6*), 4 mm parallel plate (*7–9*), and 8 mm parallel plate (*10*) as well as various analytical techniques have been investigated. However, efforts to date have focused on virgin binders and not specifically those from NC. Thus, research is needed to develop an approach for accurately obtaining low-temperature performance graded properties for recycled binders in NC.

1.2. Research Objectives

- Evaluate NCDOT RBR thresholds through a probabilistic analysis that incorporates quality assurance (QA) data for virgin binders and RAP binder samples collected from various North Carolina stockpiles.
- Evaluate and improve the accuracy for predicting RAM binder low-temperature PG properties in North Carolina using the DSR.
- Characterize the properties of RAP and RAS binders within stockpiles over time and across several asphalt plants in North Carolina.

1.3. Thesis Organization

This thesis consists of six chapters. Chapter 1 introduces the research background and objectives of this thesis. Chapter 2 provides a literature review on RBR limit selection, virgin binder selection, and alternative methods to use DSR for characterizing asphalt binders' low-temperature properties. Chapters 3, 4, and 5 present testing and analysis of 29 asphalt binders characterized as part of this thesis from 7 plants across North Carolina, including 12 virgin binders and 17 RAM binders, of which there are 3 RAS binders and 14 RAP binders. In Chapters 3, 4, and 5, methodologies are included in each chapter even though there is overlap, so that each chapter can be read as a stand-alone study. Chapter 3 presents a probabilistic evaluation of NCDOT's RBR thresholds using the RAP binders characterized as part of this this thesis, prior RAP binder characterization from NCDOT RP 2014-05, and QA data for virgin binders from the NCDOT. Chapter 4 evaluates and improves the accuracy for predicting RAP binder low-temperature PG properties using the DSR using all binders characterized as part of this thesis. Chapter 5 characterizes the properties of RAP and virgin binders within stockpiles over time and across several asphalt plants in North Carolina for a subset of this thesis' materials. Chapter 6 summarizes the conclusions and recommendations.

2. Literature Review

2.1. Overview

RAM, including RAP and recycled asphalt shingles RAS, are increasingly used in asphalt mixtures. However, their highly oxidized binders present stiffness concerns that can negatively impact cracking performance, making it critical to establish appropriate RBR percentage limits for maintaining mixture performance. While AASHTO M 323 (*11*) recommends using blending charts to set RBR% limits and selecting virgin binders when RAP content exceeds 25%, states employ varying approaches for establishing allowable RAP and RAS content limits and virgin binder specifications. This literature review examines the diverse methods states used to establish and evaluate RAP and RAS content limits. Additionally, the AASHTO M 323 (*11*) blending chart approach requires RAM binder characterization through PG grading tests using DSR for high and intermediate temperature properties and BBR tests for low-temperature properties. However, BBR testing involves practical constraints for RAM binders, including large sample requirements and time-consuming extraction and recovery processes that use expensive, hazardous solvents. Consequently, researchers have explored DSR testing with 4mm or 8mm parallel plates as an alternative method for characterizing low-temperature properties of asphalt binders. This review evaluates the relevant literature on these alternative approaches.

2.2. Approaches to Inform and Evaluate Recycled Binder Limits

Virgin binder specification according to the recycled material content or recycled binder replacement percentage (RBR%) and/or the recycled material type are measures used to mitigate variability in the performance of recycled asphalt mixtures. AASHTO M 323 (*11*), which specifies Superpave volumetric mix design, provides the virgin binder selection guidelines presented in Table 2-1 for RAP mixtures. The AASHTO M 323 guidance was derived from NCHRP Project 09-12 findings from studying the impacts of RAP on blended binder and mixture performance characteristics (*12*). The specifications address both RAP percentage by total weight of mixture and RBR%. RBR% provides better control of blended binder properties than the RAP percentage by total weight of mixture since RAP binder content can vary (*13*). Also, the AASHTO M 323 guidance recommends following a blending chart when the RAP content exceeds 25 percent. A blending chart is used to calculate the RBR% when virgin binder properties are known, or alternatively, to select the appropriate virgin binder grade at a specific RBR%. The blending chart is represented by Equation (2.1).

$$T_{\text{virgin}} = \frac{T_{\text{blend}} - (\text{RBR} \times T_{\text{RAP}})}{1 - \text{RBR}} \tag{2.1}$$

where:

T_{virgin} = critical temperature of virgin asphalt binder (high, intermediate, or low),

T_{blend} = critical temperature of blended asphalt binder (final desired) (high, intermediate, or low),

RBR = recycled binder replacement percentage, equal to weight of recycled binder divided by total weight of binder in the mixture,

T_{RAP} = critical temperature of recovered RAP binder (high, intermediate, or low).

Creating a blending chart requires the use of solvent extraction and recovery of the RAP binder with subsequent performance-graded characterization of the recovered binder properties, which is generally deemed too costly and time consuming to be practical to perform on a routine basis. These factors are likely one contributing factor to some states only permitting relatively low RAP content limits.

Table 2-1. Virgin binder selection for RAP mixtures according to AASHTO M 323.

Recommended Virgin Asphalt Binder Grade	RAP Percentage
No change in binder selection	<15
Select virgin binder one grade softer than normal (e.g., select a PG 58-28 if a PG 64-22 would normally be used)	15 to 25
Follow recommendations from blending charts	>25

While the AASHTO M 323 recommended using a blending chart to set the RBR% limits and select virgin binders when the RAP content exceeds 25 percent, states have used different approaches to set their allowable RAP and RAS content limits and virgin binder grade specifications. Therefore, relevant literature was reviewed to understand how different states use various methods to establish or critically evaluate RAP and RAS content limits. Many states have developed specific requirements for virgin binder selection according to the RBR% (defined in Equation (2.2)), informed by an evaluation of the properties of RAP and/or RAS binders within their state. NCDOT followed this practice, resulting in the RBR% limits shown in Table 2-2 and Table 2-3.

$$RBR\% = \frac{(Pb_{RAP} \times P_{RAP}) + (Pb_{RAS} \times P_{RAS})}{100 \times Pb_{total}} \times 100\% \tag{2.2}$$

where:

Pb_{RAP} = binder content of the RAP,

P_{RAP} = percentage of RAP by weight of mixture,

Pb_{RAS} = binder content of the RAS,

P_{RAS} = percentage of RAS by weight of mixture,

Pb_{total} = total binder content of the mixture.

Table 2-2 shows that the maximum RAP or RAP/RAS RBR% allowed to use in surface mixtures is 40% and only 20% for mixtures with only RAS. Furthermore, NCDOT specifies virgin binder grade requirements depending on the mixture type and the RBR%, as indicated in Table 2-3. The specification requires using a PG 64-22 for RAP only mixtures with a maximum RBR% of 30%, and the use of a PG 58-28 virgin binder when the RBR% exceeds 30% for A, B, and C mixtures. Moreover, the maximum RBR% is 18% for mixes using virgin binder PG 76-22. The NCDOT also stipulates that when the RBR% exceeds 20% and the mixture contains RAS that a PG 58-28 is used.

Table 2-2. North Carolina DOT RAP and RAS content limits.

Maximum recycled binder replacement percentage (RBR)			
Recycled material	**Intermediate and base mixes**	**Surface mixes**	**Mixes using PG 76-22**
RAS	23%	20%	18%
RAP or RAP/RAS combination	45%	40%	18%

Table 2-3. Virgin binder grade requirements based on RBR% according to NCDOT QMS.

Mix Type	RBR% ≤ 20%	21% ≤ RBR% ≤ 30%	RBR% > 30%
S4.75A, S9.5B, S9.5C, I19.0C, B25.0C	PG 64-22	PG 64-22	PG 58-28
S9.5D, OGFC	PG 76-22 B	n/a	n/a

NCDOT RP 2012-04 (*1*) proposed maximum RBR% limits based on the characterization of blended binders' rheological properties. The researchers selected two representative virgin binders in North Carolina, PG 64-22 and PG 58-28, and three recycled materials including RAP, MRAS (Manufacturer Waste Recycled Asphalt Shingles), and PRAS (Post-consumer Recycled Asphalt Shingles). Binders from recycled materials were extracted and blended with two virgin binders separately in different proportions as shown in Table 2-4, where the percentage represents the proportion of extracted binder by weight of total blended binder. For each blended binder, rolling thin film oven (RTFO) test and pressure aging vessel (PAV) test were conducted to simulate short-term aging and long-term aging of the material. The unaged level, RTFO aged level, and PAV aged level blended binders were tested on the Dynamic Shear Rheometer (DSR) to determine their rheological properties including dynamic shear modulus (G*) and phase angle (δ) at varying temperatures. Blending charts were created based on these rheological properties to determine the RAP binder limits that could be used in the pavement mixtures. The minimum limit of RAP binder content was determined from the blending charts at high temperatures, using $G^*/\sin(\delta) \geq 1.0$ kPa and $G^*/\sin(\delta) \geq 2.2$ kPa for unaged and RTFO aged binders respectively. The maximum limit was determined from the blending charts at intermediate temperatures, using $G^*\sin(\delta) \leq 5000$ kPa for PAV aged binders. From the limits determined through the blending charts, the recycled binder limits that meet the specifications of a PG 64-22 binder with respect to both high and intermediate temperatures are shown in Table 2-5. Table 2-6 shows the suggested limits for S9.5B mixtures, with conservative rounding to the nearest 5% from Table 2-5.

Table 2-4. Binder blends matrix.

Virgin Binder	RAP	MRAS	PRAS
PG 58-28	25%, 40%, 100%	10%, 20%	10%, 25%
PG 64-22	25%, 40%, 100%	10%, 20%	10%, 25%

Table 2-5. Minimum and maximum limits of recycled binders to meet PG 64-22.

Virgin Binder	Recycled Binder	High Temperature (Minimum)	Intermediate Temperature (Maximum)
PG 58-28	RAP	21.6%	42.9%
	MRAS	23.5%	56.3%
	PRAS	5.4%	26.8%
PG 64-22	RAP	12.1%	20.5%
	MRAS	15.1%	41.9%
	PRAS	4.3%	11.1%

Table 2-6. Recycled binder limits for S9.5B mixes.

Recycled Binder	Virgin Binder	Maximum Limits (% Binder)
RAP	PG 58-28	45%
	PG 64-22	20%
MRAS	PG 58-28	55%
	PG 64-22	40%
PRAS	PG 58-28	25%
	PG 64-22	10%

The limits derived from blended binders rheological properties were validated through performance tests on RS9.5B mixes designed and fabricated in the laboratory. These mixes contained the same content of recycled materials and corresponding virgin binder as listed in Table 2-6, with adjustments made to virgin aggregate and virgin binder content to account for the contributions from RAP. Each mixture was tested using the Asphalt Mixture Performance Tester (AMPT) to measure dynamic modulus, with results then input into AASHTOware Pavement ME Design software to estimate fatigue and rutting life for comparison with virgin mixtures. The recycled and virgin mixtures demonstrated satisfactory performance in the AASHTOware Pavement ME simulations and thus, the final recycled binder limits for RS9.5B mixes remained consistent with those presented in Table 2-6.

NCDOT RP 2014-05 (*14*) further assessed the impacts of RAP binder properties in the state to inform the NCDOT's RBR% specifications. The researchers characterized the high- and intermediate- performance-graded properties of 27 RAP binders acquired from 9 different stockpiles across the state, in unaged, RTFO and PAV aged conditions. The authors leveraged the results to identify the range of acceptable RBR% levels for use with PG 64-22 and PG 58-28 virgin binders, which are listed in Table 2-7. The RAP binder characterized demonstrated considerable variability with continuous high temperature grades ranging from 82 to 112°C, leading to the relatively wide ranges in applicable RBR% levels in Table 2-7.

Table 2-7. Proposed RBR% limits for RAP according to NCDOT RP 2014-05.

Virgin Binder	By RBR%	By weight of Mix
PG 64-22	0% - 17.7%	0% - 21.2%
PG 58-28	8.8% - 47.3%	10.6% - 56.8%

While the past NCDOT RP 2012-04 and RP 2014-05 proposed the RBR% limits based on blended binders rheological properties and mixture performance, NCDOT RP 2014-05 adjusted RAP RBR% limits by considering the variability of RAP binders. However, the variability of virgin binders in the state was not considered in either of these two studies. Aparicio (*15*) conducted a preliminary probabilistic analysis of RBR limits in NC leveraging the QA dataset from 2016 to 2021 provided by the NCDOT.

Austerman et al. (*16*) conducted a study to evaluate the variability of RAP stockpile and virgin binder properties being used in Massachusetts. Eight RAP producers and four regional virgin binder suppliers were evaluated, encompassing variation among stockpiles and year-to-year variation for specific stockpiles. Greater variabilities were observed among RAP stockpiles than within specific stockpiles. Virgin binders from four regional suppliers met the PG 64-28 grade requirements. However, the continuous low-temperature grades varied among these binders. While three suppliers provided binders with continuous low-temperature grades around -30°C, the binder from the fourth source showed a continuous low-temperature grade very close to the -28°C threshold. This near-threshold performance compromised its ability to accommodate RAP in asphalt mixtures without exceeding specified properties. The accuracy of the blending chart equation was verified by preparing four blended binders, combining one virgin binder with recovered RAP binders from four different sources. The low-temperature continuous grade was measured for each of these blended binders. Results indicated that the equation's predictions were accurate only at lower RAP percentages. Overall, considering the variability in both RAP and virgin binders, the predicted blended binder grades showed cases that failed intended property limits at currently permissible RBR% levels. Using the blending chart equation, only 71% of the blended binder combinations achieved the specified PG 64-28 grade, despite having a relatively low RAP content of 15% by dry weight of mixture.

Mogawer et al. (*3*) conducted another study for MassDOT to assess the impact of higher percentages of RAP in asphalt mixtures and confirmed the benefit of softer binder for mixture performance. The study used two virgin binders, including PG 64-28, which is commonly used in the Northeast, and a softer PG 52-34. The aggregates and RAP were from the same plant. The mixtures were designed and fabricated in the laboratory, with a 9.5-mm NMAS. Different RAP contents were evaluated as shown in Table 2-8.

Table 2-8. RAP content for mixture design.

Binder	%RAP
PG 64-28	0%–Control
	15%
	25%
	35%
	50%
PG 52-34	35%
	50%

The study evaluated both recovered binder properties and mixture performance. Recovered binders were extracted and recovered from the RAP mixtures and thus, constituted the blend of RAP and virgin binder. The study analyzed the rheological black space diagram, R-value, and crossover frequency. Results showed that using softer virgin binder helped reverse the increased cracking susceptibility observed when RAP content was increased to 35% and 50%. The aging-induced stiffness was effectively mitigated by the softer binder. Regarding mixture performance, the study conducted Hamburg wheel tracking test and flexural beam fatigue test. Results illustrated the impact of the softer binder in mitigating the stiffness of mixtures containing 35% and 50% RAP, as shown by increased rutting susceptibility and fatigue cracking resistance compared to the PG 64-28 mixtures. The study concluded that Superpave 9.5 mm mixtures could be designed with up to 50% RAP with the same binder content and gradation as a control mixture with 0% RAP based on volumetric design criteria. However, using the softer PG 52-34 virgin binder yielded a mixture with more rutting susceptibility at both RAP contents of 35% and 50% compared to the PG 64-28 control mixture. The mixtures with PG 52-34 binder did not meet MassDOT rutting test requirements. Therefore, the authors concluded that the use of higher percentages of RAP in HMA must be carefully developed for each specific mixture based on the properties of the RAP, the amount of RAP, and the available virgin binders.

One limitation of relying on blending charts is that the approach assumes complete blending between the recycled and virgin binder. To address this concern, Stephens et al. (*4*) conducted a study for Connecticut DOT to develop a simple physical testing procedure to determine the effective blended binder grade in asphalt mixtures with RAP. The study collected aggregate, PG 64-28 and PG 58-34 virgin binders, and RAP from a Connecticut mix plant. The determination of binder content within the RAP material and the RAP aggregate recovery were conducted using the ignition oven. One aggregate structure was chosen and maintained throughout each specimen. Half of the mix specimens contained 15% RAP, and half contained 15% reclaimed RAP aggregate. Virgin materials and reclaimed RAP aggregate were batched and mixed in laboratory. The specimens were subjected to the indirect tension test at 28°C and 3°C for correlation with high temperature and low temperature blended binder grades, respectively. For high temperature grade, the study first created a plot correlating the average tensile load measured at 28°C with the high temperature grade for specimens containing only virgin binder. Then, assuming a linear relationship between the virgin specimen average tensile loads and high-temperature grade, interpolation or extrapolation was used to obtain the effective high PG grade of the combination of RAP and virgin binder. A similar process was used to infer the low temperature grade. The effects of testing temperature, RAP content, and aggregate source were also investigated to confirm the test method is effective. The authors found that the effective PG of the mixture depends on RAP content but was not substantially impacted by aggregate source, gradation, or conditioning temperature. The authors also compared laboratory and plant mixture, which yielded unexpected trends indicating an effective PG in the plant mix exceeding what would result from complete blending. However, the authors attributed this to potential aging differences between laboratory and plant aging. While the results were not used to directly inform RBR limits, they highlight the potential impacts of partial recycled binder contribution on effective binder properties of asphalt mixtures.

Tavakol et al. (*2*) conducted research for Kansas DOT to study the effect of incorporating RAP and RAS on the performance of hot-mix asphalt mixtures and tried to identify the minimum virgin binder contents (in other words 100 – RBR%) that would result in mixture performance meeting standards. The study selected three KDOT mixture designs from two projects in Kansas as control mixtures. The first mixture design was a surface layer mixture designated as US-59-surface, which used aggregates with a 9.5-mm Nominal Maximum Aggregate Size (NMAS). The other two were intermediate course mixtures using a 19-mm NMAS, one designated as US-59-intermediate, the other designated as US-36-intermediate. All three control mixture designs contained 15% recycled materials by weight of total mixture, with US-59-surface and US-59-intermediate containing 5% RAS, while US-36-intermediate contains only RAP. To compare the impact of different recycled materials content while satisfying KDOT requirements for aggregate gradation, different percentages of recycled materials were chosen for each mixture design. The virgin binder grade was adjusted based on blending charts to achieve the intended blended binder grade, and the RBR% was calculated by considering the weight of recycled binder that was introduced into the mixture, as shown in Table 2-9.

Table 2-9. Virgin binder content and PG grade in each mixture.

Mixture Design		%RAS	RBR%	Virgin Binder Grade
US-59-surface course (SR-9.5A)	15% Rec.	5	21	64-34
	20% Rec.	5	25	64-34
	35% Rec.	5	38	58-34
US-59-intermediate course (SR-19A)	15% Rec.	5	21	64-34
	20% Rec.	5	30	64-34
	30% Rec.	5	40	58-34
US-36-intermediate course (SR-19A)	15% Rec.	0	14	70-28
	20% Rec.	5	42	64-34
	25% Rec.	5	48	58-34

The mixture performance was evaluated in terms of moisture susceptibility, rutting resistance, and fatigue cracking resistance. The testing methods included dynamic modulus test, Hamburg wheel tracking test, flow number test, and uniaxial cyclic fatigue test. The study recommended maximum RBR% limits should be required based on mixture type because of varying performance observed for SR-9.5A and SR-19A mixtures with RAP content. For SR-9.5A, lower than 25% RBR could lead to satisfactory performance. For SR-19A, 30% RBR was the maximum recycled binder content to show good performance. In addition, improved fatigue performance was observed in the mixtures incorporating both RAP and RAS compared to those RAP-only mixtures. While this study evaluated the impact of RAP binder on mixture performance, only a limited number of mixture designs could be included.

Roque et al. (*5*) investigated the relationship between RAP content and mixture cracking performance based on the dominant aggregate size range-interstitial component (DASR-IC) theory as part of a study for Florida DOT. In this theory, the dominant aggregate size range (DASR) forms an aggregate skeleton to provide shear resistance, while the interstitial component (IC) part consists of fine aggregates, binder, and air voids which fill the volume in the DASR to provide tension and shear resistance. The DASR porosity governs the interlocking and provides resistance to deformation and fracture. The study required DASR porosity to reach a range of 38-52% to ensure adequate interlocking and potentially good mixture performance. Eight RAP sources were selected based on their DASR porosity, recovered RAP binder stiffness, and RAP fineness for evaluation in mixtures. The RAP binder was according to the high-temperature continuous grade of the recovered RAP binder. The RAP binder stiffness was defined following Superpave performance grading system and grouped into high (HPG>106°C), intermediate (100°C <HPG<106°C), and low (HPG<100°C). The RAP fineness was determined from the percent passing No. 16 sieve (1.18 mm) and grouped into coarse (<40%), intermediate (40-50%), and fine (>50%). IC mixes were designed using the eight RAP sources at four RAP contents of 0%, 20%, 30%, and 40%. IC mixes were evaluated using the interstitial component direct tension (ICDT) test because the specimen preparation and testing required less effort than a full scale mixture test.

From the test, a parameter called interstitial component fracture energy (FE_{IC}) was used to evaluate cracking resistance and estimate preliminary allowable RAP content for each source. FE_{IC} is defined as the area under the stress-strain curve. The study observed FE_{IC} generally decreases as RAP content increases because the highly aged stiff RAP binder within RAP material can lead to lower FE_{IC}. FE_{IC} is also influenced by RAP fineness because finer RAP result in more RAP in the IC portion of the mixture than coarse and intermediate RAP at the same RAP content, leading to lower FE_{IC}. The result shows even at 20% RAP content, all three IC mixes with fine RAP exhibited distinctively lower FE_{IC}. Therefore, the study used coarse and intermediate RAP sources to estimate preliminary maximum RAP content and generated a preliminary guideline for maximum allowable RAP content in PMA mixture based on RAP binder stiffness and RAP fineness. After the verification using IDT test, it is concluded that for coarse (<40% passing No. 16) and low stiffness RAP, the maximum RAP content can up to 40%.

Table 2-10 summarizes the pros and cons for the different approaches identified in the literature to evaluate and inform maximum RAP and RAS contents. Some studies have focused on blended binder testing, but this approach lacks mixture-level validation, critical given the potential for partial recycled binder contribution. Additionally, the extraction and recovery process is labor-intensive, limiting the number of blends that can be evaluated. Mixture testing addresses this gap but is also time-consuming, typically restricting the number of conditions that can be studied compared to binder-level testing. Florida's ICDT method offers an alternative by testing the fine mortar fraction of the mix. While initial results are promising, standardized procedures for IC mix design and testing are still lacking. A common limitation across past studies is the narrow range of RAP, virgin binder, and RBR combinations evaluated. Future approaches could leverage large binder property databases (e.g., virgin binder QA data) to develop probabilistically informed RBR limits, with mixture testing used to validate selected scenarios.

Table 2-10. Summary of pros and cons for different approaches.

Reference	Approach	Pros	Cons
North Carolina (*1*, *14*)	Binder characterization	• Direct measurement of blended binder properties. • Well-established testing protocols with acceptable thresholds. • Follows traditional binder specifications, familiar to industry.	• Binder extraction and recovery are time-consuming. • RAP impact on mixture performance remains unknown. • Variability of virgin binder is not considered.
Kansas (*2*)	Mixture performance evaluation	• RAP impact on mixture performance is directly evaluated. • Accounts for aggregate structure effects, not just binder properties. • Eliminates assumptions about binder blending and interaction.	• Limited mixture design scenarios are evaluated. • Performance tests can be highly variable. • Difficult to tie findings directly to influence of the binder.
Massachusetts (*3*)	Binder and mixture evaluation	• Considers impacts of RAP on both binder and mixture properties.	• Extensive testing requirements limit number of mixtures/RAP sources that can be evaluated.
Connecticut (*4*)	Comparison of mixtures prepared with RAP and RAP aggregate to binder properties	• Do not need extraction and recovery. • Considered partial blending between RAP and virgin binders. • Can be easily implemented by agencies.	• Requires validation against established methods.
Florida (*5*)	New method for IC mix specimen evaluation	• IC mix specimen preparation and testing require less effort than full scale mixture and capture interactions between binder and aggregate.	• Requires validation. • IC preparation is not practical.

2.3. Approaches to Predict BBR from DSR

Low-temperature performance evaluation plays a critical role in the asphalt performance grading system. It determines thermal crack resistance of asphalt binders. The BBR test currently serves as the standard method for determining these low-temperature properties. However, the BBR test requires significantly more long-term aged binder compared to DSR testing. This binder demand is challenging when characterizing RAM binders in particular given the extraction and recovery processes needed to obtain samples is time consuming and require hazardous, expensive solvents. Researchers have attempted to use DSR testing to evaluate low-temperature properties as an alternative to BBR testing. Therefore, this review examines relevant literature to understand different methods for evaluating low-temperature asphalt binder properties.

2.3.1. Geometry

The DSR is an instrument that applies torsion to a cylindrical sample. The DSR can control stress or strain through applied torque. Larger sample radius requires proportionally higher forces to achieve the same stress or strain levels as smaller samples. The combination of increased radius and higher force in larger samples results in proportionally higher torque demands.

Testing at low temperatures creates two challenges. First, asphalt binders have a higher modulus at low temperatures for a given loading rate or time, requiring much higher torque for low-temperature measurements. Second, as specimen stiffness approaches the stiffness of the instrument frame, the measurements recorded by the system include deformation of the loading components themselves. Consequently, using sample geometry with smaller diameters is helpful for low-temperature testing, and it is critical to measure and eliminate the compliance effect of the instrument when conducting measurements at low temperatures.

Table 2-11 compares three different geometries used for testing asphalt binder properties in the DSR for the prediction of BBR results. The torsion bar geometry (3.3 mm-thick × 12.7 mm-wide × 38.1 mm-long) offers higher stress capability for very low temperature conditions and produces measurable deformation within instrument limits. However, it requires significant binder volume compared to 4 mm and 8 mm geometries and requires more complex specimen preparation, leading to somewhat comparable effort requirements to BBR testing. The 4 mm parallel plate geometry with 4 mm diameter samples with 1.75 mm height, provides an excellent torque multiplication for higher stress testing with lower compliance, though it still demands careful machine compliance corrections during analysis. The primary challenge with the 4 mm parallel plate geometry set up is trimming the very small, delicate sample. The 8 mm parallel plate geometry uses 8 mm diameter and 2 mm tall samples. This setup employs the standard DSR geometry already used for intermediate-temperature performance grading and is compatible with equipment typically available in asphalt laboratories. The literature review focuses on 4 mm and 8 mm parallel plates because the torsion bar geometry requires relatively large binder volumes and complex specimen preparation.

Table 2-11. Summary of pros and cons for different geometries.

Geometry	Sample Size	Pros	Cons
Torsion Bar (*6*)	3.3 mm-thick × 12.7 mm-wide × 38.1 mm-long	• Higher stress capability suitable for very low temperature testing, • Achieves measurable deformation within instrument capacity.	• Still requires a substantial volume of binder compared to smaller geometries, • Specimen preparation as complicated as BBR setup.
4 mm Parallel Plate (*7–9*)	4 mm-diameter × 1.75 mm-height	• High torque multiplication factor, allowing for higher stresses and lower compliance compared to larger geometries.	• Requires careful compliance correction, • Tedious sample preparation.
8 mm Parallel Plate (*10*)	8 mm-diameter × 2 mm-height	• Uses the standard DSR geometry, • Does not require the complex compliance corrections since testing limited to intermediate temperatures.	• Testing at intermediate temperatures requires extrapolation of time-temperature shift factors to low temperatures, rather than direct testing at BBR conditions.

2.3.2. Models

To convert DSR measurements to BBR parameters, two steps are necessary. First, convert the dynamic shear modulus from the frequency domain to creep compliance in the time domain. Second, convert the shear response to uniaxial response using Poisson's ratio.

Researchers have developed several methods to use the DSR testing for evaluating low-temperature asphalt binder properties as an alternative to the BBR testing. Each approach employs different models and correlation techniques to translate DSR results with BBR parameters.

Sui et al. (*7*) established direct correlations between DSR and BBR results by empirically observing that both tests measure similar material characteristics. They observed the similarity between the shear stress relaxation modulus $G(t)$ from step strain tests using the DSR and the BBR creep stiffness $S(t)$. Additionally, they found that the slope of the log-log scale relaxation modulus curve represents the apparent relaxation rate (m_r value), which is comparable to BBR's m_c value, as shown in Figure 2-1. Since step strain tests require impractical constant initial strain, the researchers conducted dynamic frequency sweep tests and converted complex shear modulus $G^*(\omega)$ to shear stress relaxation modulus. They evaluated two interconversion methods: fitting dynamic data using the generalized Maxwell model and fitting with the Christensen-Anderson-Marasteanu (CAM) model. They used the resultant master curve model combined with the empirical conversion equation developed by Ninomiya and Ferry (*17*) to obtain $G(t)$, the conversion equation is given in Equation (2.3). Both master curve models produced nearly identical results that matched measured data for three asphalt binders, leading them to select the first method for simplicity.

$$G(t) = G'(\omega) - 0.4G''(0.4\omega) + 0.014G''(10\omega) \tag{2.3}$$

where:

$G'(\omega)$ = storage modulus,

$G''(\omega)$ = loss modulus.

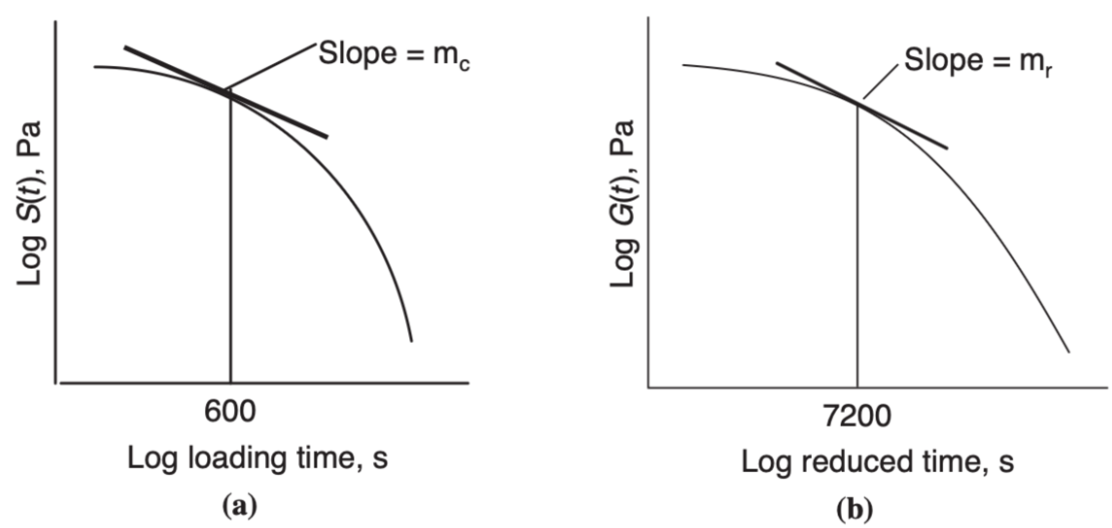

Figure 2-1. Illustration showing similarity between (a) creep stiffness versus loading time from BBR and (b) stress relaxation modulus versus reduced time from DSR (Figure cited from Sui et al (*7*)'s study).

Based on the time-temperature superposition principle used in the BBR test (where testing temperature increases 10°C above PG temperature to reduce data collection from 2 hours to 60 seconds), Sui et al. (*7*) found strong correlations between *S*(*t*) at 60 seconds and *G*(*t*) at 7,200 seconds, as well as between m_c and m_r values. Using six asphalt binder results from the February 2009 Binder Expert Task Group meeting in Irvine, California, they obtained linear correlation coefficients of 0.969 for *S*(*t*) vs. *G*(*t*) and 0.945 for m_c vs. m_r. When they expanded their dataset to eleven binders by adding five more samples, correlation coefficients improved to 0.986 and 0.957 respectively, demonstrating that larger datasets strengthen these relationships.

Lu et al. (*8*) found an empirical correlation between dynamic shear modulus measured by 4 mm geometry using DSR and creep stiffness measured by BBR. The correlation at higher frequency (100 rad/s) was not very strong, with R^2 values of 0.33 and 0.41 for the best fit line at -15°C and -25°C, respectively. The correlation became stronger at lower frequency (0.1 rad/s) with R^2 values of 0.50 and 0.70 at -15°C and -25°C, respectively. They used an interconversion equation developed by Anderson et al. (*18*) to convert $G^*(\omega)$ to *S*(*t*), deriving dynamic shear modulus and phase angle from master curves at 0.0167 rad/s frequency (corresponding to 60 s in BBR), the equation is given in Equation (2.4). This approach yielded a clear trend between DSR-estimated and BBR-measured stiffness, but with some deviation, showing an R^2 value of 0.64 for the best fit line at a reference temperature of -25°C. They attributed this deviation to wax crystallization from the waxy binders or physical hardening that occurred during different thermal histories due to sample size difference. When they removed one waxy binder with the highest wax content of 6.2% (leaving seven binders total, five of which were waxy binders with wax content ranging from 1.9% to 4.2%), the R^2 improved from 0.64 to 0.77. They also evaluated DSR-estimated *m*(60) with BBR-measured *m*(60), Equation (2.5) from Anderson et al. (*18*) was used to estimate *m*(60). Similar to the *S*(*t*) correlation, the *m*-value correlation was stronger at lower frequency (0.1 rad/s) with R^2 values of 0.60 and 0.47 at -15°C and -25°C, respectively.

$$S(t) \approx \frac{3G^*(\omega)}{[1+0.2\sin(2\delta)]} \tag{2.4}$$

where:

G^* = dynamic complex modulus,

δ = phase angle.

$$m-\text{value}\approx\frac{\delta}{90} \tag{2.5}$$

Hajj et al. (*9*) investigated exact viscoelastic interconversion from frequency sweep testing in the DSR as a BBR replacement. They created master curves using sigmoidal functions applied to creep compliance $J^*(\omega)$ data obtained by inverting the dynamic shear modulus $|G^*|(\omega)$ values. The researchers converted master curves to $J(t)$ using the Ninomiya and Ferry approach, then to $D(t)$ using Equation (2.6). They inverted compliance at different time points to obtain stiffness versus time curves, extracting stiffness and *m*-value parameters at various temperatures for continuous grade determination.

$$D(t)=\frac{J(t)}{1+2v} \tag{2.6}$$

where:

$D(t)$ = tension/compression creep compliance,

$J(t)$ = shear creep compliance,

v = Poisson's ratio.

Zeng et al. (*10*) investigated $S(60)$ and $m(60)$ prediction using only LVE properties measured with 8 mm parallel plates at intermediate temperatures. Their approach relied on time-temperature superposition (t-TS) theory, which allows mechanical response prediction at different temperature-time combinations by adjusting loading frequency. This enables data shifting along the log frequency axis to form master curves for interpolation at any temperature-frequency combination. Since DSR measurements only reached temperatures as low as 0-15°C, they used Arrhenius equation for extrapolation to obtain time-temperature shift factors for BBR temperatures. The researchers evaluated two interconversion methods: rigorous calculation involving retardation spectrum conversion and approximate method using idealized relaxation and retardation spectra. Both methods required the master curve construction using the 2S2P1D model. They proposed using approximate conversion for creep stiffness $S(60)$ calculations and rigorous calculations for $m(60)$ predictions to achieve the best accuracy. A more detailed description of Zeng et al. (*10*)'s modeling framework is presented in Chapter 4 of this thesis.

Table 2-12. Summary of master curve models and conversion methods.

Reference	Master Curve Model	Conversion from Frequency to Time Domin	Translate G(t) to S(t)
Sui et al. (*7*)	• Generalized Maxwell model • CAM model	Ninomiya and Ferry empirical conversion equation	Direct correlations between DSR $G(t)$ and BBR $S(t)$
Lu et al. (*8*)	Built-in model from commercial software	Anderson et al. interconversion equation to convert $G^*(\omega)$ to $S(t)$	Complex modulus correlation with BBR creep stiffness
Hajj et al. (*9*)	Sigmoidal function	Ninomiya and Ferry approach to convert master curves to $J(t)$, then to $D(t)$	Exact viscoelastic interconversion
Zeng et al. (*10*)	2S2P1D model	• Rigorous calculation (retardation spectrum conversion) • Approximate method (idealized relaxation/retardation spectra) *(Recommended approximate for S(t), rigorous for m-value)*	Convolution integral and Poisson's ratio

2.3.3. Evaluation of Accuracy

Researchers have progressively refined DSR-based prediction methods for low-temperature binder evaluation, achieving varying levels of accuracy through different approaches and criteria adjustments.

Sui et al. (*7*) established equivalent DSR criteria to current BBR thresholds, reporting that G(7,200 s) = 162 MPa is approximately equivalent to S(60 s) = 300 MPa at a temperature 10°C lower. Similarly, they found m_r(7,200 s) = -0.261 coincides with m_c = -0.3 at a temperature 10°C lower. Rounding these values produced practical criteria: $G(t) \leq 160$ MPa and $m_r \geq -0.26$ at the actual PG temperature. When they compared continuous low temperatures determined from $G(t)$ versus $S(t)$ and m_r versus m_c for four asphalt binders using line of equality plots, they achieved R^2 values of 0.74 for $G(t)$ vs. $S(t)$ and 0.96 for m_r vs. m_c.

Lu et al. (*8*) applied criteria proposed by Farrar et al. (*19*) to compare DSR-determined continuous low temperatures with BBR measurements. They found good correlation for stiffness-based continuous temperatures with $R^2 = 0.8$, but poor correlation for m-value-based continuous temperatures. Additionally, DSR-predicted stiffness temperatures were generally lower than BBR values, with differences exceeding 10°C in some cases.

Hajj et al. (*9*) achieved accurate stiffness continuous grade predictions with 7% average error when comparing predicted grades with BBR-based continuous grades. However, m-value continuous grade predictions showed an average error of 27%. The authors explain this poor m-value performance resulted from the parameter's high sensitivity, where small differences at critical frequencies and temperatures cause large variations in grade calculations due to localized slope changes. To improve accuracy, they developed a second approach that fit sigmoidal functions to single-temperature data without constructing master curves using time-temperature superposition. They repeated this process for each BBR test temperature (16°C, 10°C, and 4°C above the lower grade temperature) and applied identical interconversion processes. This method produced strong linear correlation with slight bias between predicted and BBR-measured m-values. They addressed this bias by changing the *m*-value criteria from 0.3 to 0.28, following Farrar et al. (*19*) recommendations, which reduced average error to 8%.

Zeng et al. (*10*) found good correlation between DSR-predicted and BBR-measured creep stiffness $S(60\text{ s})$ with $R^2 = 0.83$. However, correlation between predicted and measured m-values was less accurate at $R^2 = 0.76$. To improve prediction accuracy, the researchers calibrated predicted results using linear equations fitted to all predicted results. After calibration, R^2 values increased to 0.85 and 0.81, respectively.

Table 2-13. Criteria and accuracy of each method.

Reference	Criteria to Yield Current BBR Thresholds	Reported S(60) Prediction Accuracy	Reported m-value Prediction Accuracy
Sui et al. (*7*)	G(t) ≤ 160 MPa m-value ≥ 0.26 at t = 7,200 s	R^2 = 0.74 G(t) vs. S(t)	R^2 = 0.96
Lu et al. (*8*)	Farrar et al. (*19*) criteria: G(t) ≤ 143 MPa at t = 60 s m-value ≥ 0.28 from G(t) at t = 60 s	R^2 = 0.8 continuous temperature based on stiffness	R^2 = 0.3 continuous temperature based on m-value
Hajj et al. (*9*)	Approach 1: Standard criteria of the BBR test S(t) ≤ 300 MPa, m ≥ 0.3 Approach 2: m-value ≥ 0.28	Approach 1: 7% average error Approach 2: 7% average error	Approach 1: 27% average error Approach 2: 8% average error
Zeng et al. (*10*)	Standard criteria of the BBR test	Before calibration: R^2 = 0.83 After calibration: R^2 = 0.85	Before calibration: R^2 = 0.76 After calibration: R^2 = 0.81

2.3.4. Poisson's Ratio

Poisson's ratio serves as a critical value for converting shear creep compliance J(t) to normal creep compliance D(t). To simplify analysis and avoid measuring the time-temperature-binder specific Poisson's ratio, researchers assume it remains constant. Different studies have adopted various constant Poisson's ratio values, as shown in Table 2.

Hajj et al. (*9*) assessed how Poisson's ratio sensitivity affects the accuracy of stiffness predictions. They found that an assumed time-independent Poisson's ratio influences only the stiffness parameter while not affecting the m-value parameter. This occurs because constant Poisson's ratio creates vertical scaling of the compliance curve without changing its slope. When they tested two different constant Poisson's ratio values (0.35 and 0.45), results showed small changes in the calculated stiffness-based continuous grading temperature. Zeng et al. (*10*) referenced previous studies to select a Poisson's ratio of 0.5 without providing additional rationale or evaluating alternatives. In contrast, Lu et al. (*8*) and Sui et al. (*7*) directly developed correlations between $G(t)$ and $S(t)$ without using Poisson's ratio for conversion.

Table 2-14. Poisson's ratio of each method.

Reference	Poisson's Ratio	Author's Justification
Hajj et al. (*9*)	0.35	The asphalt binder approaches this value at low temperatures and/or high frequencies based on previous work.
Zeng et al. (*10*)	0.5	Selected based on previous studies.

2.3.5. Test Conditions

Table 2-15 presents the testing conditions and correction requirements for different parallel plate configurations in DSR measurements as an alternative to BBR testing for evaluating the low-temperature grade of asphalt binder. Hajj et al. (*9*) evaluated a total of eleven virgin asphalt binders, with six polymer-modified binders. Zeng et al. (*10*) evaluated a total of 45 virgin binders, with five polymer-modified binders. The 4 mm parallel plate provides the advantage of measuring at very low temperatures using the DSR, though this requires implementing complex machine compliance correction procedures. Conversely, the 8 mm parallel plate operates at relatively warm intermediate temperatures, with the benefit that machine compliance correction is not required.

Table 2-15. Summary of testing conditions.

Reference	Geometry	Test Material	Temperature Range	Frequency Range
Sui et al. (*7*)	4 mm	16 Virgin Binders	–40°C to 30°C	Not specified
Lu et al. (*8*)	4 mm	8 Virgin Binders	–35°C to 0°C	0.1–100 rad/s
Hajj et al. (*9*)	4 mm	11 Virgin Binders	–30°C to 60°C	Not specified
Zeng et al. (*10*)	8 mm	45 Virgin Binders	0°C–54°C Recommend: Low PG+30°C to Low PG+60°C	0.1–100 rad/s, or 1–100 rad/s, or 0.628–188 rad/s Recommend: 0.628 to 188 rad/s

2.4. Critical Summary

Establishing RBR% limits as a function of virgin binder performance grade is one way of reducing inconsistencies in the performance of recycled asphalt mixtures. AASHTO M 323 provides guidelines for virgin binder selection based on RAP percentage. Many states, such as North Carolina, have developed their own requirements for virgin binder selection based on

RBR% through evaluation of region-specific RAP and/or RAS binder properties. Other states have implemented various approaches to establish or critically evaluate RAP and RAS content limits: Kansas used mixture performance evaluation, Massachusetts employed both binder and mixture evaluation, Connecticut compared mixtures prepared with RAP and RAP aggregate to binder properties, and Florida evaluated the fine mortar fraction of the mix.

However, previous studies establishing RBR% limits use deterministic analysis methods that evaluate limited selections of virgin binders, RAM binders, and their blends. This approach cannot assess the risk of blended binders failing to meet performance-graded criteria at different RBR% levels because it does not account for combined variability effects in virgin and RAM binder properties. Accordingly, one objective of this thesis is to evaluate NCDOT RBR thresholds through a probabilistic analysis that incorporates quality assurance (QA) data for virgin binders and RAP binder samples collected from various North Carolina stockpiles over multiple research projects.

Low-temperature performance evaluation plays a critical role in the asphalt performance grading system. It determines thermal crack resistance of asphalt binders. The BBR test currently serves as the standard method for determining these low-temperature properties. However, the BBR test requires significantly more long-term aged binder compared to DSR testing, posing challenges especially for testing recycled binders given the extensive extraction and recovery processes.

Researchers have attempted to use DSR testing to evaluate low-temperature properties as an alternative to BBR testing. Two parallel plate approaches have been explored: 4 mm parallel plates offer an ability to measure properties at very low temperatures but require complex machine compliance correction, while 8 mm parallel plates enable measurements at relatively warm intermediate temperatures with lower machine compliance correction requirements. Additionally, 8 mm parallel plates are compatible with equipment typically available in asphalt laboratories.

Among the available analytical approaches in the literature, Zeng et al. (*10*)'s approach was selected for further evaluation herein because it achieved relatively good prediction accuracy compared to other reviewed studies and used the largest dataset for validation. However, previous studies focused exclusively on virgin asphalt binders and did not include recycled binders. Therefore, one objective of this thesis is to evaluate and improve the accuracy of predicting RAM binder low-temperature properties using 8 mm parallel plates on the DSR.

3. Probabilistic Analysis of Recycled Binder Replacement Limits

3.1. Introduction

Selecting appropriate virgin binders and establishing recycled material content limits are critical factors for reducing performance inconsistencies in recycled asphalt mixtures. Current practice relies on established guidelines and state-specific requirements to guide these decisions. AASHTO M 323 (*11*) provides guidelines for selecting virgin asphalt binder grades based on the percentage of RAP or the recycled binder replacement (RBR) level in a mixture. When the RAP content or RBR exceeds 25%, the standard recommends the use of a blending chart to determine the appropriate virgin binder grade. AASHTO M 323 provides guidelines for selecting virgin binder grades based on percentage of RAP or the RBR of the mixture. When the RAP content or RBR exceeds 25%, AASHTO M 323 recommends the use of a blending chart to determine the appropriate virgin binder grade. These recommendations stem from the findings of NCHRP Project 09-12 (*12*). Many states have developed region-specific requirements that account for local RAP and RAS binder characteristics.

North Carolina has established virgin binder selection criteria based on RBR that were informed by systematic evaluation of regional recycled materials (*14*). As shown in Table 3-1, NCDOT currently limits RAP content to 0.4 for surface mixtures and 0.45 for intermediate and base mixtures. However, mixtures using PG 76-22 are restricted to a maximum RBR of 0.18. Virgin binder selection depends on RBR, as listed in Table 3-2. PG 64-22 virgin binder is required when RAP content is 0.3 or less. When RAP content exceeds 0.3, a softer PG 58-28 virgin binder must be used to compensate for the stiffness of highly oxidized RAP binders. Other states have used various approaches to inform and evaluate virgin binder grade selection and maximum recycled material content limits. Kansas used mixture performance evaluation (*2*), Massachusetts employed both binder and mixture evaluation (*3*), Connecticut compared mixtures prepared with RAP and RAP aggregate to binder properties (*4*), and Florida evaluated the fine mortar fraction of the mix (*5*).

Table 3-1. Maximum RBR% requirements according to NCDOT QMS.

Mix Type	Surface Mixes	Intermediate and Base Mixes	Mixes Using PG 76-22
Maximum RAP Content	40%	45%	18%

Table 3-2. Virgin binder grade requirements based on RBR% according to NCDOT QMS.

Mix Type	RBR% ≤ 20%	21% ≤ RBR% ≤ 30%	RBR% > 30%
S4.75A, S9.5B, S9.5C, I19.0C, B25.0C	PG 64-22	PG 64-22	PG 58-28
S9.5D, OGFC	PG 76-22	n/a	n/a

However, these previous studies all used deterministic analysis methods that evaluate a limited selection of virgin binders, RAP binders, and their blends. This approach cannot assess the risk of blended binders failing to meet performance-graded criteria at different RBR levels. Quality assurance (QA) data for virgin binders provides a robust dataset representing the variability of virgin binder properties within a given state. When combined with representative RAP binder characterization, this information can be used to generate frequency distributions of blended binder properties as a function of RBR. These distributions can then inform the selection of RBR limits that achieve compliance with PG specifications at a desired probability level, offering a more data-driven approach to determine RBR thresholds.

3.2. Objectives

The objective of this chapter is to evaluate NCDOT RBR thresholds through a probabilistic analysis that incorporates quality assurance (QA) data for virgin binders and RAP binder samples collected from various North Carolina stockpiles. The analysis focuses on mixture designations that do not require PG 76-22, as these mixtures have significantly lower maximum RBR limits compared to the other mixture designations.

3.3. Methodology

3.3.1. Materials

This study used three data sets: (1) RAP binders specifically characterized as part of this study under NCDOT Research Project (RP) 2023-03, (2) RAP binder data from the earlier NCDOT RP 2014-05 (*14*), and (3) virgin binder QA data provided by NCDOT. In total, these data sets encompass 44 RAP binders and 342 virgin binders.

The NCDOT asphalt binder specifications are based on AASHTO M 320. Accordingly, the data sets focused on AASHTO M 320 performance-graded (PG) binder properties evaluated at the critical temperatures for North Carolina’s climatic grade of PG 64-22. These properties include the Dynamic Shear Rheometer (DSR)-derived characteristics used for high- and intermediate-temperature grading, based on measurements of the dynamic shear modulus, $|G^*|$, and phase angle, δ. Specifically, these include $|G^*|/\sin(\delta)$ at 64°C for high-temperature grading and $|G^*|\times\sin(\delta)$ at 25°C for intermediate-temperature grading. The low-temperature properties measured using the Bending Beam Rheometer (BBR), include creep stiffness at a loading time of 60 seconds, $S(60)$, and the slope of the logarithmic stiffness-time curve at a loading time of 60 seconds, $m(60)$, both measured at -12°C.

The study materials include 17 RAP stockpiles sampled from seven plants across North Carolina. A subset of RAP binders are from the same plants used in Chapter 5 and hence, the same plant identification scheme is used in this chapter for consistency. Details on the extraction, recovery, and testing of these samples are provided in the subsequent section. To support a more comprehensive analysis, a second data set was incorporated, consisting of 27 additional RAP binders characterized in previous NCDOT RP 2014-05 (*14*). The continuous high grading temperatures for these 27 RAP binders varied from 82°C to 112°C. However, it is important to note that these additional samples include only high- and intermediate-temperature PG characterization results.

The virgin binder dataset consisted of QA data acquired from 2022 to 2024 by the North Carolina Department of Transportation (NCDOT). This dataset contains 273 PG 64-22 samples and 69 PG 58-28 samples. High-, intermediate-, and low-temperature PG properties were available for PG 64-22 binders. The high-temperature results utilized were acquired at the rolling thin film oven (RTFO) age level whereas the intermediate and low temperature PG properties were measured after RTFO and pressurized aging vessel (PAV) aging. The QA data for PG 58-28 binders provide only high- and intermediate-temperature data because existing low temperature measurements at -18°C do not match NC's critical climate temperature of -12°C.

3.3.2. RAP Binder Test Methods

The study RAP binders were extracted using a centrifuge extractor with trichloroethylene (TCE) as the solvent according to Method A of AASHTO T 164 (*20*). The asphalt binder recovery was completed using a rotary evaporator according to ASTM D5404 (*21*). The recovered RAP binders were subjected to RTFO aging according to AASHTO T 240 for characterization (*22*). The RAP binders were not subjected to further aging in the PAV in accordance with Appendix X2 of AASHTO M 323 .

DSR testing was conducted on RAP binders at the RTFO age level according to AASHTO T 315 (*23*) for high- and intermediate-temperature grading at 64°C and 25°C, respectively. Testing was performed at a minimum of two additional high- and intermediate-temperature grading levels: one at which the binder met the PG criterion and one at which it did not. This approach enabled calculation of the continuous grading temperatures in accordance with ASTM D7643

. To shorten the testing time, a measurement module and a temperature-setting module were added to the DSR high-temperature grading test. Initially, the temperature was set at 64°C. After the first measurement module, the temperature was increased to 100°C for the second measurement. If the result passed the AASHTO M 320 specification for high temperature, the temperature was then increased in 6°C increments for subsequent measurements until a failing result was obtained. In contrast, if a failing result was obtained at 100°C, the temperature was then decreased in 6°C increments for subsequent measurements until a passing result was obtained. The results were used to determine the continuous high-temperature grade. The same practice was applied to the intermediate-temperature grading test, with the initial temperature set at 25°C. After the first measurement module, the temperature was increased to 34°C for the second measurement. Depending on the pass or fail results, the temperature was then decreased or increased in 3°C increments for subsequent measurements until a fail or pass result was obtained. The results were used to determine the continuous intermediate-temperature grade.

AASHTO M 320 (2023) requires that $|G^*| \times \sin(\delta)$ is less than or equal to 6,000 kPa at 25°C for NC's climatic grade of PG 64-22. AASHTO M 320 (2023) and NCDOT specifications (2024) also require that δ must be greater than or equal to 42° when $|G^*| \times \sin(\delta)$ falls between 5,000 kPa and 6,000 kPa at this temperature. To evaluate the potential implications of the δ requirement, the blended binder δ values were estimated using Equation ((3.1)) at 25°C. None of the estimated δ values that fell below the minimum limit despite some $|G^*| \times \sin(\delta)$ values exceeding 5,000 kPa and thus, it is inferred that the $|G^*| \times \sin(\delta)$ rather than the δ criterion is most restrictive. In addition, conversations with the NCDOT Materials and Tests personnel indicate no binders have been rejected for failing the δ requirement. Consequently, the 6,000 kPa limit for $|G^*| \times \sin(\delta)$ was used as the basis for calculating continuous grading intermediate-temperatures.

$$\delta_{\text{Blend}} = RBR_{\text{RAP}} \times \delta_{\text{RAP}} + (1 - RBR_{\text{RAP}}) \times \delta_{\text{Virgin}} \tag{3.1}$$

where:

δ_{Blend} = δ of the blend of RAP and virgin binder,

$\delta_{RAP} = \delta$ of the RAP binder,

$\delta_{Virgin} = \delta$ of the virgin binder.

Original binder testing of the RAP binder was avoided to ensure any residual solvent from the recovery was fully removed, which was confirmed following RTFO aging via Fourier Transform Infrared Spectroscopy (FTIR). The results were analyzed to obtain $|G^*|/\sin(\delta)$ and $|G^*|\times\sin(\delta)$ at the critical high- and intermediate-temperatures, respectively (*24*). Two replicate tests were initially conducted. If the results met the repeatability requirements in AASHTO T 315 (*23*), testing ceased. If the requirement was not met, additional replicates test was conducted until the requirement was satisfied.

Bending beam rheometer (BBR) testing was performed for low-temperature characterization in accordance with AASHTO T 313. RAP binders were tested at the RTFO age condition as specified in Appendix X2 of AASHTO M 323. The testing temperature of -12°C was selected to match North Carolina's critical climate temperature. Testing was also conducted at -6°C and the results were used to calculate the continuous grading temperature according to ASTM D7643. All BBR tests were conducted by the NCDOT's Materials and Tests Unit.

Figure 3-1 to Figure 3-3 present continuous high grading temperatures (HPG), intermediate grading temperatures (IPG), and low grading temperatures (LPG) values of the study RAP binders. Figure 3-1 shows the continuous HPG of RAP binders. The RAP HPG values span from 94.2°C to 109.2°C. Figure 3-2 displays the continuous IPG values, which shows a span from 30.5°C to 43.9°C. Figure 3-3 presents the continuous LPG values, revealing a span from -8.8°C to -20.4°C. Notably, RAP binder sample L cracked immediately when a load was applied to the sample during the BBR testing at -12°C because of the high brittleness. Thus, the LPG of RAP binder L is not available in this study.

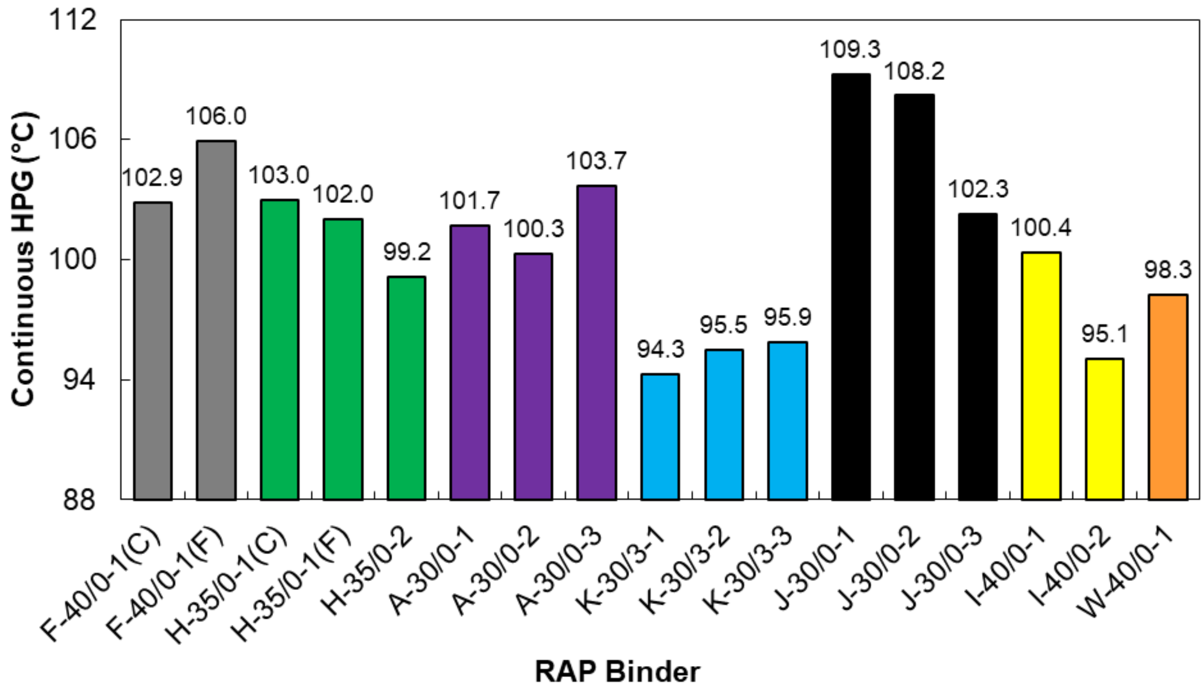

Figure 3-1. Continuous HPG of RAP binders.

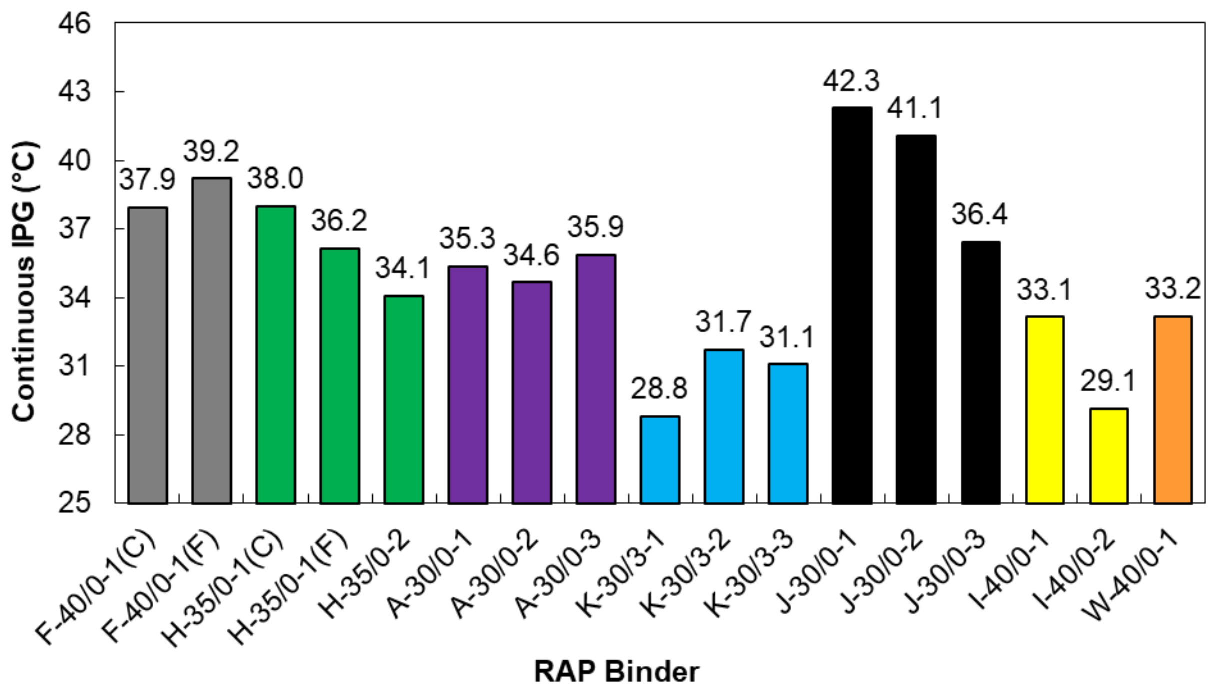

Figure 3-2. Continuous IPG of RAP binders.

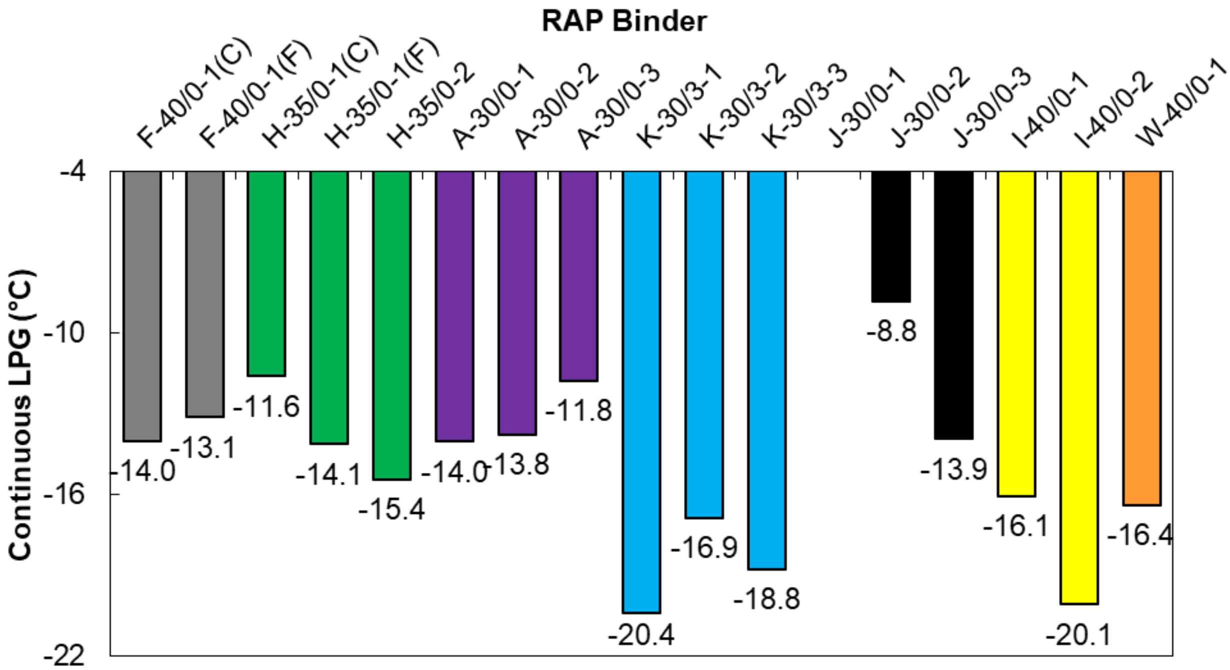

Figure 3-3. Continuous LPG of RAP binders.

3.3.3. Blended Binder Analysis

Blending charts equations were used to virtually blend RAP binders with virgin binders to generate all possible combinations of blended binder properties at a given RBR level for a given virgin binder PG. This analysis yielded over 12,000 simulated binder blends, which would not be feasible to evaluate through direct experimentation. Such analysis approach was chosen because the distributions of virgin and/or RAP binder value for a given parameter failed statistical tests for normality in all cases, which precluded generating distributions of blended binder properties analytically from the distributions of virgin and recycled binder properties. Therefore, all possible combinations were chosen to virtually generate the distributions of blended binder properties. High- and intermediate-temperature blended binder parameters $|G^*|/\sin(\delta)$ and $|G^*|\times\sin(\delta)$, along with the low temperature stiffness parameter $S(60)$, were calculated using Equation(3.2). The blended binder parameter $m(60)$ was calculated using Equation (3.3). These equations were selected based on the blending charts prescribed in AASHTO M 323, which suggest a linear relationship between blended binder continuous grading temperatures and RBR combined with the relationships between the PG parameters and temperature suggested by ASTM D7643. ASTM D7643 indicates linear relationships between the logarithm of each PG parameter and temperature, with the exception of $m(60)$, which is assumed to vary linearly with temperature.

$$\log(P_{\text{Blend}}) = RBR_{\text{RAP}} \times \log(P_{\text{RAP}}) + (1 - RBR_{\text{RAP}}) \times \log(P_{\text{Virgin}}) \tag{3.2}$$

where:

P_{Blend} = property of the blend of RAP and virgin binder,

RBR_{RAP} = RAP binder recycled binder ratio, equal to the weight of RAP binder in the mix divided by total binder weight in the mix,

P_{RAP} = property of the RAP binder,

P_{Virgin} = property of the virgin binder.

$$m(60)_{\text{Blend}} = RBR_{\text{RAP}} \times m(60)_{\text{RAP}} + (1 - RBR_{\text{RAP}}) \times m(60)_{\text{Virgin}} \tag{3.3}$$

where:

$m(60)_{\text{Blend}}$ = the absolute value of the slope of the logarithm of stiffness curves versus the logarithm of time for the blend,

$m(60)_{\text{RAP}}$ = the absolute value of the slope of the logarithm of stiffness curves versus the logarithm of time for the RAP binder,

$m(60)_{\text{Virgin}}$ = the absolute value of the slope of the logarithm of stiffness curves versus the logarithm of time for the virgin binder.

The analysis was repeated across a range of RBR levels to critically assess existing thresholds and identify alternative limits that would minimize the likelihood of blended binder systems failing to meet specification requirements. For each RBR level, histograms of performance indices were generated like the example shown in Figure 3-4 and compared against standard specification thresholds to determine the percentage of blended binders meeting the required criteria. The PG 64-22 binder data set was used as a benchmark to compare the recycled binder blends against. PG 64-22 is the climatic grade specified in North Carolina for virgin mixtures. As such, it serves as a reference for the target performance properties that the recycled binder blends should achieve.

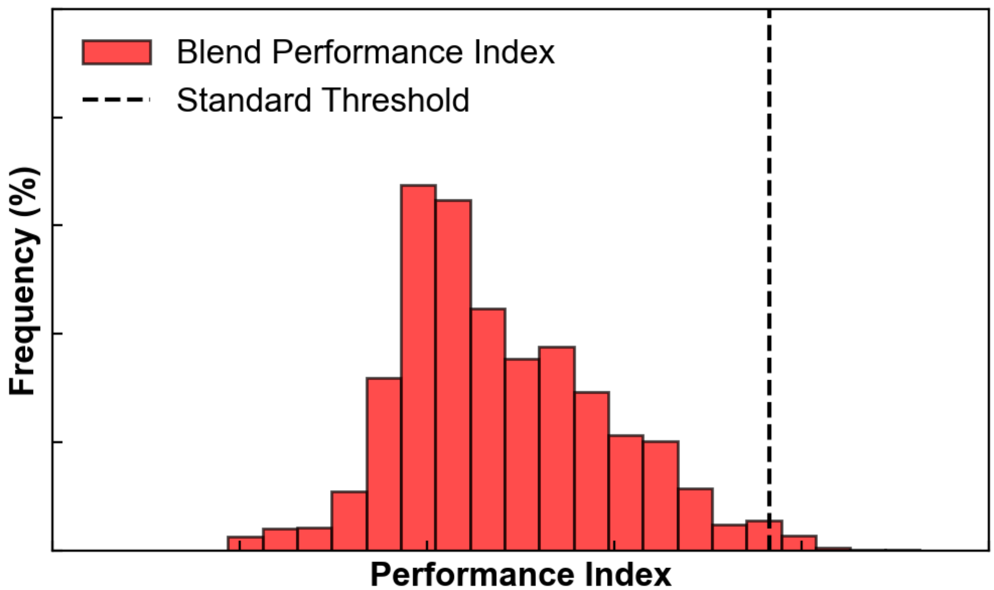

Figure 3-4. Example of distribution analysis.

Studies have noted the blending chart equations in Appendix X2 of AASHTO M 323 can be inaccurate, especially at high RBR levels (*12*). Therefore, the accuracy of the blending charts equations used was verified for select blends evaluated in this study. Six RAP binders encompassing the range of continuous high grading temperatures of the study materials were physically blended with virgin binders in the laboratory at different RBR levels as shown in Table 3-3. The blended binders were aged using RTFO and PAV procedures and the high- and intermediate-temperature PG properties were evaluated using the DSR, respectively. The results were compared to the values predicted using Equation (3.2). Figure 3-5 shows the results, which yield an R^2 value of 0.99 relative to the line of equality. The data is centered along the line of equality indicating no apparent bias. The average percent error was 8% for the high-temperature property and 3% for the intermediate-temperature property on a log scale.

Table 3-3. Virgin and RAP binders blended at different RBR levels.

Virgin Binder	RBR	RAP HPG (ºC)
PG 64-22	0.2	109.3
		95.5
PG 58-28	0.3	94.5
		95.5
	0.4	94.3
		108.2

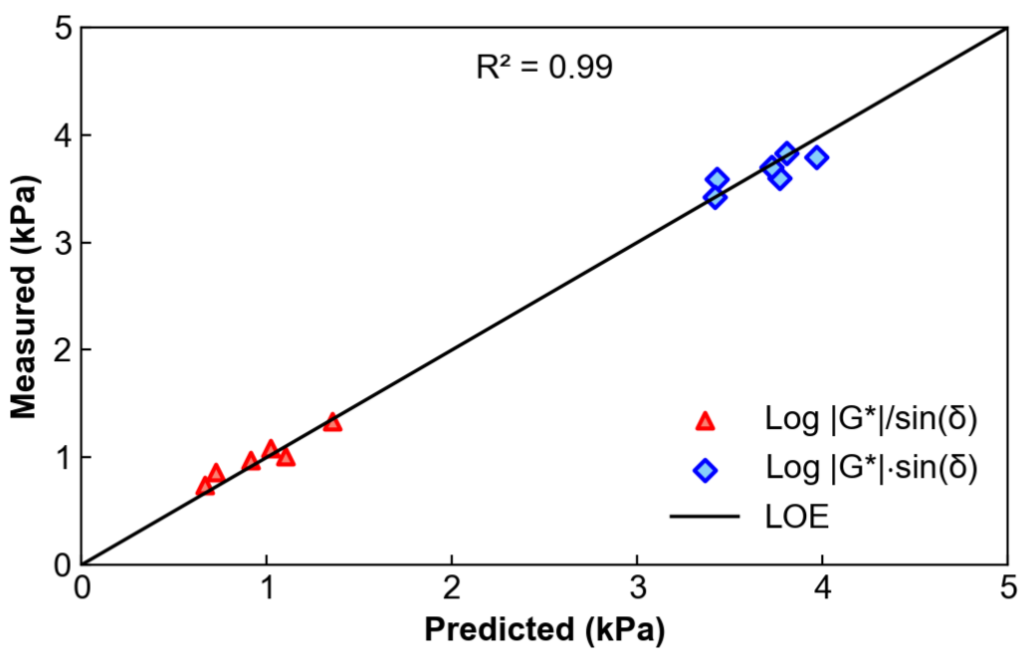

Figure 3-5. Comparison of blending chart predictions and measured values.

3.4. Results

3.4.1. Distributions of Virgin and RAP Binder Properties

Figure 3-6 to Figure 3-10 present histograms of the PG parameters for the virgin and RAP binders. Figure 3-6 shows the histograms of log $|G^*|/\sin(\delta)$ at 64°C for PG 64-22 and PG 58-28 virgin binders. When compared against the AASHTO M 320 requirement, that $|G^*|/\sin(\delta)$ is at least 2.2 kPa at the RTFO age level, it is evident that all PG 64-22 virgin binders satisfy the specification. In contrast, most PG 58-28 binders fall below the threshold with only two samples exceeding it. This outcome is expected because PG 58-28 binders are not designed to meet the specification at 64°C.

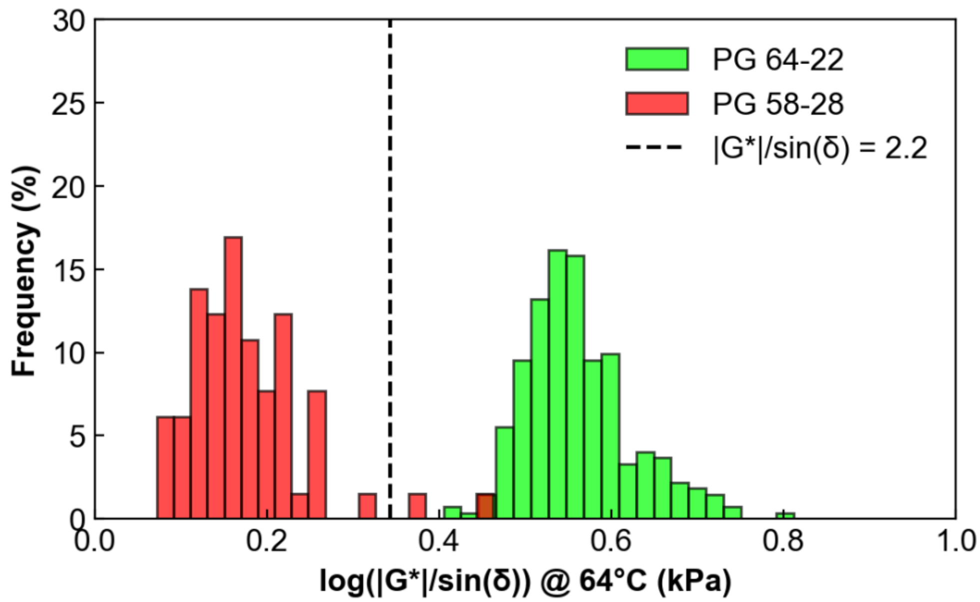

Figure 3-6. Distribution of log ($|G^*|/\sin(\delta)$) for virgin binders PG 64-22 and PG 58-28 at 64°C.

Figure 3-7 presents the histograms of log $|G^*|\times\sin(\delta)$ at 25°C for the same set of virgin binders. All virgin binders satisfy the AASHTO M 320 specification that $|G^*|\times\sin(\delta)$ must not exceed 6,000 kPa at 25°C. AASHTO M320 and NCDOT specifications require that the phase angle δ must be equal to or above 42° when $|G^*|\times\sin(\delta)$ falls between 5,000 kPa and 6,000 kPa. However, the phase angle δ information was not reported in the NCDOT QA database, and thus, this additional requirement could not be evaluated for the two binders that fall within this range. Most virgin binders had values well below 5,000 kPa, with only two PG 64-22 binders falling between 5,000 kPa and 6,000 kPa.

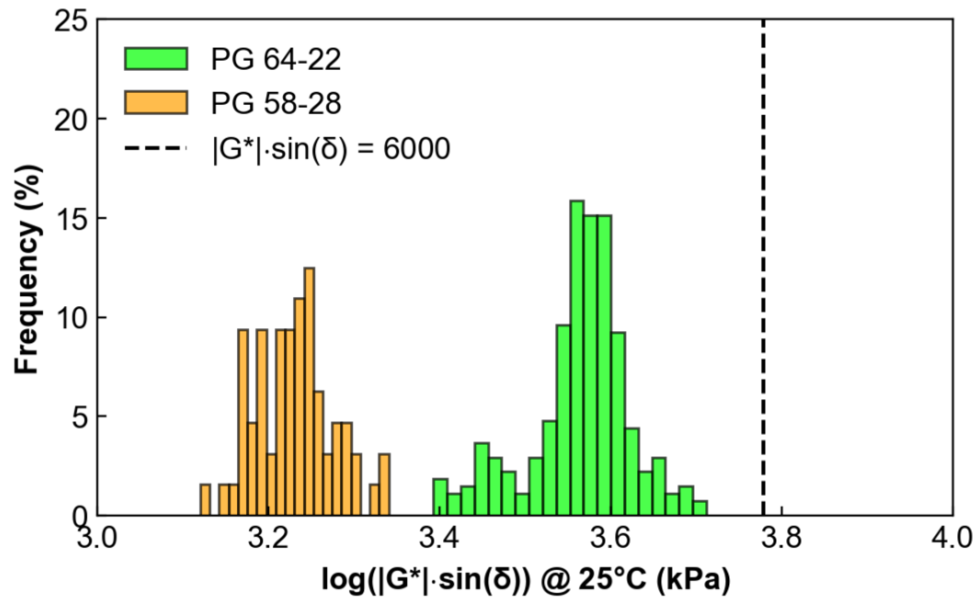

Figure 3-7. Distribution of log (|G^*|×sin(δ)) for virgin binders PG 64-22 and PG 58-28 at 25°C.

Figure 3-8 displays histograms of the low-temperature properties at -12°C. As QA data was unavailable at -12°C for the PG 58-28 virgin binders, only PG 64-22 binder results are presented. Figure 3-8(a) displays the distribution of log *S*(60) values, evaluated against the AASHTO M 320 threshold requiring that *S*(60) is less than or equal to 300 MPa. All PG 64-22 virgin binders meet this threshold. Figure 3-8(b) presents the corresponding distribution of *m*(60) values compared to the AASHTO M 320 threshold requiring that the *m*(60) is greater than or equal to 0.3. All PG 64-22 virgin binders meet this specification.

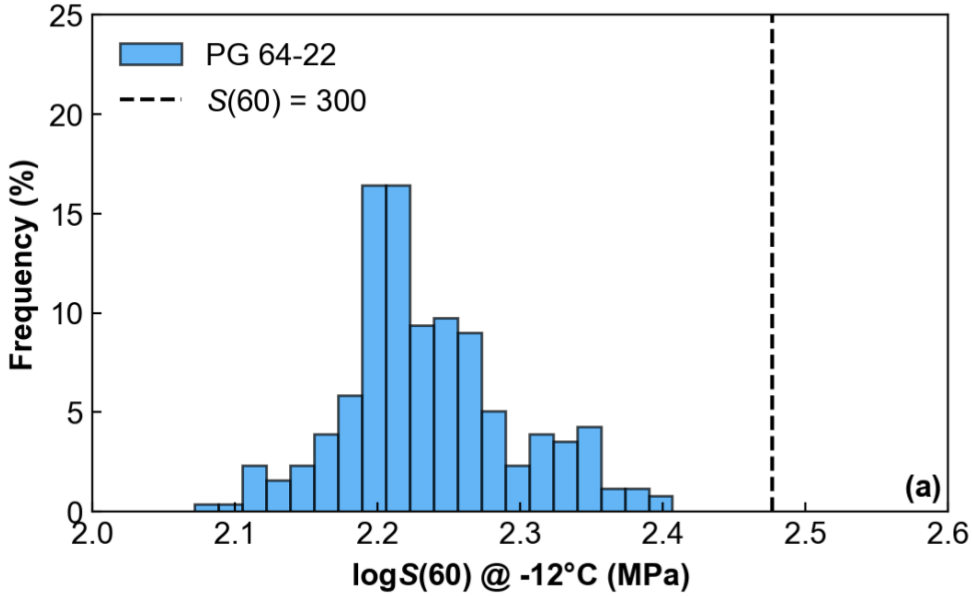

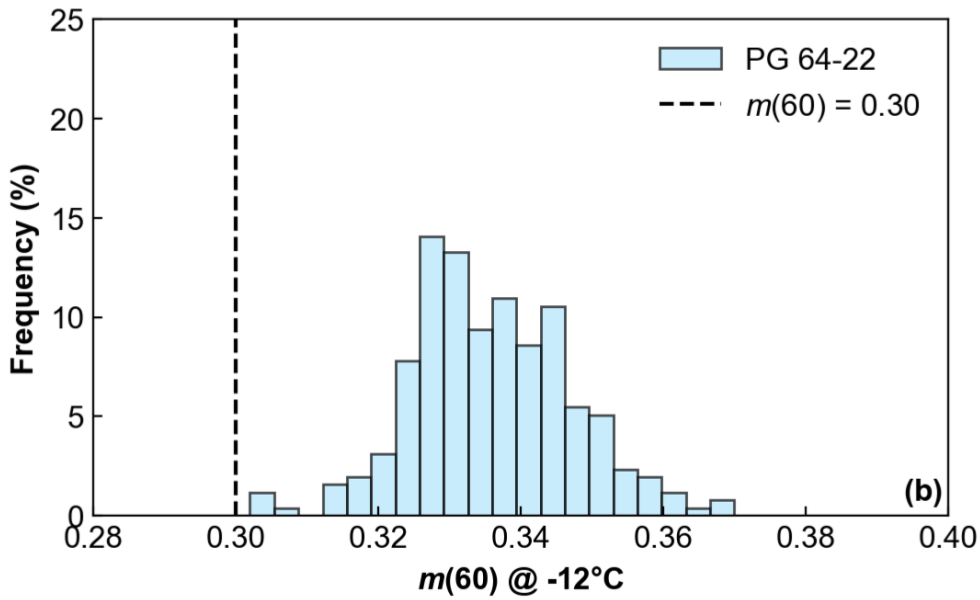

Figure 3-8. Distribution of low-temperature properties from BBR test at -12°C for virgin binder PG 64-22: (a) log S(60), (b) m(60).

Figure 3-9 shows the histogram of log $|G^*|/\sin(\delta)$ at 64°C for the RAP binders. The logarithm of the 2.2 kPa minimum limit specified by AASHTO M 320 is approximately 0.34. Thus, the entire distribution of RAP binder properties greatly exceeds the specification, matching expectations since RAP binders are generally highly oxidized and exhibit high stiffness.

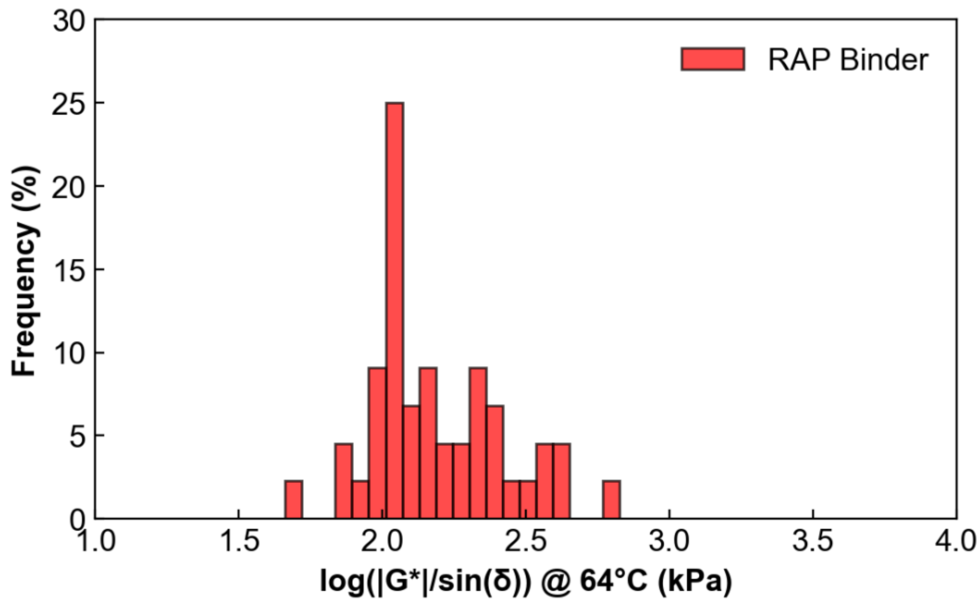

Figure 3-9. Histogram of log (|G*|/sin(δ)) for RAP binders at 64°C.

Figure 3-10 presents the histogram of log |G*|×sin(δ) at 25°C for the RAP binders. The entire distribution exceeds the maximum limit of 6,000 kPa specified by AASHTO M 320 due to high stiffness of the RAP binders, indicating poor cracking susceptibility.

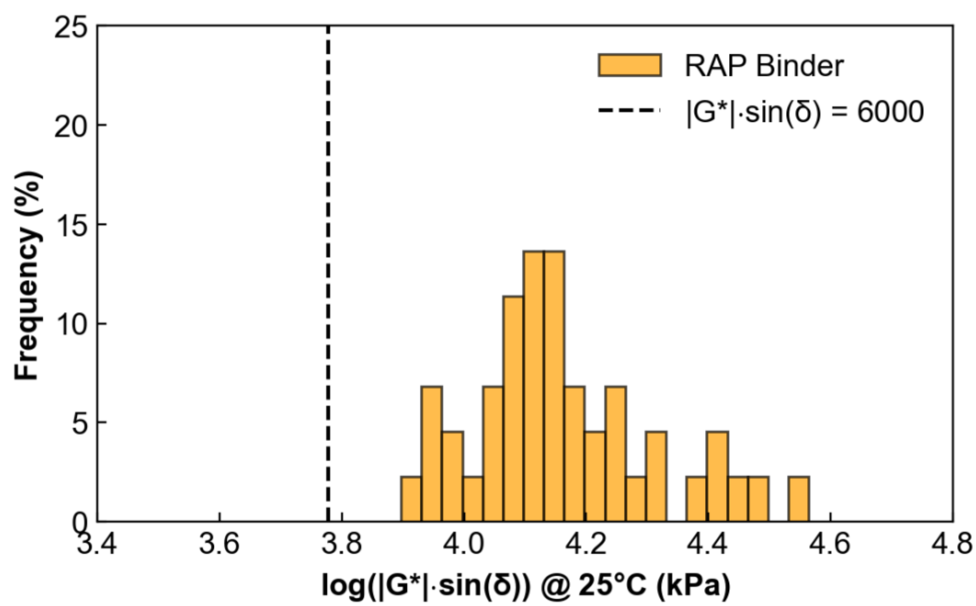

Figure 3-10. Histogram of log (|G*|×sin(δ)) for RAP binders at 25°C.

Figure 3-11 presents the histograms of the low temperature properties at -12°C of RAP binders. The distribution of low-temperature properties is more sparse than the intermediate- and high-temperature properties given that BBR testing at -12°C was conducted only on the 17 RAP binders tested in this study, of which only 16 RAP binder results are available as mentioned previously. Two RAP binders meet the AASHTO M 320 low-temperature specification criteria requiring that *S*(60) falls at or below 300 MPa. None of the RAP binders meet the criteria requiring that *m*(60) is equal to or greater than 0.30. Overall, none of the RAP binders satisfy both low-temperature specification criteria.

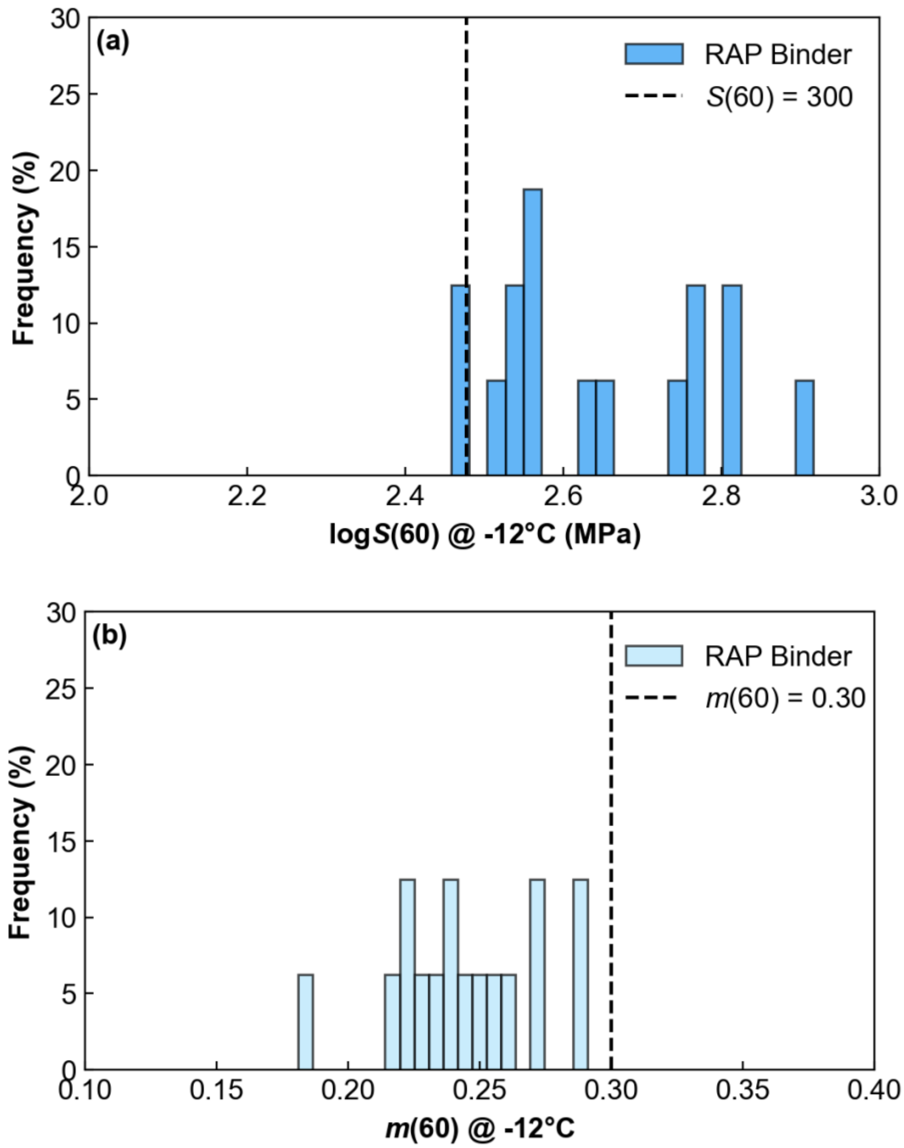

Figure 3-11. Distribution of low-temperature properties from BBR test for RAP binders at -12°C: (a) log *S*(60), (b) *m*(60).

Analytical solutions are available for deriving the distribution of a functional combination of two normally distributed variables (*25*). Thus, if the distributions of a given property for both the virgin and RAP binders are normally distributed, the distribution of the blended binder property at a given RBR level can be analytically derived using the blending chart equations. The normality of the RAP and virgin binder property distributions was assessed using the Shapiro-Wilk test to inform the appropriate methodology for generating the distribution of blended binder properties. Table 3-4 shows p-values from Shapiro-Wilk (*26*) tests assessing the normality of each virgin and RAP binder parameter distribution. The null hypothesis for the Shapiro-Wilk test is that the data are normal distributed. Thus, higher p-values indicate a higher likelihood that the data follow a normal distribution. At a significance level of 0.05, the null hypothesis is rejected when the p-value is less than or equal to 0.05, indicating the data deviates from a normal distribution.

Table 3-4 shows the p-value results of the Shapiro-Wilk tests. The results show that the distribution of RAP $|G^*|/\sin(\delta)$, PG 58-28 $|G^*|\times\sin(\delta)$, RAP $|G^*|\times\sin(\delta)$, and PG 64-22 $m(60)$ have p-values greater than 0.05. However, despite the p-value exceeding the threshold, the distribution of RAP $|G^*|/\sin(\delta)$ presented in Figure 3-9 displays a sharp, narrow peak around 2.0 with an asymmetric shape, suggesting a visual deviation from normality. PG 58-28 $|G^*|\times\sin(\delta)$, RAP $|G^*|\times\sin(\delta)$, and PG 64-22 $m(60)$ distributions are normal based on the p-values shown in Table 3-4. However, there are no cases where the distributions of both RAP and virgin binders for a given parameter are normally distributed, which would allow them to be combined analytically. Therefore, all possible combinations of RAP and virgin binder blends were evaluated through blending charts to generate the probability distributions of blended binder properties.

Table 3-4. p-values from Shapiro-Wilk normality tests.

Performance	p-value
PG 64-22 $G^*/\sin(\delta)$	0.0000
PG 58-28 $G^*/\sin(\delta)$	0.0000
RAP $G^*/\sin(\delta)$	0.0922
PG 64-22 $G^*\sin(\delta)$	0.0000
PG 58-28 $G^*\sin(\delta)$	0.8239
RAP $G^*\sin(\delta)$	0.0566
PG 64-22 log $S(60)$	0.0003
PG 64-22 $m(60)$	0.0991

3.4.2. Evaluation of Blends of PG 64-22 Virgin Binder and RAP

Table 3-2 shows that the NCDOT specifies the use of PG 64-22 virgin binder when RBR is less than or equal to 0.3 for the mixture designations under consideration herein. To evaluate the effectiveness of this threshold and explore alternatives that may reduce the risk of failing AASHTO M 320 intermediate and low temperature specifications, the distribution of blended binder (i.e., RAP + PG 64-22 virgin binder) properties was assessed at RBR levels of 0.2 and 0.3, with PG 64-22 virgin binder included as a benchmark. Figure 3-12 presents the corresponding histograms of $|G^*|\times\sin(\delta)$ for these blends along with PG 64-22 virgin binders. As the RBR increases, the histograms shift to the right, confirming that RAP binders increase the blended binder $|G^*|\times\sin(\delta)$. AASHTO M 320 requires that $|G^*|\times\sin(\delta)$ is less than or equal to 6,000 kPa. At the current RBR threshold of 0.3, only 74% of the blended binders meet this requirement. In contrast, reducing the RBR to 0.2 increases compliance to 96%, suggesting that a lower RBR threshold for PG 64-22 may better ensure conformance with the intermediate-temperature specification.

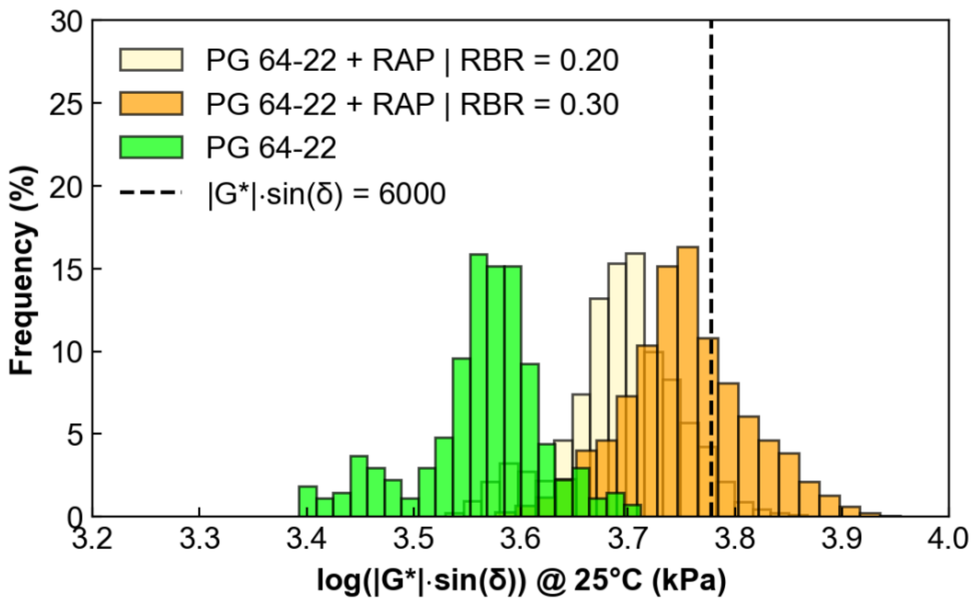

Figure 3-12. Histogram of log ($|G^*|\times\sin(\delta)$) at 25°C for blends of PG 64-22 and RAP at various RBR levels compared to PG 64-22 virgin binder.

Figure 3-13 and Figure 3-14 show the histograms of the *S*(60) and *m*(60) at -12°C for the blended binders at RBR levels of 0.2 and 0.3 alongside PG 64-22 virgin binder as a reference. Figure 3-13 shows that 97% of blends meet the maximum *S*(60) limit of 300 MPa specified by

AASHTO M 320 at the NCDOT's current RBR limit of 0.3. When the RBR is reduced to 0.2, the compliance rate increases to 99%. Figure 3-14 demonstrates that only 76% of blended binders exceed the minimum $m(60)$ requirement of 0.3 at the current RBR limit of 0.3, suggesting that the low-temperature grades of the blends tend to be m-controlled rather than S-controlled. Reducing the RBR to 0.2 improves the pass rate to 95%.

Collectively, the results indicate that reducing the maximum RBR limit for PG 64-22 virgin binder from 0.30 to 0.20 increases the likelihood that blended binders will meet AASHTO M 320 intermediate- and low-temperature specifications to approximately 96%, thereby reducing the probability of cracking. However, an important consideration when evaluating this potential change is whether using a softer PG 58-28 at an RBR of 0.20 would negatively impact rutting resistance.

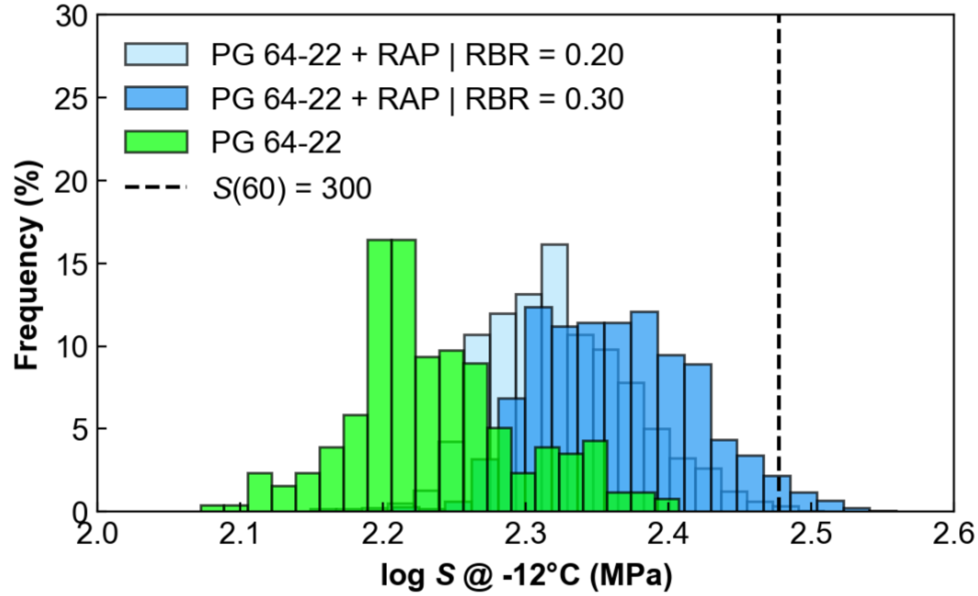

Figure 3-13. Histogram of log *S*(60) at -12°C for blends of PG 64-22 and RAP at various RBR levels compared to PG 64-22 virgin binder.

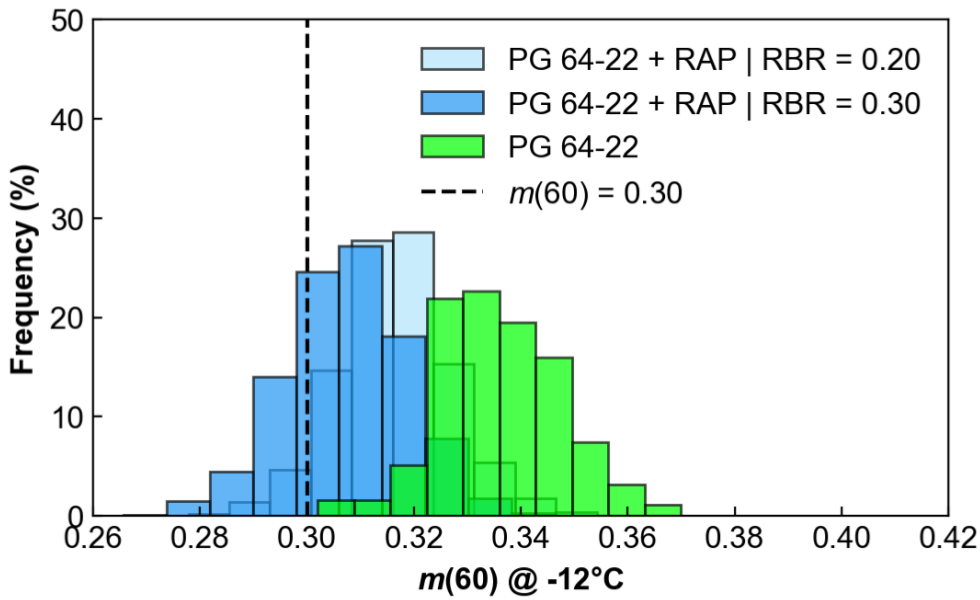

Figure 3-14. Histogram of *m*(60) at -12°C for blends of PG 64-22 and RAP at various RBR levels compared to PG 64-22 virgin binder.

3.4.3. Evaluation of Blends of PG 58-28 Virgin Binder and RAP

NCDOT specifies the use of PG 58-28 virgin binder when the RBR exceeds 0.30, with maximum allowable RBRs of 0.40 for surface layers and 0.45 for intermediate and base layers. To evaluate the effectiveness of these thresholds and to explore the potential impact of lowering the minimum RBR at which PG 58-28 is used to 0.2, the properties of blended binders (i.e., RAP + PG 58-28 virgin binder) were assessed. These blended binder properties were benchmarked against those of PG 64-22 virgin binders and the criteria specified in AASHTO M 320.

Figure 3-15 shows histograms of $|G^*|/\sin(\delta)$ at 64°C for blends of RAP and PG 58-28 at RBR levels of 0.2 and 0.3 along with PG 64-22 virgin binders. The results reveal that that 100% of blended binders exceed the minimum limit specified by AASHTO M 320 at both 0.2 and 0.3 RBR levels. Therefore, reducing the minimum RBR where PG 58-28 virgin binder is used to 0.2 maintains adequate rutting resistance. Moreover, at an RBR of 0.2, the blended binder distribution becomes very similar to that of PG 64-22 virgin binders.

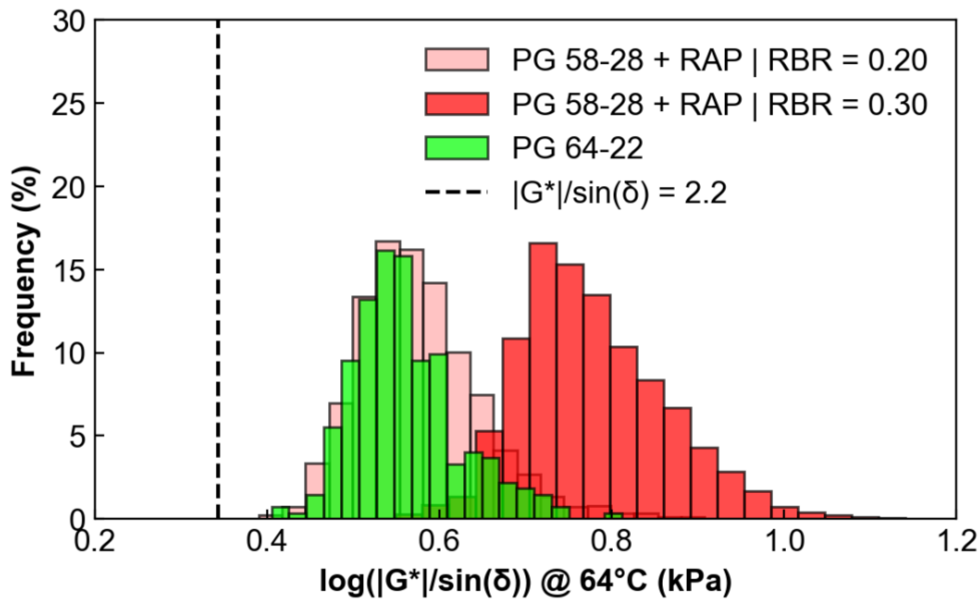

Figure 3-15. Histogram of log ($|G^*|/\sin(\delta)$) at 64°C for blends of PG 58-28 and RAP at various RBR levels compared to PG 64-22 virgin binder.

The maximum RBR limits for using PG 58-28 virgin binder are 0.4 for surface layers and 0.45 for intermediate and base layers. To evaluate the effectiveness of these limits, the distribution of $|G^*|\times\sin(\delta)$ at 25°C for blended binders containing PG 58-28 at these RBR levels along with 0.2 were evaluated. These distributions were compared to PG 64-22 virgin binders and the AASHTO M 320 specification limit. Figure 3-16 shows the corresponding histograms. At an RBR level of 0.45, 93% of blended binders fall below the maximum $|G^*|\times\sin(\delta)$ limit of 6,000 kPa. This compliance rate increases to 99% when the RBR is reduced to 0.4, indicating the current maximum RBR limits yield a high probability of compliance with the intermediate-temperature binder specifications. At an RBR of 0.2, the distribution of blended binder properties shifts to the left, indicating these blends are softer than PG 64-22 virgin binder.

Interestingly, the distribution $|G^*|\times\sin(\delta)$ at 25°C values for blended binders at an RBR of 0.4 is similar to that of PG 64-22 virgin binders. This finding contrasts with the results for $|G^*|/\sin(\delta)$ at 64°C where the blended binder properties most closely aligned with PG 64-22 virgin binder at an RBR of 0.2.

Unfortunately, the effectiveness of the maximum RBR limits in ensuring compliance with low temperature properties could not be fully evaluated, as QA data for PG 58-28 binders was only available at –18°C.

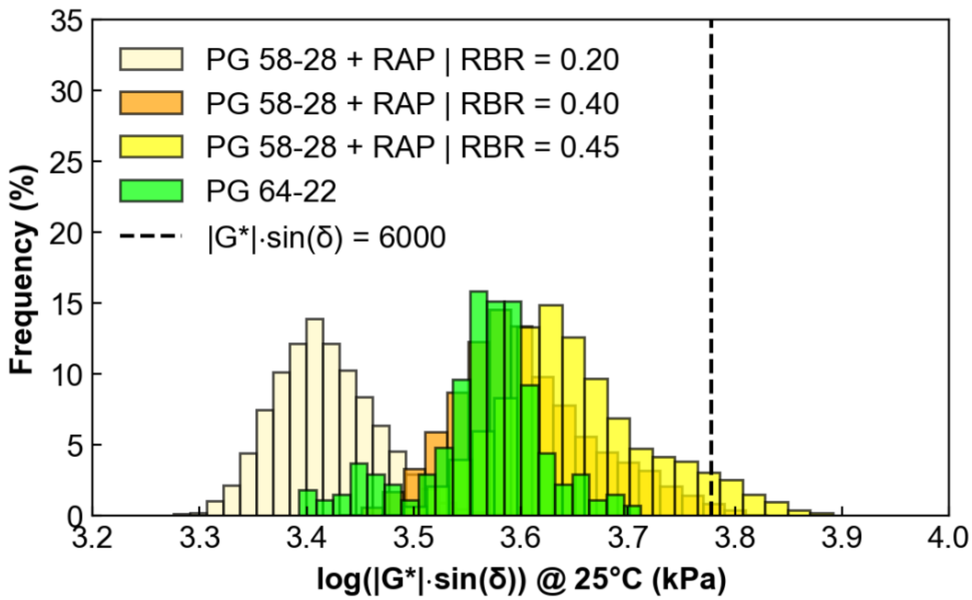

Figure 3-16. Histogram of log ($|G^*|\times\sin(\delta)$) at 25°C for blends of PG 58-28 and RAP at various RBR levels compared to PG 64-22 virgin binder.

3.4.4. Probabilistic Approach to Select RBR Limits

This section presents a probabilistic approach to inform the selection of RBR limits. The properties of all possible combinations of virgin and RAP binder blends were calculated using fine increments of RBR. At each RBR level, the percentage of blends with a given virgin binder PG that met the AASHTO M 320 specification criteria was determined. These results were used to generate plots showing the percentage of blends meeting a given specification requirement as a function of RBR. Such plots, when paired with an agency's target probability for compliance, can be used to select an RBR threshold. For demonstration purposes herein, a 90% compliance probability was selected as a benchmark for identifying potential RBR limits.

Figure 3-17 shows the relationship between the percentage of blends meeting the intermediate-temperature specification for $|G^*|\times\sin(\delta)$ and RBR. The vertical arrows indicate the RBR levels at which 90% of the blends meet the specification. The results show that achieving at least 90% compliance with intermediate-temperature thresholds requires limiting the RBR to 0.24 for PG 64-22 virgin binder and 0.47 for PG 58-28 virgin binder. It is noted that the 0.47 limit closely aligns with NCDOT's current maximum RBR limit of 0.45 for using PG 58-28 in intermediate and base layers. However, the analysis suggests a 0.24 limit for PG 64-22 binders, which is notably lower than NCDOT's current limit of 0.30.

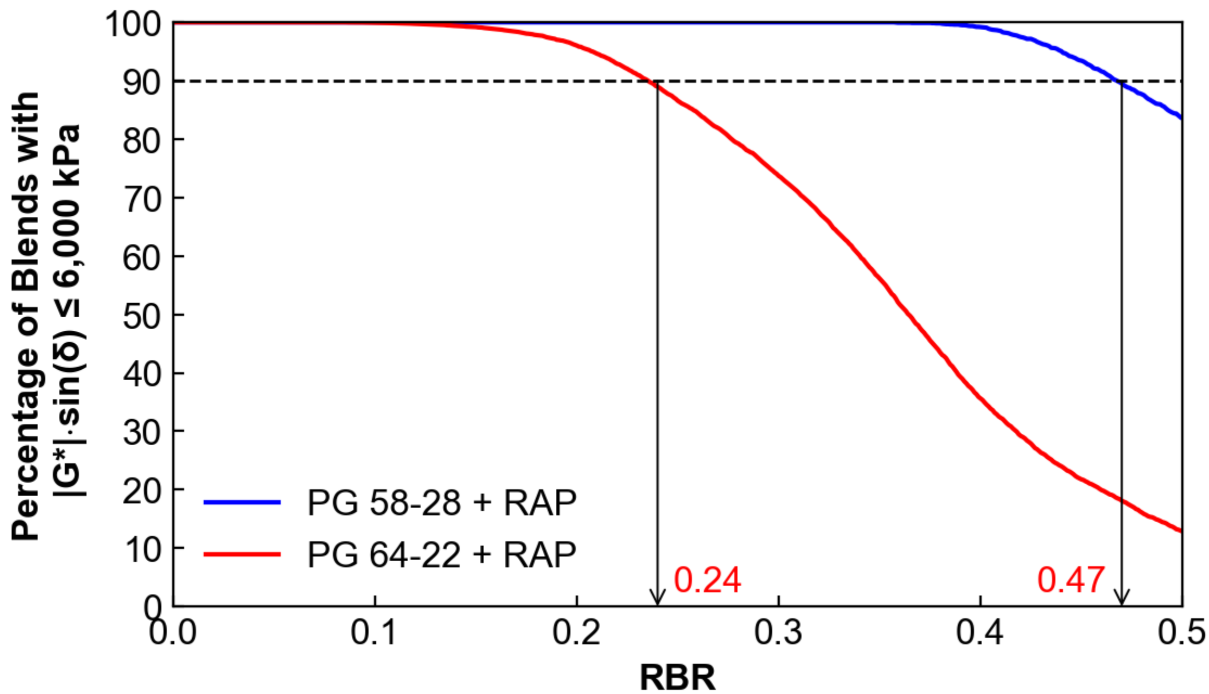

Figure 3-17. Selecting RBR limits to achieve a 90% probability of meeting the $|G^*|\times\sin(\delta)$ specification.

Figure 3-18 presents the relationship between the percentage of blends meeting the high-temperature specification for $|G^*|/\sin(\delta)$. Since the PG 64-22 virgin binders exceed the minimum $|G^*|/\sin(\delta)$ and adding RAP increases the value further, high temperature requirements meet at all RBR levels for this virgin binder grade. For blends with PG 58-28, 90% of the blends meet the minimum limit for $|G^*|/\sin(\delta)$ at an RBR of 0.12. At an RBR level of 0.17, all blends of PG 58-28 and RAP meet the intermediate-temperature specification,

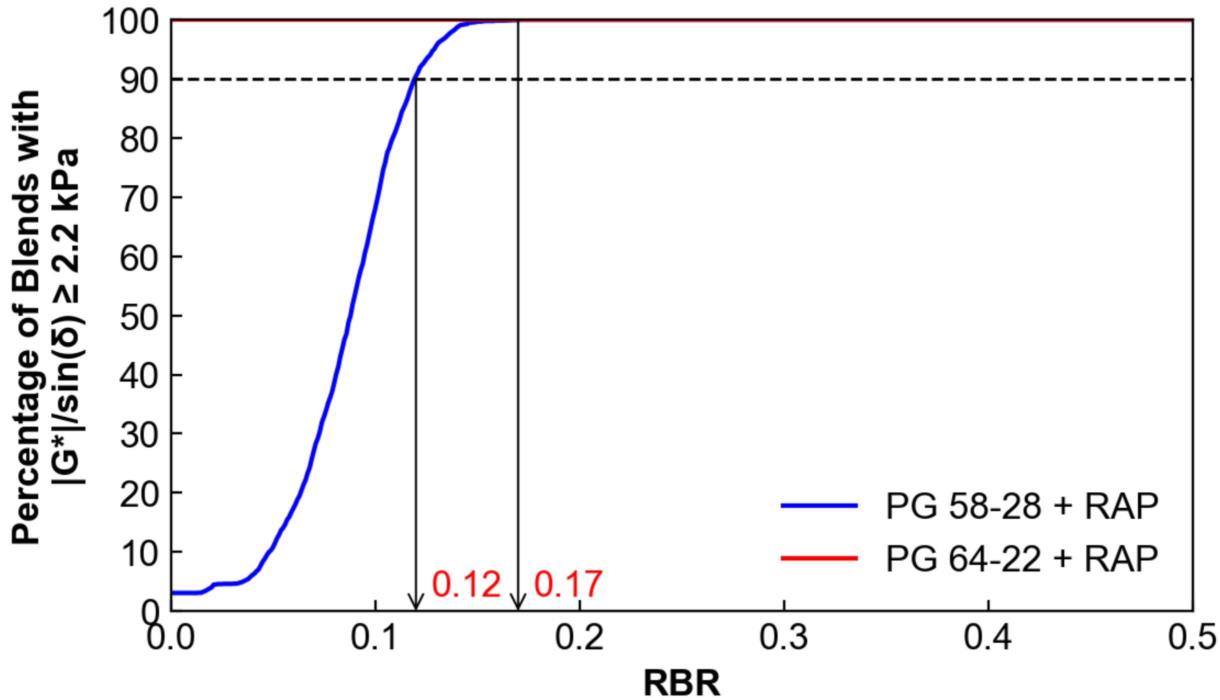

Figure 3-18. Selecting RBR limits to achieve a 90% probability of meeting the |*G|/sin(*δ*) specification.**

Figure 3-19 shows the relationship between the percentage of blends incorporating PG 64-22 virgin binder that meet low-temperature specifications for both *S*(60) and *m*(60), plotted as a function of RBR. To achieve a 90% probability of meeting the specifications, the RBR must be less than 0.38 based on *S*(60) criterion and less than 0.21 based on *m*(60) criterion. These results indicate that the *m*(60) is the controlling specification parameter at low temperature. Furthermore, the results indicate that to achieve a 90% probability of compliance with the *m*(60) specification, the maximum allowable RBR limit for PG 64-22 should be reduced from the current value of 0.30.

Collectively, the example probabilistic analysis presented herein suggests that lowering the RBR threshold for specifying PG 58-28 from 0.30 to 0.20, while maintaining a maximum RBR limit of 0.45, results in an approximate 90% probability of meeting the intended blended binder performance properties.

It is important to note that selecting appropriate RBR limits involves many additional considerations and satisfying asphalt binder specifications alone does not guarantee adequate mixture performance. Nevertheless, the probabilistic approach demonstrated in this section offers a useful framework for leveraging QA data and RAP binder characterization as one component of establishing reliable specifications.

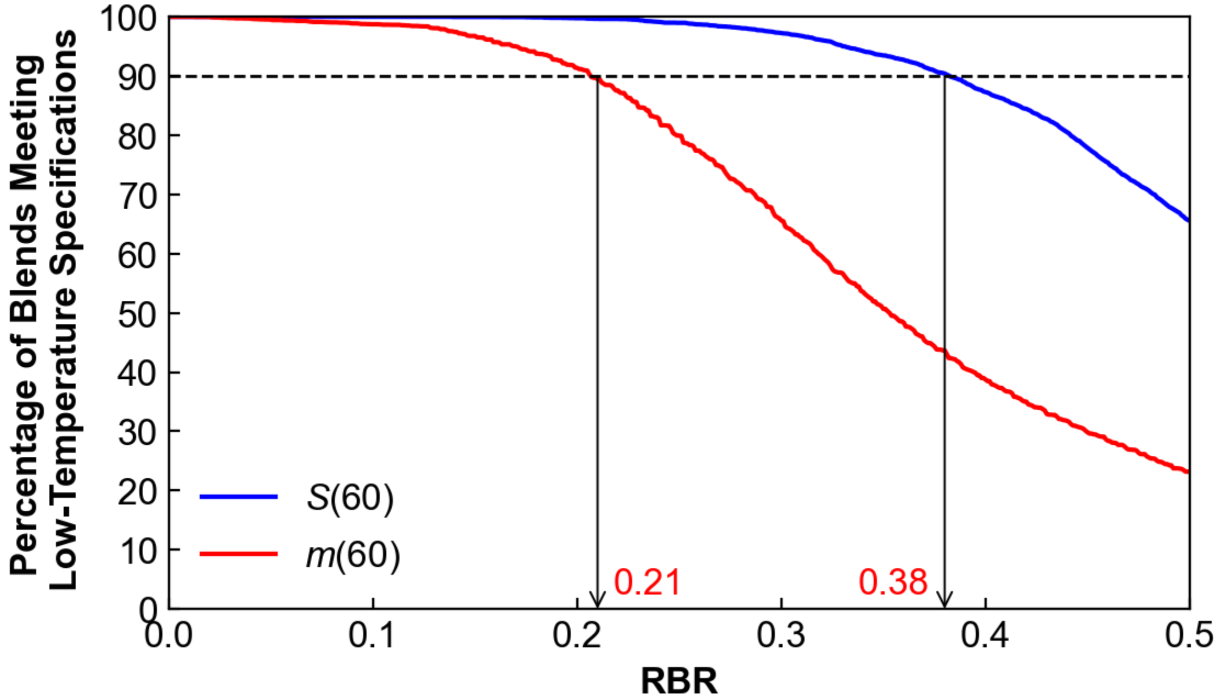

Figure 3-19. Selecting RBR limits to achieve a 90% probability of meeting the low-temperature specifications when PG 64-22 virgin binder is used.

3.5. Conclusions and Recommendations

The probabilistic approach used in this study offers a method for leveraging virgin binder QA data and RAP binder results to assess the probability of meeting targeted blended property requirements as a function of RBR. Applying this method to analyze existing NCDOT RBR thresholds indicates that:

- Lowering the maximum RBR limit for PG 64-22 virgin binder from the permitted 0.30 to 0.20 increased the probability of binder blends meeting intermediate- and low-temperature requirements in AASHTO M 320 to approximately 96% while maintaining compliance with high-temperature requirements.
- NCDOT's maximum RBR limits of 0.40 and 0.45 provide a high (>90%) probability of meeting intermediate-temperature grading requirements.
- Different RBR levels yielded similar blended binder property distributions to PG 64-22 virgin binder at high-temperature (RBR = 0.2) and intermediate-temperature (RBR = 0.4).

- It is suggested that QA data collection is expanded to include low-temperature properties at -12°C for PG 58-28 binders and phase angle at 25°C since these characteristics could not be considered in the present study.
- Future research should incorporate blending chart uncertainty into the probabilistic analysis of blended binder properties.
- Future research should also validate the proposed RBR thresholds using an evaluation of mixture performance to ensure field applicability.

4. Prediction of BBR Properties from DSR Test Results

4.1. Introduction

Low-temperature performance evaluation plays a critical role in the asphalt performance grading system by determining the thermal crack resistance of asphalt binders. The bending beam rheometer (BBR) test currently serves as the standard method for determining these low-temperature properties. However, the BBR test requires significantly more binder than the dynamic shear rheometer (DSR) test, which poses challenges when characterizing RAM binder samples due to the extensive solvent extraction and recovery needed to obtain sufficient binder. Extraction and recovery are time-consuming and requires hazardous, expensive solvents. In contrast, smaller DSR samples are more readily extracted and recovered. Furthermore, the DSR is used for high- and intermediate-temperature performance grading. Thus, eliminating the BBR would streamline the equipment required for performance grading.

Researchers have attempted to use DSR testing to evaluate low-temperature properties of asphalt binders as an alternative to BBR testing. Different geometries, including the torsion bar (*6*), 4 mm parallel plate (*7–9*), and 8 mm parallel plate (*10*), as well as various analytical techniques have been investigated. However, efforts to date have focused on virgin binders and not specifically those from NC. Thus, research is needed to develop an approach for accurately obtaining low-temperature performance graded (PG) properties for both virgin and recycled binders in NC. Herein, the approach proposed by Zeng et al. (*10*) is adopted. This approach uses the 8 mm parallel plate geometry at intermediate temperatures, which is compatible with equipment typically available in asphalt laboratories. Furthermore, among available analytical approaches in the literature, Zeng et al. (*10*)'s approach was selected because it achieved relatively good prediction accuracy among the reviewed studies and used the largest dataset for validation.

4.2. Objectives

The objective of this chapter is to evaluate and improve the accuracy of Zeng et al.'s (*10*) model for obtaining the low-temperature performance graded properties from the DSR for both virgin and RAM binders in NC.

4.3. Methodology

4.3.1. Materials

This study evaluated 29 asphalt binders from across North Carolina, including 12 virgin binders and 17 RAM binders, of which there are 3 RAS binders and 14 RAP binders. The RAP binders and BBR characterization presented in this chapter are consistent with those included in Data Set #2 from the previous chapter. However, the methodology is briefly restated here to ensure this chapter can be read as a standalone study. The RAM materials were collected from seven plants across North Carolina, many sampled at multiple times over the span of 1-2 years. The RAM stockpiles were replenished between each sampling. The virgin binders correspond to those used in combination with these RAM materials at the source asphalt plants. The RAM binders were obtained through extraction and recovery of the sampled RAM material. Details on the extraction, recovery, and testing of these samples are provided in the subsequent section. The binder source and PG information are summarized in Table 4-1.

Table 4-1. Summary of the materials.

Binder ID	Binder Type	PG Grade
F1	Virgin Binder	58-28
H2		64-22
A1		64-22
A2		64-22
A3		64-22
K1		58-28
K2		58-28
J1		64-22
J2		64-22
J3		64-22
W&I1		58-28
I2		58-28
F#1-C	RAP Binder	100-10
H#1-F		100-10
H#1-C		100-10
H#2		94-10
A#1		100-10
A#2		100-10
A#3		100-10
K#1		94-16
K#2		94-16
K#3		94-16
J#3		100-10
I#1		100-16
I#2		94-16
W#1		94-16
K#1-RAS	RAS Binder	NA
K#2-RAS		NA
K#3-RAS		NA

4.3.2. Test Methods

The RAP and RAS binders were extracted using a centrifuge extractor with trichloroethylene (TCE) as the solvent according to Method A of AASHTO T 164 (*20*). The asphalt binder recovery was completed using a rotary evaporator according to ASTM D5404 (*21*). The recovered RAP binders were subjected to RTFO aging according to AASHTO T 240 for characterization (*22*). The RAP binders were not subjected to further aging in the PAV in accordance with Appendix X2 of AASHTO M 323 . The RAS binders were tested after blending with virgin binder using a blend ratio that matched a plant-produced mixture from which the RAS was sourced. Fried et al. suggested avoiding testing RAS alone because the potentially excessive PG of RAS binders can make casting samples and obtaining reliable rheological measurements difficult (*27*). To prepare blends containing RAS, the virgin binder was preheated to 140°C and the RAS binder was preheated to 165°C (*28*). The two binders were then thoroughly blended with a power drill equipped with a paddle attachment. Within the results, the RAS blends are included in the RAM binder data series along with RAP. The virgin binders and blends were conditioned in the RTFO and PAV according to AASHTO R 28 (*29*) to produce short- and long-term aged binder, respectively. No RAS particles persisted after blending and conditioning in the RTFO. Attenuated Total Reflectance (ATR) Fourier Transform Infrared Spectroscopy (FTIR) was performed before testing to ensure that any residual solvent from the recovery was fully removed.

The temperature-frequency sweep (TFS) test and BBR test were conducted for all the prepared binders. The TFS tests were performed in a DSR using the 8 mm parallel plate geometry following the general requirements in AASHTO T 315 (*23*). The test temperatures were 5°C, 20°C, 35°C, and 50°C with test frequencies that ranged from 0.1 Hz to 15 Hz for the virgin and RAS blends. The RAP binder was tested at 10°C rather than 5°C to avoid the potential debonding between the sample surface and the parallel plate. In Zeng et al.'s (*10*) prediction method, only data from 5°C (or 10°C), 20°C, and 35°C were included. The dynamic shear modulus, $|G^*|$, and the phase angle, δ, were measured in the TFS test. Two replicate tests were initially conducted. If the results met the repeatability requirements in AASHTO T 315 (*23*), testing ceased. If the requirement was not met, additional replicates tests were conducted until the requirement was satisfied.

The BBR test was performed for low temperature characterization in accordance with AASHTO T 313. The RAP and RAS binders were tested at -6°C and -12°C, while the virgin binders were tested at -12°C and -18°C. All BBR tests were conducted by the NCDOT's Materials and Tests Unit.

4.3.3. Model Framework

This study used the method developed by Zeng et al. (*10*) to predict the low-temperature BBR properties, creep stiffness at 60 seconds, *S*(60), and the absolute value of the slope of creep stiffness versus time in log space at a loading time of 60 seconds, *m*(60), from DSR tests. Accordingly, initially three data quality and preparation steps were conducted: raw data checking, stiffness extrapolation verification, and $|G^*|$ smoothing. The raw data quality checking ensures that results are smooth and continuous by using Cole-Cole plots and Black Space diagrams (*6*). The stiffness extrapolation check determines whether extrapolation is necessary because the converted highest creep stiffness from the DSR test was smaller than the maximum *S*(60) in the reported BBR test results. To check this, Equation (4.1) is used to estimate *S*(60) and the values are compared to the BBR measurements. If the maximum *S*(60) calculated is smaller than the maximum from the BBR results, it suggests extrapolation is necessary (*10*) but results can still be estimated. In this study, the blends with the three RAS binders required extrapolation because the calculated maximum *S*(60) converted from the DSR test results was around 200 MPa, which was smaller than the BBR threshold of 300 MPa. In addition, J#1 and J#2 RAP binders had a minimum *S*(60) values of 363 MPa and 345 MPa, requiring minor extrapolation. All other binders did not require extrapolation. While these cases where extrapolation are noted, they were analyzed in the same way as the other binders and did not demonstrate larger errors than the remaining binder samples.

$$S(t) = \frac{2(1+v)}{J'(\omega)} \tag{4.1}$$

$$\omega = \frac{2}{\pi t} \tag{4.2}$$

where:

$S(t)$ = creep stiffness,

v = Poisson's ratio,

$J'(\omega)$ = storage shear compliance.

The $|G^*|$ smoothing was achieved by constructing master curves using two steps. First, the time-temperature shift factors for each temperature were determined using the pairwise interpolation method proposed by Fried and Castorena (*27*). This approach relies on linear interpolation of $|G^*|$ versus frequency in log–log space between successive isotherms to identify the frequencies at the two isotherms that yield equivalent $|G^*|$ values. Thus, the method requires that adjacent isotherms have an overlapping span of $|G^*|$ values. These differences in these frequencies define the shift factor between the two isotherms of interest. After calculating the shift factor for each pair of isotherms, the time-temperature shift factors, a_T, are calculated relative to a selected reference temperature.

Subsequently, the E_a parameter in Arrhenius time-temperature shift factor model in Equation (4.3) and 2S2P1D model fitting parameters in Equation (4.4) are optimized simultaneously to minimize the sum of squared errors for storage and loss moduli.

$$\log a_T = \frac{E_a}{2.303R}\left(\frac{1}{273+T} - \frac{1}{273+T_{ref}}\right) \tag{4.3}$$

where:

E_a = the activation energy and a material dependent constant,

R = 8.314 J/(K·mol),

T = temperature,

T_{ref} = the reference temperature.

$$G^*(\omega) = G_e + \frac{G_g - G_e}{1+\delta(i\omega\tau_0)^{-k} + (i\omega\tau_0)^{-h} + (i\omega\beta\tau_0)^{-1}} \tag{4.4}$$

where:

G^* = complex shear modulus,

ω = reduced frequency, equal to the actual frequency multiplied by a_T,

G_g = the glassy modulus, fixed as 10^9 Pa in this study,

G_e = the static modulus,

δ, τ_0, β, k and h = constant coefficients determined by optimization.

The fitting accuracy of this study was evaluated by calculating the mean absolute percentage error (MAPE). The maximum MAPE of $|G^*|$ among all binders evaluated is 4.79% and the maximum MAPE of the phase angle, δ, is 3.05%, indicating good agreement between the measurements and model predictions.

These models smooth the data and enable calculation of properties at any temperature. Since DSR measurements only reach temperatures of 5-10°C, the system uses Arrhenius equation extrapolation to obtain time-temperature shift factors for BBR temperatures using Equation (4.3)

The general definition of the creep stiffness, $S(t)$ is given in Equation (4.5). Thus, translating from the above master curve model to $S(t)$ requires conversion from the unit response function $G^*(\omega)$ to $J(t)$.

$$S(t) = \frac{1}{D(t)} = \frac{2(1+\nu)}{J(t)} \tag{4.5}$$

where:

$D(t)$ = flexural creep compliance,

ν = Poisson's ratio which Zeng et. al assumed equal to 0.5,

$J(t)$ = shear creep compliance.

Two methods are used to convert from the frequency to the time domain and obtain the desired properties, one for $S(60)$ and a second for $m(60)$ determination. An approximate interconversion method is used to obtain $S(60)$ using idealized relaxation and retardation spectra. In contrast, the $m(60)$ is determined through rigorous computation involving retardation spectrum conversion. The respective methods were found to be most accurate by Zeng et al. (*10*).

The rigorous method converts from the frequency to time domain through retardation spectrum conversion following Equation (4.6). The reader is referred to Zeng et al. (*10*) for further details on how the $|G^*|$ master curve is used to arrive at this equation. In summary, G^* is first converted to the complex compliance, J^*, using the Carson transformation. The retardation spectrum is then calculated according to a mathematic transformation and input to (4.6). Then, $J(t)$ is input into Equation (4.5) to calculate $S(t)$ and ultimately $S(60)$. In addition, $S(t)$ is calculated at 8, 15, 30, 60, 120, and 240 seconds and a second order polynomial is fit to the log $S(t)$ versus log t results in accordance to calculate $m(60)$ in accordance with the AASHTO T 313 procedure.

$$J(t) = J_g + \int_{-\infty}^{\infty} L(\tau)(1 - e^{-t/\tau}) d\ln\tau \tag{4.6}$$

where:

J_g = glassy shear compliance,

t = time,

τ = retardation time,

$L(\tau)$ = retardation spectrum.

The approximate conversion method resembles the rigorous method except for $J(t)$ is obtained from $J'(\omega)$ in frequency domain as originally proposed by Christensen and defined in Equation (4.7).

$$J(t) = J'(\omega)\Big|_{\omega=\frac{2}{\pi t}} \tag{4.7}$$

4.3.4. Empirical Calibration

The BBR parameters, $S(60)$ and $m(60)$, were predicted from the DSR results at each test temperature according to Section 4.4.3. To improve the prediction of BBR properties, separate linear regression models were calibrated to relate the measured and predicted values. The goal here was to provide an empirical calibration to improve accuracy.

Initially, linear regression models with interaction terms (i.e., an Analysis of Covariance (ANCOVA)) was developed for $S(60)$ and $m(60)$ using all of the data. This initial regression analysis was used to assess if there was a bias between the relationship between measured and predicted values between the virgin and RAM binders. Equation (4.8) shows the general form of the regression model.

$$Measured = \beta_0 + \beta_1 \times Predicted + \beta_2 \times Group + \beta_3 \times Group \times (Predicted - Mean_{Predicted}) \tag{4.8}$$

where:

$Measured$ = measured parameter value from the BBR test,

$Predicted$ = predicted parameter value from the DSR test,

$Group$ = dataset indicator (Group 1 = virgin binders, assigned a value of 0, Group 2 = RAM binders, assigned a value of 1),

$Mean_{Predicted}$ = mean predicted value among the two groups,

β_0 = intercept for the virgin binder group,

β_1 = slope for the virgin binder group,

β_2 = change in intercept for the RAM binder group,

β_3 = change in slope for the RAM binder group.

Model significance was evaluated at a significance level of $\alpha = 0.05$. A statistically significant β_0 indicates a nonzero intercept, while a significant β_1 confirms the slope parameter is significant. A significant β_2 suggests the intercept differs between the virgin and RAM binder groups, and a significant β_3 indicates a difference in slope between the two groups. equations were fit to relationship between measured and predicted properties.

Subsequently, linear regression equations were calibrated without interaction terms according to the findings of the initial regression analysis (i.e., if the slopes were found to be different between groups, separate slopes were calculated for the virgin and RAM binder groups). To enable both optimization and testing of these empirical calibrations, these regression equations were calibrated using 80% of the study binders. To ensure the verification binders are independent from the calibration binders, the binders sampled only one time from a given plant were selected for verification, which means in the calibration binders there are no binders from the same plants as the verification binders.

4.3.5. Calibrated Model Evaluation

The prediction accuracy of the calibrated models was evaluated by comparing the predicted continuous low grading temperatures (CPG) calculated according to ASTM D7643 (*30*) and ΔT_c calculated according to AASHTO R 118 (*31*) values with those determined from BBR measurements. To determine these parameters, the continuous grading temperatures for $S(60)$ and $m(60)$ are first calculated, termed $T_{c,s}$ and $T_{c,m}$, respectively. $T_{c,s}$ represents the CPG based on $S(60)$ values at two temperatures and is calculated using Equation (4.9). $T_c(m)$ represents the CPG based on $m(60)$ values at two temperatures and is calculated using Equation (4.10). Once these values are obtained, ΔT_c is calculated using Equation (4.11). The final CPG determination follows a conditional criterion based on the ΔT_c sign: when $\Delta T_c > 0$, CPG = $T_{c,s}$; when $\Delta T_c < 0$, CPG = $T_{c,m}$.

$$T_{c,s} = T_x + \left[\frac{(T_x - T_y) \times (\log 300 - \log S_x)}{\log(S_x) - \log(S_y)} \right] - 10 \tag{4.9}$$

where:

- T_x = a lower temperature,
- T_y = a higher temperature,
- S_x = the $S(60)$ at a specific temperature T_x,
- S_y = the $S(60)$ at a specific temperature T_y.

$$T_{c,m} = T_x + \left[\frac{(T_x - T_y) \times (0.300 - m_x)}{m_x - m_y} \right] - 10 \tag{4.10}$$

where:

m_x = the $m(60)$ at a specific temperature T_x,

S_y = the $m(60)$ at a specific temperature T_y.

$$\Delta T_c = T_{c,s} - T_{c,m} \tag{4.11}$$

4.4. Results

4.4.1. Model Prediction without Calibration

This section presents the comparison of DSR-predicted and BBR-measured properties. The DSR-predicted values were calculated without any calibration. Figure 4-1(a) and (b) show the comparison of measured and predicted $S(60)$ and $m(60)$, respectively. A small bias is visually evident between virgin binders and RAM binders when comparing the measured and predicted $S(60)$ values. The virgin binders exhibit closer agreement with the line of equality than the RAM binders. In general, the DSR-predicted $S(60)$ values tend to be higher than the measured values while the $m(60)$ tend to be underestimated. The coefficient of determination (R^2) with respect to the line of equality for $S(60)$ and $m(60)$ is 0.83.

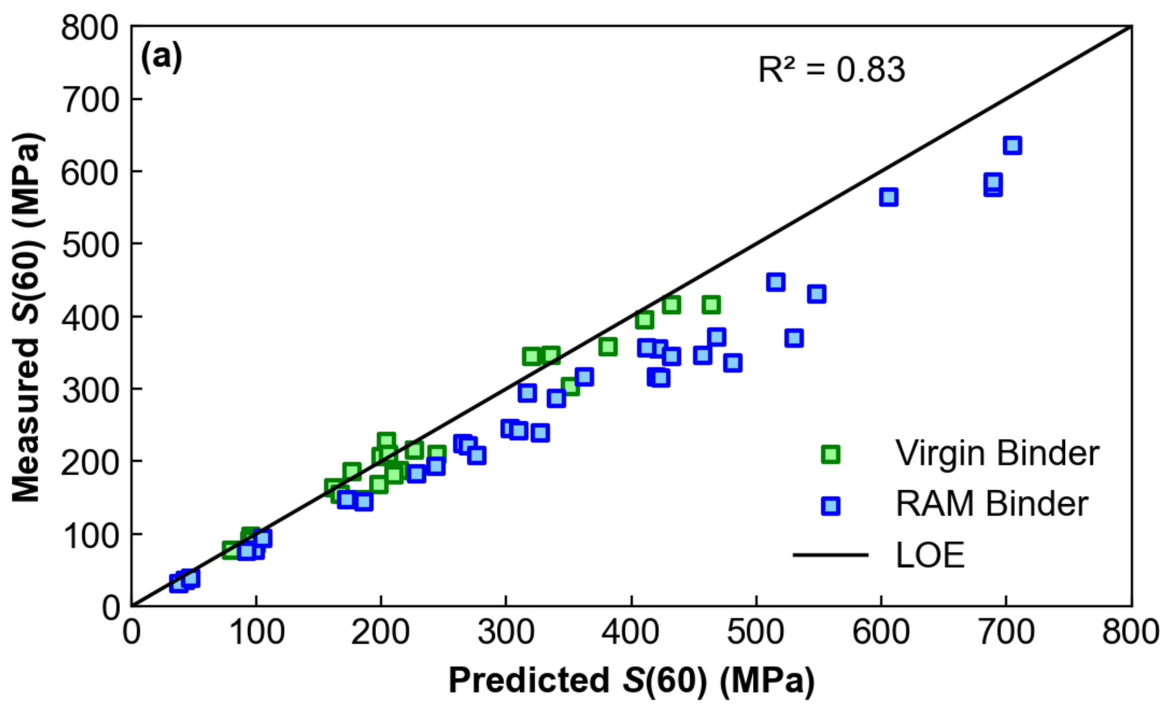

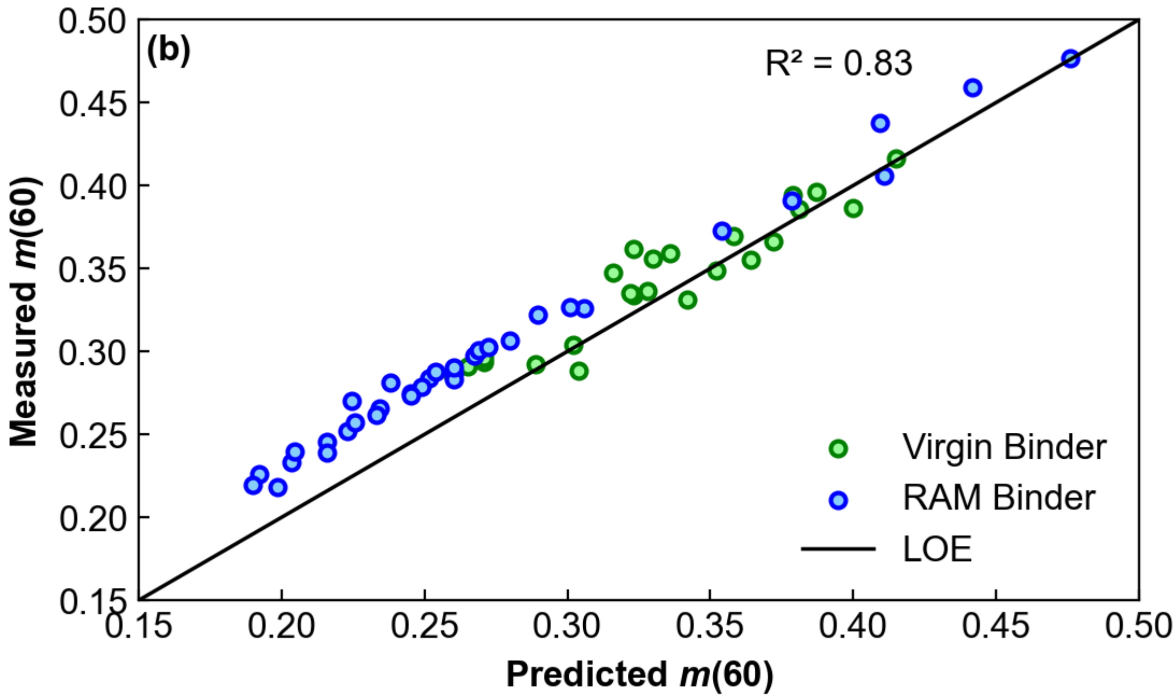

Figure 4-1. Comparison of *S*(60) and *m*(60) from DSR-predicted and BBR-measured: (a) *S*(60), (b) *m*(60).

Figure 4-2 presents the comparison of CPG values calculated based on BBR measurements and DSR predictions without calibration. The results show a bias between the virgin binder and RAM binders. Virgin binders are well aligned along the line of equality, while a bias exists for the RAM binders. However, the overall R^2 with respect to the line of equality is 0.82. The CPGs of the RAM binders were all *m*-controlled (meaning ΔT_c *is* less than zero), whereas only one virgin binder was *m*-controlled, which seems to at least partially explain the observed bias. Interestingly, there are three RAM binder results that align with those of the virgin binders. They are all RAS binders, which were blended with virgin binders before being measured. Therefore, their CPG values are closer to those of virgin binders. However, even though the RAS percentages are from 12% to 16%, the impact is still noticeable, with all RAS binders being *m*-controlled like the RAP binders.

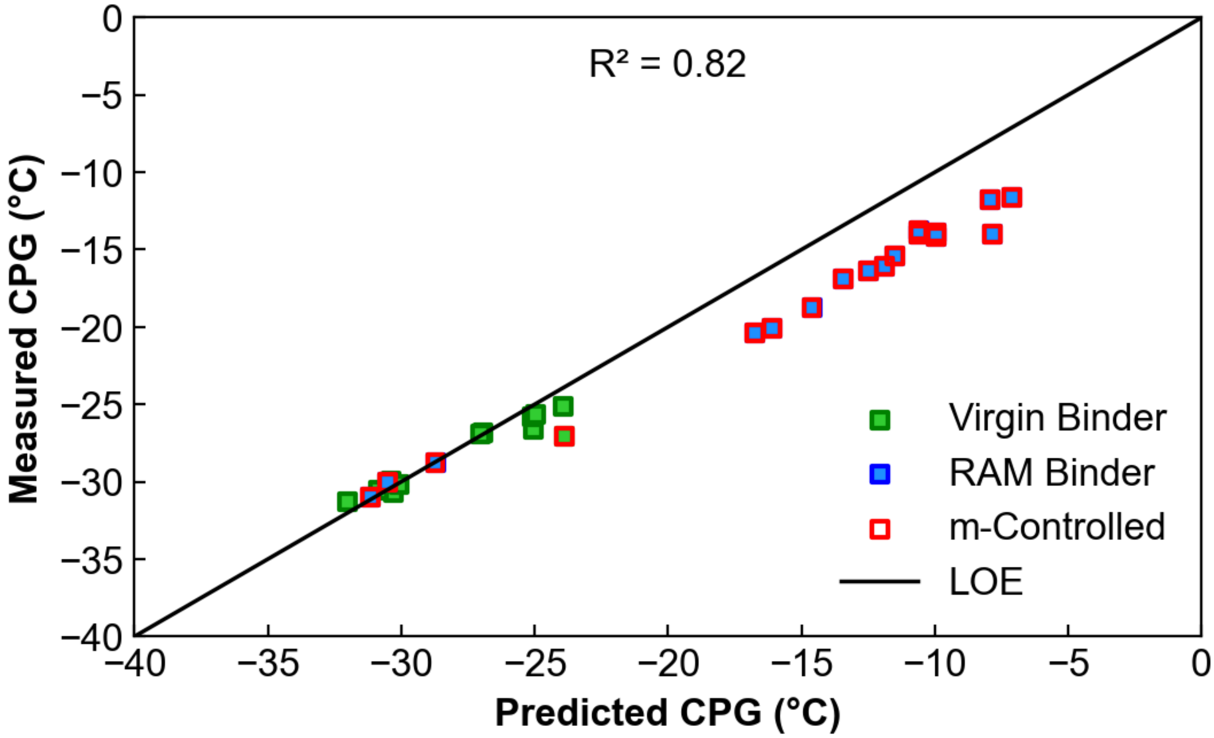

Figure 4-2. Comparison of CPG from DSR-predicted and BBR-measured.

Figure 4-3 presents the comparison of ΔT_c values calculated based on BBR measurements to those calculated based on DSR predictions. The prediction accuracy is not as good as for *S*(60), *m*(60), and CPG. The R^2 with respect to the line of equality of 0.54. The virgin binder and RAM binder ΔT_c values are distinct. Most measured ΔT_c values of the virgin binders are greater than zero, while all RAM binders have ΔT_c values less than zero. This aligns with the virgin binders being *S*-controlled and RAM binders being *m*-controlled as shown in Figure 4-2.

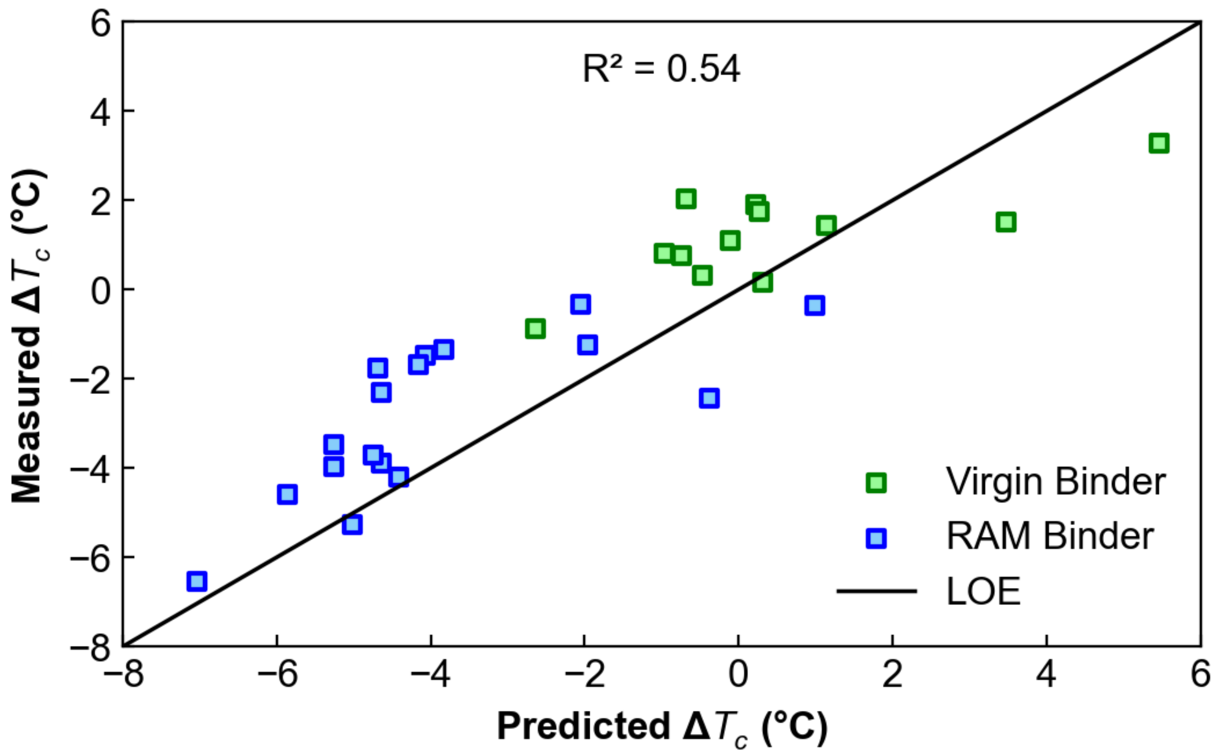

Figure 4-3. Comparison of ΔT_c from DSR-predicted and BBR-measured.

4.4.2. Linear Regression with Interactions

Table 4-2 presents the linear regression with interaction terms results. P-values less than 0.05 are deemed significant. The results indicate that the virgin binder intercept (β_0) and slope (β_1) parameters are significant, except for the intercept term for $S(60)$. Furthermore, the results indicate that both the slopes and intercepts of the relationships between BBR measurements and DSR predictions of $S(60)$ values are significantly different for the virgin binder and RAM binder groups based on the interaction terms β_2 and β_3. For $m(60)$ values, the slopes of the virgin and RAM binder groups do not differ significantly based on the β_3 parameter p-values but the intercepts are different based on the β_2 p-values. Based on this results, the linear regression equations for $S(60)$ and $m(60)$ were fitted separately for virgin binders and RAM binders in Section 4.4.3, using a consistent slope for virgin and RAM binder groups when developing the $m(60)$ regression equations. In addition, given that β_0 is insignificant, linear regression equations for $S(60)$ were evaluated using intercept terms and fixed intercepts of zero.

Table 4-2. Linear regression with interactions results.

Parameter	Equation Term	Estimate	p-value
$S(60)$	Intercept Virgin (β_0)	-3.273	0.6522
	Slope Virgin (β_1)	0.891	<0.0001
	Intercept Interaction (β_2)	-20.396	<0.0001
	Slope Interaction (β_3)	-0.0511	0.0450
	$Mean_{Predicted}$	299.726	NA
$m(60)$	Intercept Virgin (β_0)	0.0592	<0.0001
	Slope Virgin (β_1)	0.8693	<0.0001
	Intercept Interaction (β_2)	0.0043	0.0112
	Slope Interaction (β_3)	0.03518	0.1997
	$Mean_{Predicted}$	0.2978	NA

4.4.3. Empirical Calibrations

This section presents the linear regression equations identified to improve the accuracy of $S(60)$ and $m(60)$ predictions from DSR test results for virgin binders and RAM binders, respectively. To enable both optimization and testing of these empirical calibrations, the equations were fit using 80% of the study binders that were independent from others.

Figure 4-4 shows the best-fit lines for relating measured and predicted $S(60)$ of virgin binders and RAM binders. For virgin binders, the slope of the measured versus predicted $S(60)$ is 0.95, and the intercept is -5.79, while for RAM binders, the slope is 0.83, and the intercept is -2.90. Since the intercept terms are small relative to the magnitude of the measured $S(60)$ values, and the linear regression with interaction terms suggested the intercept is insignificant for the virgin binder group, regression equations were also fitted using a fixed intercept of zero. Given that the regression equations with and without intercept terms produced identical R^2 values relative to the line of equality for both the virgin and RAM binder groups, the intercept is deemed unnecessary.

Building on Equation (4.5), the calibrated $S(t)$ equations with the fixed intercept of zero can be conveyed by Equation (4.12). Equation (4.12) shows that an alternative way to implement this calibration is through an update to Poisson's ratio. Zeng et al. (*10*) used a Poisson's ratio of 0.5, citing Di Benedetto et al. (*32*). Di Benedetto et al. (*32*) reported Poisson's ratios of asphalt binders spanning from 0.35 at low temperatures and/or high frequencies to 0.50 at high temperatures and/or low frequencies for a single 50/70 penetration-graded virgin binder.

$$S(t)_{calibrated} = \frac{2(1+v_{=0.5})}{J(t)} \times slope = \frac{2(1+v_{calibrated})}{J(t)} \tag{4.12}$$

Where:

$S(t)_{calibrated}$ = calibrated creep stiffness prediction from the DSR test,

$\nu_{=0.5}$ = Poisson's ratio, assumed to equal 0.5,

slope = slope of the best fix line between DSR-predicted $S(t)$ without calibration and BBR measurements,

$\nu_{calibrated}$ = refined Poisson's ratio to provide equivalent $S(t)$ to that with Poisson's ratio set at 0.5 and the slope calibration.

Accordingly, the calibrated slopes of 0.93 for virgin binders and 0.82 for RAM binders in Figure 4-4 are equivalent to changing Poisson's ratio in Equation (4.5) from 0.50 to 0.40 and 0.23 for virgin and RAM binders, respectively. The trend in Poisson's ratio values is deemed reasonable among virgin and RAM binders based on the literature, which shows that stiffer asphalt binders exhibit lower Poisson's ratio values. However, it is noted that the RAM value is lower than those reported in the literature (*32*, *33*). Kim et al. (*33*) showed that at –5°C, a penetration grade 30/45 asphalt binder maintained a relatively constant complex Poisson's ratio of 0.26 ± 0.04 across different frequencies. In contrast, the softer penetration grade 50/70 asphalt binder exhibited slightly higher values that varied with frequency, ranging from 0.32 ± 0.04 at 10 Hz to 0.30 ± 0.04 at 0.1Hz, near the lower end of the range reported by Di Benedetto et al.(*32*). Given that these were virgin binders, it seems plausible that the RAM binders may exhibit lower values than those reported in the literature. It is recommended that the empirical calibration of $S(60)$ be adopted using updates to Poisson's ratios in Equation (4.5).

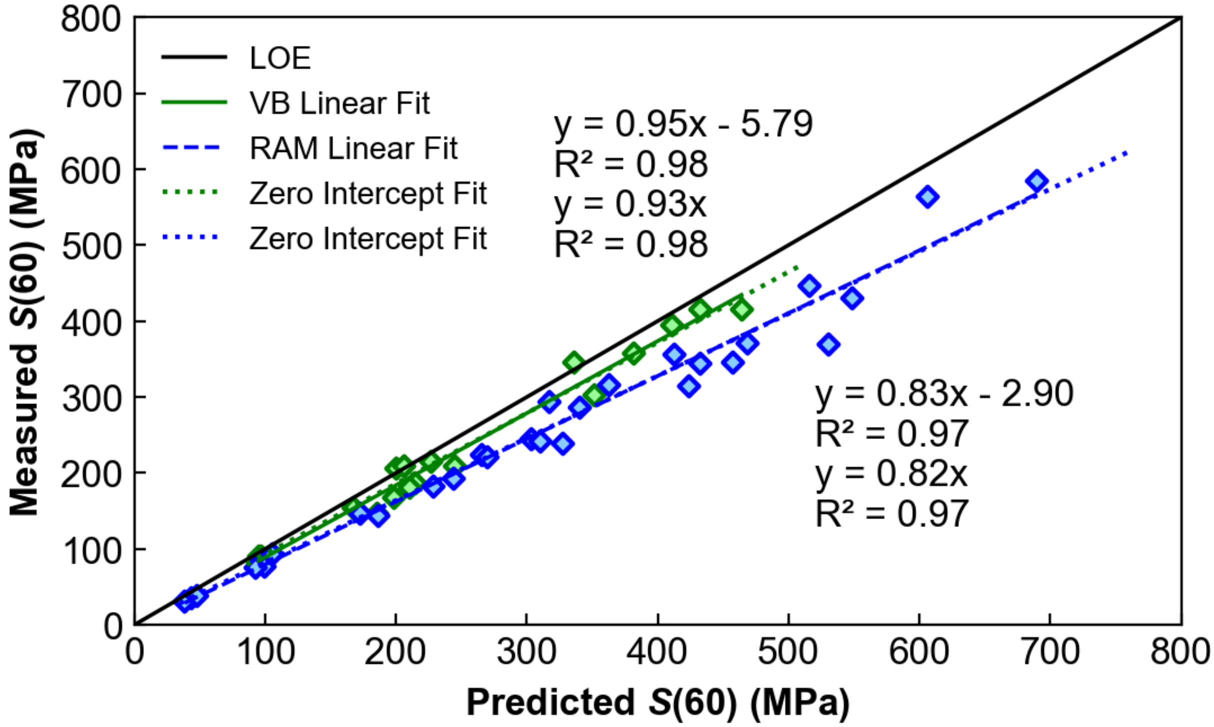

Figure 4-4. Linear fit equations of *S*(60) for virgin binder and RAM binder separately.

Figure 4-5 shows the comparison between measured and calibrated DSR predictions of S(60) using updated Poisson's ratios of 0.40 for virgin binders and 0.23 for RAM binders in Equation (4.5). The calibration improved the R^2 for the line of equality from 0.83 without calibration to 0.97. In addition, the R^2 values concerning the line of equality are similar for the calibration and verification data sets. The R^2 for the 80% study binders used to calibrate the regression equations with respect to the line of equality is 0.98, while the R^2 for the line of equality for the remaining 20% of the data used for verification is 0.96.

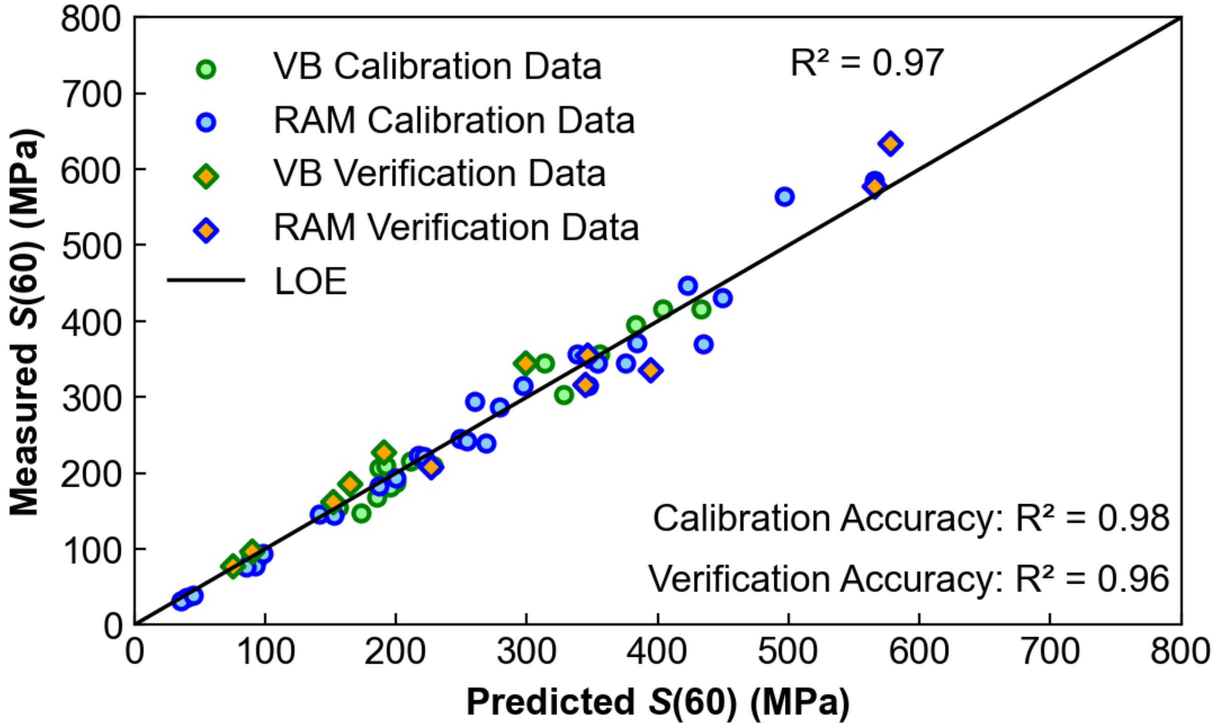

Figure 4-5. Comparison of predicted and measured *S*(60) with Poisson's ratio = 0.40 for virgin binders and Poisson's ratio = 0.23 for RAM binders.

Table 4-2 indicates that the slope of the relationship between BBR measurements and DSR predictions of *m*(60) values does not differ between virgin and RAM binders; however, the two groups exhibit different intercepts. Accordingly, the calibrated equations for predicting *m*(60) using DSR measurements were made using a common slope with distinct intercepts for each binder type. To determine these parameters, a least squares optimization was performed in which the two intercepts (for virgin and RAM binders) and a single slope parameter were simultaneously estimated. The objective function minimized the sum of squared errors between the measured *m*(60) values and those predicted by the calibrated equations for both binder groups. Figure 4-6 shows the resultant calibrated equations and their accuracy. This analysis yielded a slope of 0.8924 and an intercept of 0.0492 for virgin binders and 0.0563 for RAM binders. It is noted that the predicted *m*(60) value is insensitive to the chosen Poisson's ratio since *m*(*t*) is the slope of the log *S*(*t*) versus log(*t*) curve.

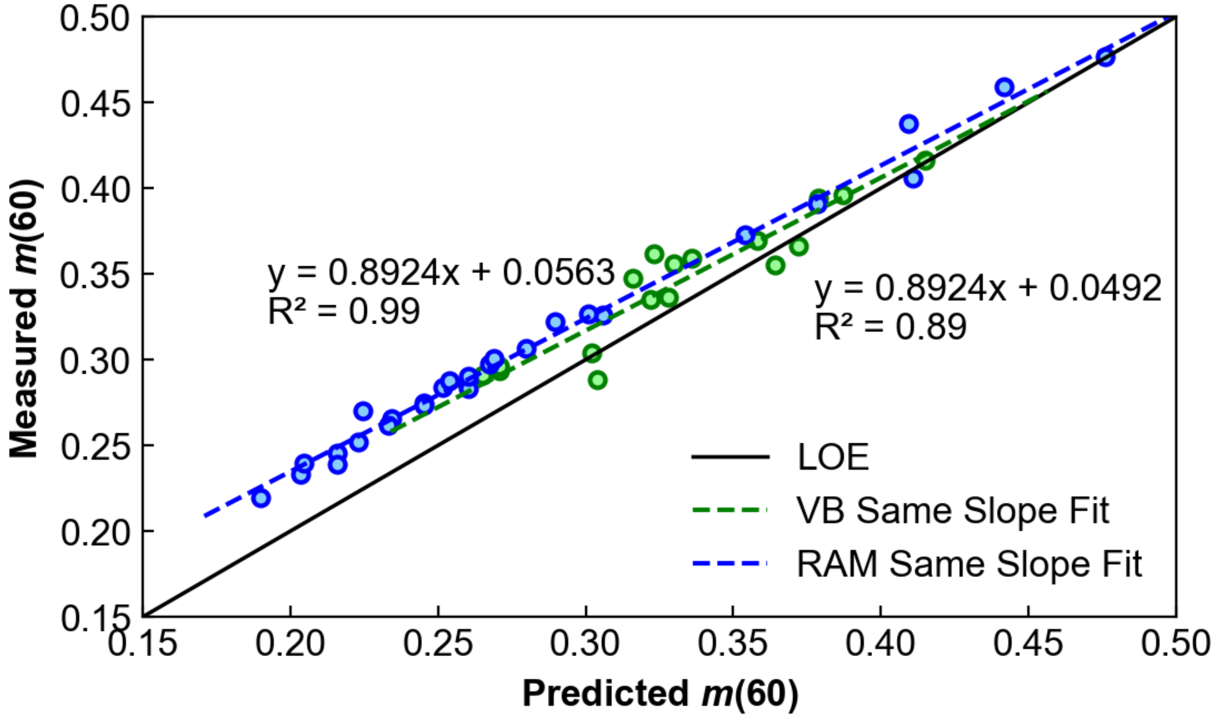

Figure 4-6. Linear fit equations of *m*(60) of virgin and RAM binder separately with a constrained slope.

Figure 4-7 shows the comparison of measured BBR *m*(60) values and those from the calibrated DSR predictions for all binders. The calibrations improved the R^2 with respect to the line of equality from the 0.83 to 0.97 for the collective data. Additionally, the R^2 with respect to the line of equality is comparable for the calibration and verification data sets. 80% of study binders used to calibrate the regression equations have an R^2 with respect to the line of equality of 0.97, while the R^2 for the line of equality for the remaining 20% of the data used for verification is 0.95.

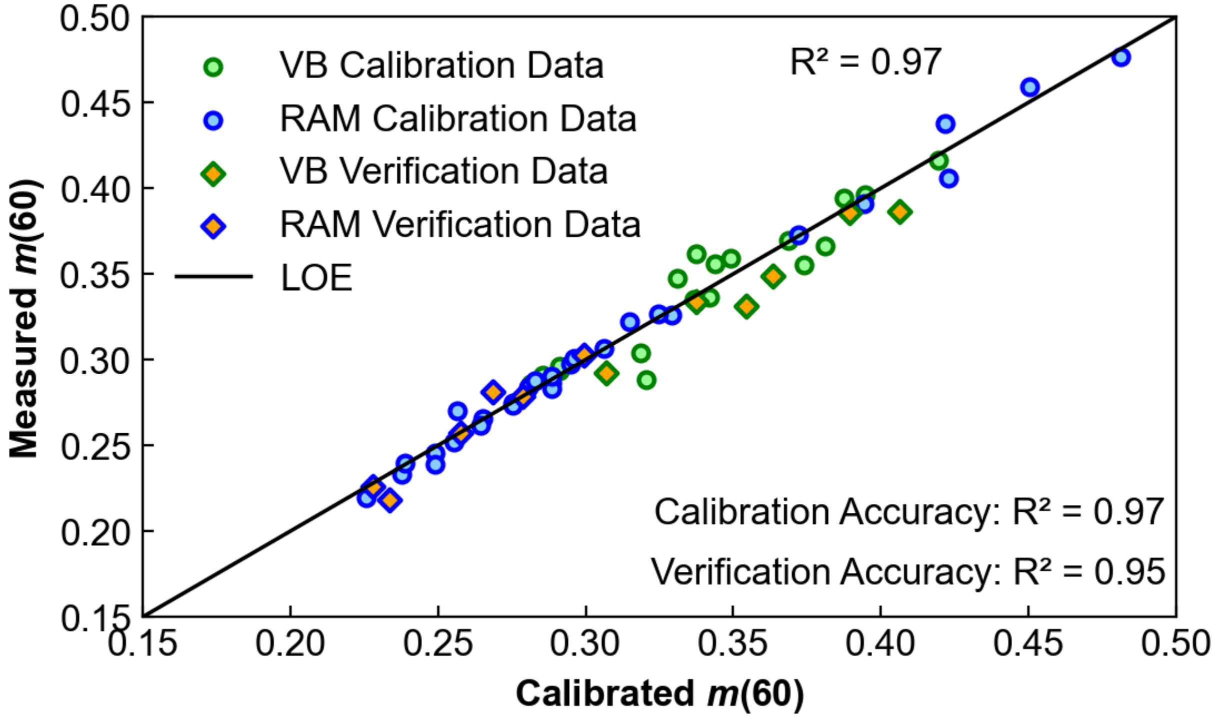

Figure 4-7. Comparison of linear calibrated and measured *m*(60).

4.4.4. Evaluation of the Calibrated Models

Based on the results presented in the previous section, Equation (4.13) is suggested for the prediction of *S*(60) and Equations (4.14) and (4.15) are suggested for the prediction of *m*(60) values for virgin and RAM binders, respectively, from DSR test results.

$$S(60) = \frac{2(1+v)}{J'(\omega = \frac{2}{\pi t})} \tag{4.13}$$

where:

v = 0.40 for virgin binders and 0.23 for RAM binders.

$$m(60) = 0.0492 + 0.8924 \times m_{predicted} \tag{4.14}$$

$$m(60) = 0.0563 + 0.8924 \times m_{predicted} \tag{4.15}$$

where:

$m_{predicted}$ = *m*(60) calculated according to Section 4.4.3. It is noted that *m*(60) does not depend on the Poisson's ratio.

Figure 4-8 shows the comparison between the CPG values calculated using BBR test results to those calculated based on the above equations. The R^2 with respect to the line of equality for the entire data set improved from 0.82 without calibration to 0.98 with calibration. Furthermore, the verification data set maintains a high R^2 with respect to the line of equality of 0.96. Figure 4-9 provides another visual means to compare CPGs determined from BBR results versus those from the calibrated DSR predictions. The average error in CPG is –0.02°C, the average absolute error is 0.69°C, the maximum error is 2.6°C.

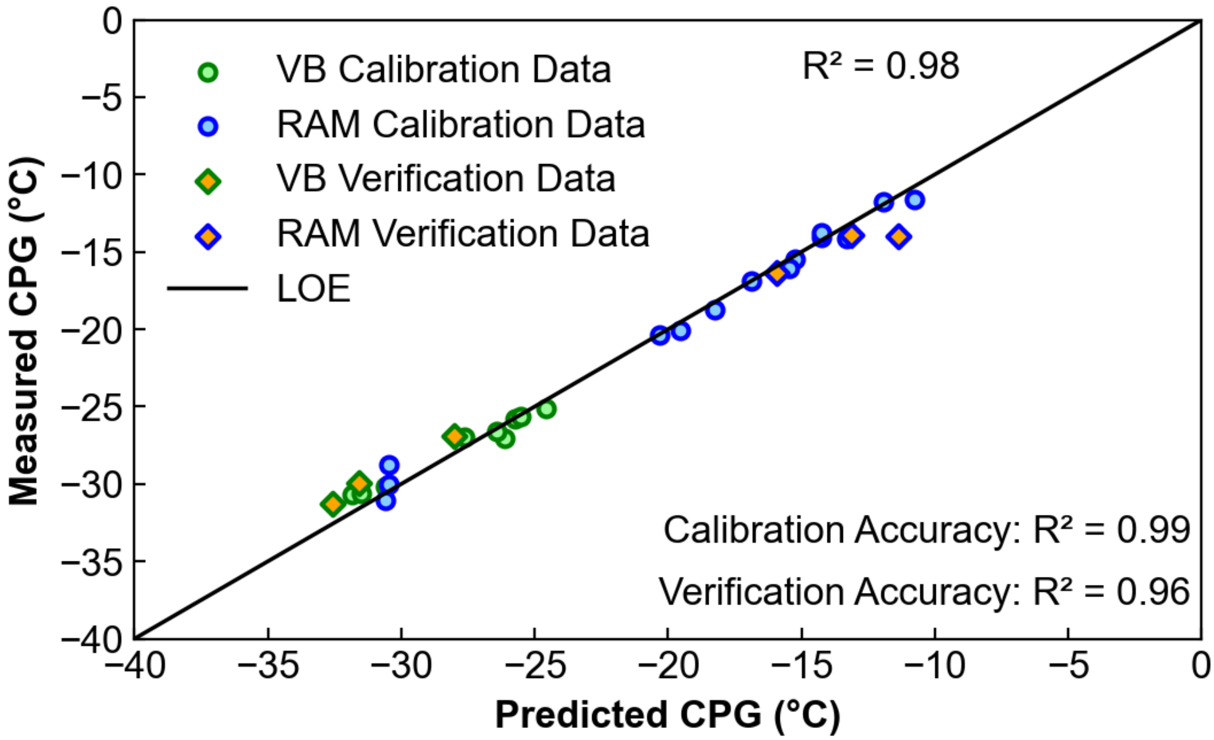

Figure 4-8. Comparison of calibrated predictions and measured CPG values.

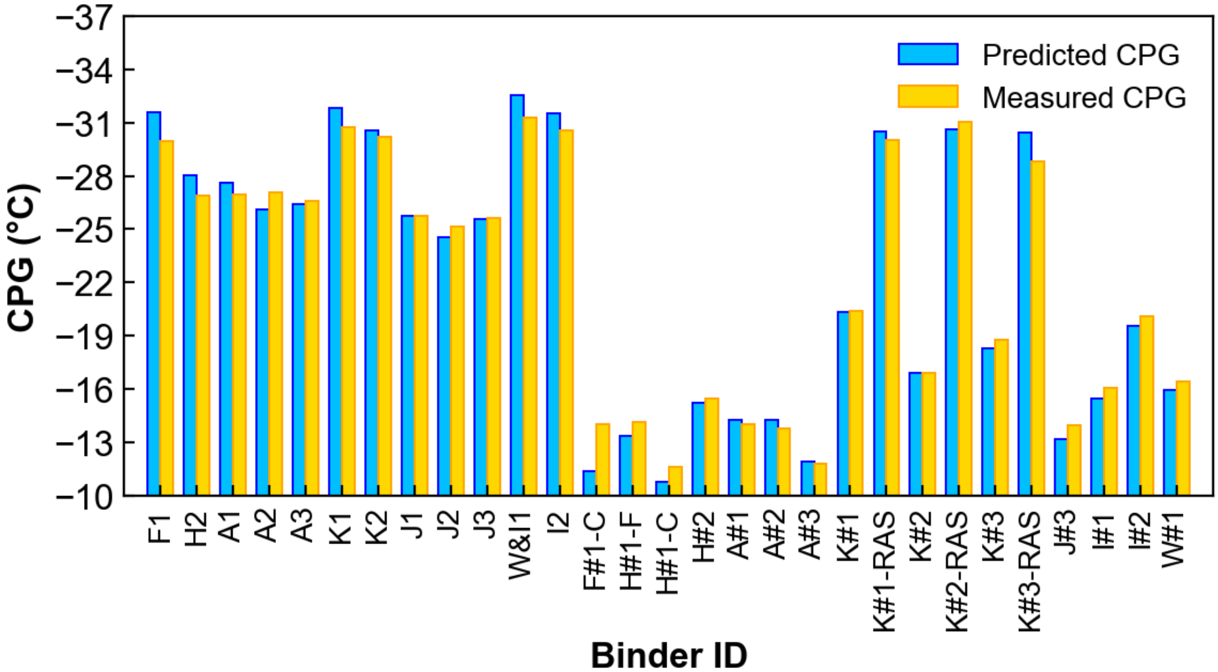

Figure 4-9. Comparison of calibrated predictions and measured CPGs for each binder.

Figure 4-10 shows the corresponding relationships between ΔT_c determined using the BBR and calibrated DSR predictions, indicating an R^2 of 0.63 concerning the line of equality. This is a moderate improvement in prediction of ΔT_c compared to that without any calibration, where the R^2 was 0.54, but it is still not as good as the other parameters evaluated.

To further evaluate the potential implications of the errors in ΔT_c predictions, the determination of passing vs. failing the limits established by Elwardany et al. (*34*) were evaluated. They proposed: (1) accepting all binders with ΔT_c > -2°C, (2) rejecting all binders with ΔT_c < -6°C, and (3) accept binders with ΔT_c values between the critical range of -6°C and 2°C only if cracking resistance is verified via the Asphalt Binder Cracking Device (ABCD) test. Correspondingly, the decision if a binder is accepted, rejected, or in the critical range based on the calibrated DSR predictions was compared to that from BBR measurements.

The calibrated DSR predictions identified the same decision for 23 out of the 29 binders evaluated based on these criteria. One binder that failed based on the BBR measurements was identified as in the critical range based on the calibrated DSR predictions. In addition, four binders that were accepted based on BBR results were identified as falling in the critical zone based on the calibrated DSR predictions, and one binder that fell in the critical range based on BBR results was identified as acceptable based on the calibrated DSR predictions.

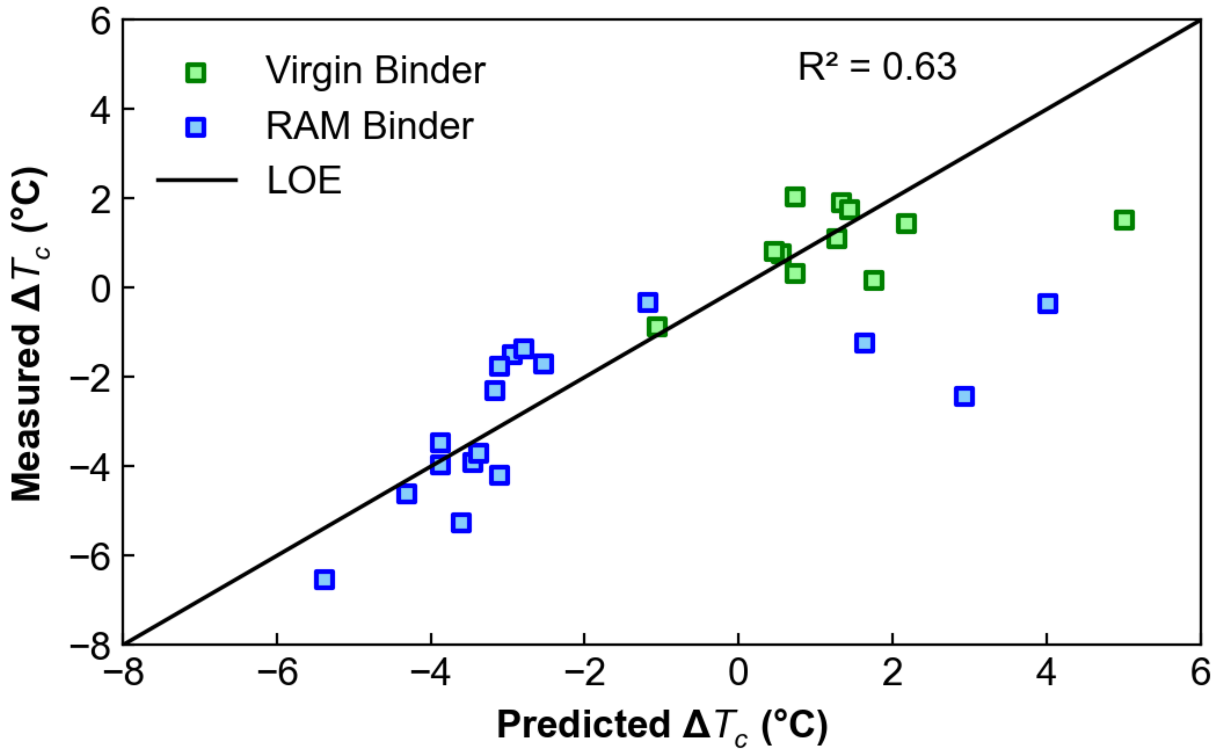

Figure 4-10. Comparison of predicted and measured ΔT_c with Poisson's ratio = 0.40 for virgin binders and Poisson's ratio = 0.23 for RAM binders.

4.4.5. Comparison of Empirical Calibration Equations with Previous Research

Linear equation calibrations of the Zeng et al. (*10*) models to best match BBR results have been reported in two prior studies. Table 4-3 summarizes the comparison of linear equations from those studies and the present study's recommended equations, where the term *predicted* represents the predicted values without calibration and the term *measured* represents the measured values from BBR testing. In Zeng et al.'s study, the linear equation for *S*(60) yielded a slope of 0.87 and an intercept of 21.04, while the *m*(60) equation had a slope of 0.8106 and an intercept of 0.0661. In Preciado et al.'s (*35*) research, the *S*(60) equation showed a slope of 0.90 and an intercept of -14.67, and the *m*(60) equation had a slope of 0.847 and an intercept of 0.045.

The comparison reveals that the linear equations for both *S*(60) and *m*(60) differ significantly across all three studies. The discrepancy in linear equations can likely be attributed to the different materials used in each study and potentially biases among laboratories. Zeng et al. (*10*) evaluated 45 materials consisting entirely of virgin binders, including five polymer-modified binders from throughout the U.S. In contrast, Preciado et al. (*35*) examined 26 binder blends containing various combinations of virgin binders, recycled binders, and different in some cases recycling agents.

Table 4-3. Comparison of linear calibrate equations from previous research.

	$S(60)$	$m(60)$
Zeng et al. (*10*)	$measured = 0.87 \times predicted + 21.04$ $R^2 = 0.85$	$measured = 0.8106 \times predicted + 0.0661$ $R^2 = 0.81$
Preciado et al. (*35*)	$measured = 0.90 \times predicted - 14.67$ $R^2 = 0.94$	$measured = 0.847 \times predicted + 0.045$ $R^2 = 0.87$
Current study	Virgin Binder: $measured = 0.93 \times predicted$ $R^2 = 0.98$ RAM Binder: $measured = 0.82 \times predicted$ $R^2 = 0.97$	Virgin Binder: $measured = 0.8924 \times predicted + 0.0492$ $R^2 = 0.89$ RAM Binder: $measured = 0.8924 \times predicted + 0.0563$ $R^2 = 0.99$

4.5. Conclusions and Recommendations

The following conclusions and recommendations are drawn from the results of this chapter:

- Using Zeng et al.'s approach without empirical calibration, both $S(60)$ and $m(60)$ achieved an R^2 of 0.83 relative to the line of equality, while the CPG yielded an R^2 of 0.82 with respect to the line of equality.
- The linear regression-based calibrations developed in this chapter, specific to RAM and virgin binders, improved the DSR predictions of BBR test results for both $S(60)$ and $m(60)$, achieving an R^2 of 0.97 relative to the line of equality. The average absolute error in continuous low-grading temperature predictions was 0.7°C. The empirical calibration for $S(60)$ suggests that Poisson's ratio is approximately 0.40 for virgin binders and 0.23 for RAM binders at the BBR test conditions.

- Predictions of ΔT_c were poorer than those for $S(60)$, $m(60)$, and the continuous low grading temperature. Future research should evaluate alternative parameters that could serve as more reliable predictors than ΔT_c from DSR test results.
- The calibrated equations provide a promising means to predict BBR properties using DSR test results. It is suggested that the calibrations be validated using a broader data set. Notably, this study did not consider polymer-modified binders.

5. Variability of Plant-produced High Recycled Content Asphalt Mixtures within a State

The work presented in this chapter has been published in the Transportation Research Record, Journal of the Transportation Research Board, © National Academy of Sciences: Transportation Research Board 2025. https://doi.org/10.1177/03611981251315680. It has been reprinted here according to SAGE's author archiving and re-use guidelines. In this work, Wei Xie completed the asphalt binder testing and corresponding data analysis, and contributed to the writing on asphalt binder testing and results in in Sections 5.3.2 and 5.4.2 as well as the associated conclusions. It is noted that the binder characterization and performance-graded binder test results in this section coincide with a subset of those tested and analyzed in Chapters 3 and 4.

5.1. Introduction

Reclaimed asphalt pavement (RAP) has been used in the production of asphalt mixtures in the United States for decades, with its initial usage dating back to the 1970s. Incorporating RAP into asphalt mixtures reduces the demand for raw materials such as virgin aggregate and asphalt binder, thereby preserving natural resources, decreasing landfill waste from construction debris, and lowering costs (*36*, *37*). Recycled asphalt shingles (RAS) have also gained significant interest within the asphalt pavement industry in recent years to reduce shingle waste and offset the need for virgin binder by making use of their high binder content, typically ranging from 20 to 30 percent (*38*, *39*). Nevertheless, the binder present in these recycled asphalt materials (RAM) is oxidized and therefore, stiffer and more brittle compared to virgin asphalt binder. Consequently, state agencies limit the quantity of RAP and RAS allowed in asphalt mixtures due to concerns about long-term pavement performance, particularly related to cracking and raveling (*40*, *41*).

Another limiting factor for incorporating high RAM content into asphalt mixtures is the variability of RAM properties within a given stockpile over time and across stockpiles within a state, as this can lead to inconsistencies in the properties and performance of asphalt mixtures (*42*–*44*). Studies have shown that RAP stockpile properties, such as the theoretical maximum specific gravity (G_{mm}), asphalt content, gradation, and performance grade (PG) of extracted and recovered binder, can vary greatly across different regions within a state and even within a single stockpile over time (*14*, *16*). While state agencies require the measurement of some of these RAM properties as part of quality assurance (QA) procedures, the PG is typically not included because it involves solvent extraction and recovery of the RAM binder, which is time-consuming and impractical. Consequently, variability in the recycled binder properties is generally not accounted for.

The incorporation of performance measures into mixture design and QA procedures is one way to mitigate the potentially detrimental impacts of RAM variability on performance. Many state agencies are shifting from a solely volumetric mixture design approach to a balanced mix design (BMD) approach that incorporates measures of rutting and cracking performance into the design process (*45–48*). However, most state agencies implementing BMD still rely on traditional compositional measures (e.g., gradation, volumetrics) as quality acceptance characteristics (AQCs) during production. Thus, understanding the impacts of variability in the composition of asphalt mixtures on their performance is crucial to ensure adequate controls are implemented during production to mitigate performance variability. Accordingly, several studies have investigated the impacts of variability in asphalt binder content and aggregate gradation on mixture performance (*49–51*). These studies have reported that mixtures meeting performance threshold limits during the design phase can fail to meet those same thresholds during production due to variations in binder content and aggregate gradation, even when these variations are within tolerance limits. However, these investigations were conducted on laboratory-mixed, laboratory-compacted specimens, and not actual plant-produced mixtures and did not consider the impacts of variability in the RAM. Rahman et al. (*52*) evaluated the variability of the performance of plant-produced asphalt mixtures containing RAP and RAS. They observed differences in the performance of mixtures sampled at different times during mixture production, which they speculated could be due to variations in aging caused by different silo storage times at the asphalt plant before transportation to the construction site. However, this study involved mixtures with low recycled material content, capped at 10% RAP and 3% RAS.

The North Carolina Department of Transportation (NCDOT) permits relatively high recycled binder replacement percentages (RBRs) in surface mixtures. The NCDOT allows up to 40% RBR for surface mixtures containing RAP or a combination of RAP and RAS, and up to 20% RBR for RAS-only mixtures (*53*, *54*). Thus, understanding the variability of recycled material properties and their impacts on the performance of plant-produced asphalt mixtures in North Carolina is critically important to ensure that adequate measures are in place to achieve consistent performance.

5.2. Objectives

The objectives of this study are to:

- Characterize the properties of RAP and RAS within stockpiles over time and across several asphalt plants in North Carolina.
- Evaluate the variability in the performance of plant-produced asphalt mixtures containing high percentages of recycled asphalt material (RAM) in North Carolina.
- Evaluate the causes for the observed variability in plant-produced mixture performance.

5.3. Methodology

5.3.1. Materials

Plant-produced surface asphalt mixtures and their constituent materials (RAM and virgin binder) were acquired and characterized from four asphalt plants in North Carolina. All mixtures evaluated in this study have a 9.5 mm nominal maximum aggregate size. Table 5-1 provides a summary of the characteristics of the plant-produced asphalt mixtures reported on the job mix formula (JMF). The mixtures from Plants H and A are classified as RS9.5C according to NCDOT specification (*54*) and are designed for traffic loading between 3 to 30 million equivalent single axle loads (ESALs), while the mixtures from Plant K and J are classified as RS9.5B and are designed for traffic loading up to 3 million ESALs. It is noteworthy that all materials (i.e., RAP, virgin binder, and plant-produced asphalt mixture) were sampled on two different dates spanning from several months to up to one year apart to assess the variability in their properties and performance after a prolonged time gap. The reason for the relatively long time gap was to try to encompass a gap during which the recycled material stockpiles would have been replenished with new sources.

Table 5-1. Characteristics of the plant-produced asphalt mixtures reported on the JMF.

Plant	H	A	K	J
Mix type	RS9.5C	RS9.5C	RS9.5B	RS9.5B
RAP content (% by weight of aggregate)	35	30	30	30
RAS content (% by weight of aggregate)	0	0	3	0
Asphalt binder content (% by weight of mixture)	6.1	6.0	6.3	6.0
Recycled binder replacement (%)	25	25	30	27
Voids in mineral aggregate VMA (%)	16.9	17.1	18.2	17.1
Virgin binder performance grade	64-22	64-22	58-28	64-22

Note: In the designations RS9.5C and RS9.5B, "RS" stands for recycled surface course; "9.5" indicates the nominal maximum aggregate size of 9.5 mm; "C" and "B" designate the mixture's design traffic loading, where "C" mixtures are designed for 3 to 30 million ESALs and "B" mixtures are designed for up to 3 million ESALs.

Figure 5-1 presents the plant locations and sampling dates. Plant-produced mixture and RAM were sampled on the same dates. The selected plants encompass the coastal and piedmont geologic regions in North Carolina to encompass different aggregate mineralogies and regional practices. The study did not include plants from the mountain region of North Carolina because high RAM content mixtures are not commonly used in that area.

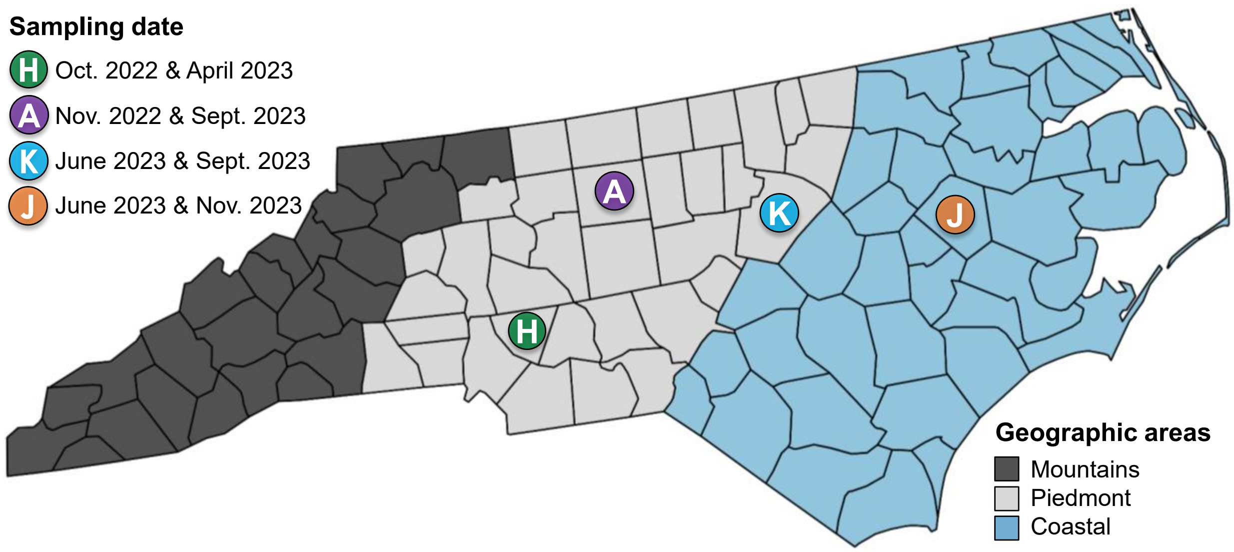

Figure 5-1. North Carolina map indicating the location and sampling date of the material sources.

Naming Convention

A naming convention was created to represent each mix and the different conditions at which the mixture is evaluated. An example is H-35/0-1 where "H" reflects the Plant ID, "35" denotes the RAP content and "0" denotes the RAS content, and "1" indicates this was the first sample acquired from the plant. Thus, when this mixture was resampled, the name for that sample was H-35/0-2.

5.3.2. Test Methods

Characterization of the RAM Materials

The RAM materials were oven-dried at 60°C prior to characterization. The mass of the RAM before and after drying was used to determine its moisture content. The RAM materials were characterized in terms of asphalt content, theoretical maximum specific gravity (G_{mm}), and performance grade (PG) of extracted and recovered RAM binder. The asphalt content of the recycled materials was measured via ignition oven according to AASHTO T 308 (*55*). The G_{mm} was measured using automatic vacuum sealing method according to ASTM D6857 (*56*).

Characterization of the Virgin and Recycled Binders

The recycled binders were extracted using a centrifuge extractor with trichloroethylene (TCE) as the solvent according to Method A of AASHTO T 164 (*20*). The asphalt binder recovery was completed using a rotary evaporator according to ASTM D5404 (*21*). The recovered RAP binders were subjected to Rolling Thin Film Oven (RTFO) aging according to AASHTO T 240 for characterization (*22*). The RAP binders were not subjected to further aging in the pressurized aging vessel in accordance with Appendix X2 of AASHTO M 323. The RAS binders were tested after blending with virgin binder using a blend ratio that matched the plant-produced mixture. Fried et al. suggested avoiding testing RAS alone because the potentially excessive PG of RAS binders can make casting samples and obtaining reliable rheological measurements difficult (*27*). To prepare blends containing RAS, the virgin binder was preheated to 140°C and the RAS binder was preheated to 165°C (*28*). The two binders were then thoroughly blended with a power drill equipped with a paddle attachment. The virgin binders and blends were conditioned in the RTFO and pressurized aging vessel (PAV) according to AASHTO R 28 (*29*) to produce short- and long-term aged binder, respectively. No RAS particles persisted after blending and conditioning in the RTFO.

DSR testing was conducted on all binders at the RTFO age level according to AASHTO T 315 (*57*) for high-temperature grading. Original binder testing was avoided for the RAP to ensure any residual solvent from the recovery was fully removed, which was confirmed via Fourier Transform Infrared Spectroscopy (FTIR). DSR testing was also conducted for intermediate temperature grading according to AASHTO T 315 (*57*). Intermediate temperature tests were performed on RAP at the RTFO age level in accordance with Appendix X2 of AASHTO M 323 and at the PAV age level for the virgin binders and blends in accordance with AASHTO M 320 (*24*). The results were analyzed to determine the standard high- and intermediate-temperature grades according to AASHTO M 320 (*24*) and the continuous grading high-temperatures (PGH) and continuous grading intermediate temperatures (PGI) according to ASTM D7643 (*30*). DSR testing was conducted at a minimum of two temperatures, one passing the AASHTO M 320 high-temperature grading criteria and one failing. Two replicate tests were initially conducted. If the results met the repeatability requirements in AASHTO T 315 (*57*), testing ceased. If the requirement was not met, additional replicate tests were conducted until the requirement was satisfied.

The continuous grading temperatures of the blend of virgin and recycled binders in the plant-produced mixtures were approximated using linear blending charts in accordance with Appendix X2 of AASHTO M 323. For the RAP-only mixtures, the blended binder continuous grading temperatures were estimated using Equation (5.1). For the mixtures containing RAP and RAS, the blended binder continuous grading high-temperatures were estimated using Equation (5.2), inputting the continuous temperature of the blend of virgin and RAS binder as the PG_{Virgin} (*58*). The measured mixture and RAM binder contents for each sample were used to calculate the RBR values, thereby accounting for the observed variability in mixture composition.

$$PG_{\text{Blend}} = RBR_{\text{RAP}} \times PG_{\text{RAP}} + (1 - RBR_{\text{RAP}}) \times PG_{\text{Virgin}} \tag{5.1}$$

where:

PG_{Blend} = continuous grading temperature of the blend of recycled and virgin binder (°C),

RBR_{RAP} = RAP binder recycled binder ratio, equal to the weight of RAP binder in the mix divided by total binder weight in the mix,

PG_{Virgin} = virgin binder continuous grading temperature (°C).

The RAS blend results combined with the virgin binder results were used to estimate the RAS binder continuous high-temperature using Equation (5.2).

$$PG_{\text{RAS}} = \frac{PG_{\text{Blend}} - (1 - BR_{\text{RAS}}) \times PG_{\text{Virgin}}}{BR_{\text{RAS}}} \tag{5.2}$$

where:

PG_{RAS} = continuous grading temperature of the RAS (°C),

BR_{RAS} = RAS blend ratio in the blend of virgin and RAS binder, equal to the weight of RAS binder by the combined weight of RAS and virgin binder.

In addition, temperature-frequency sweep (TFS) tests were carried out using the DSR at the PAV age level for the virgin binders and blends and RTFO age level for the RAP binders according to the general requirements of AASHTO T 315 (*23*). For virgin binders and blends, TFS testing was implemented using the 8-mm parallel plate geometry with a 2-mm gap using test temperatures of 5°C, 20°C, 35°C, and 50°C and a frequency span of 0.1 to 15 Hz. For the RAP binders, tests temperatures of 10°C, 20°C, 35°C, and 50°C were used as challenges maintaining proper adhesion were encountered at 5°C. Two replicate tests were conducted for each binder and blend. The results generally met the repeatability requirements of AASHTO T 315.

Dynamic shear modulus ($|G^*|$) and phase angle (δ) master curves were constructed and modeled following the recommendations of Fried and Castorena (*59*). This procedure involves free shifting of the isotherms in a pair-wise approach to first construct the master curve and then employing linear regression to calculate the Christensen Anderson master curve model coefficients. The coefficient of determination (R^2) values for the resultant dynamic shear modulus master curves were all 1.00 and at least 0.99 for phase angle master curves. The master curve models were used to calculate the Glover-Rowe (G-R) parameter (*60*), $|G^*|\cos^2\delta/\sin\delta$, at the condition of 15°C and 0.005 rad/s. The G-R parameter has been proposed as a better indicator of cracking resistance than the AASHTO M 320 intermediate-temperature parameter, $|G^*|\times\sin\delta$, for two reasons. First, the G-R parameter is an indicator of ductility and thus, cracking susceptibility, for non-polymer-modified asphalts. Lower G-R values are associated with higher ductility (*61*, *62*). Second, an increase in G-R, along with an expected reduction in ductility, occurs due to an increase in $|G^*|$ and/or a decrease in δ, which aligns with changes imparted by oxidative aging. In contrast, the AASHTO M 320 parameter suggests an improvement in cracking resistance when δ decreases, which is counterintuitive to the effects of oxidation known to induce embrittlement.

The blended binder G-R values were approximated using estimates of the blended $|G^*|$ and δ obtained using Equation (5.3) and Equation (5.4), respectively based on Elkashef et al. (*63*).

$$\log|G^*|_{\mathrm{Blend}} = RBR_{\mathrm{RAP}} \times \log|G^*|_{\mathrm{RAP}} + (1 - RBR_{\mathrm{RAP}}) \times \log|G^*|_{\mathrm{Virgin}} \quad (5.3)$$

where:

$|G^*|_{\mathrm{Blend}}$ = dynamic shear modulus of the blend of recycled and virgin binder (Pa),

$|G^*|_{\mathrm{RAP}}$ = dynamic shear modulus of the RAP (Pa),

$|G^*|_{\mathrm{Virgin}}$ = virgin binder dynamic shear modulus or blend of virgin and RAS binder dynamic shear modulus for RAP/RAS mix case (Pa).

$$\delta_{\mathrm{Blend}} = RBR_{\mathrm{RAP}} \times \delta_{\mathrm{RAP}} + (1 - RBR_{\mathrm{RAP}}) \times \delta_{\mathrm{Virgin}} \quad (5.4)$$

where:

δ_{Blend} = phase angle of the blend of recycled and virgin binder (°),

δ_{RAP} = phase angle of the RAP (°),

δ_{Virgin} = virgin binder phase angle or blend of virgin and RAS phase angle for RAP/RAS mix case (°).

Characterization of the Plant-produced Asphalt Mixtures

The plant-produced asphalt mixtures were characterized in terms of extracted aggregate gradation, asphalt binder content, and G_{mm}. The asphalt binder content and extracted aggregate were obtained via ignition oven, and the extracted aggregate gradation was determined according to AASHTO T 30 (*64*). The G_{mm} was measured according to AASHTO T 209 (*65*). Additionally, all mixtures were tested for rutting and cracking susceptibility using the asphalt pavement analyzer (APA) and the indirect tensile cracking test (IDEAL-CT), respectively. The APA was conducted in accordance with AASHTO T 340 (*66*) and NCDOT requirements (*54*) on four replicate specimens with 150 mm in diameter by 75 mm tall, with target air void of 4% at 64°C. The output of the APA test is the rut depth after 8,000 wheel passes. The IDEAL-CT was conducted according to ASTM D8225 (*67*) on five replicate specimens with 150 mm in diameter by 62 mm tall, with target air void of 7% at 25°C. It should be noted that all plant-produced asphalt mixtures were obtained in 5-gallon buckets. The loose mixes were then divided into small samples following LaCroix (*68*).

5.3.3. Statistical Analysis

JMP Pro software version 17 was used to perform statistical analysis of the mixture performance test results. A one-way analysis of variance (ANOVA) was conducted to identify statistically significant differences between the mixture mean CT_{Index} and rut depth values among the different mixtures and samples. After verifying significant differences exist, the post-hoc Tukey-Kramer test was conducted to compare all pairs of means and identify which pairs are significantly different from each other. The statistical tests were conducted at a significance level (α) of 0.05.

5.4. Results

5.4.1. Recycled Asphalt Material Characteristics

Table 5-2 summarizes the properties of the RAM samples. It is important to note that the only case that contained fractionated RAP was H-35/0-1. Plant H used two RAP stockpiles (coarse and fine) for the first sample, but later switched to using only one RAP stockpile (fine). Consequently, only one RAP stockpile result is shown for H-35/0-2, which is compared most directly to the blend from H-35/0-1. Variability in the RAP properties is observed across the different plants, with binder contents spanning from 4.8 to 5.8 percent (neglecting the fractionated stockpiles) and G_{mm} values spanning from 2.451 to 2.625. However, when looking at the variability within stockpiles, the stockpiles show generally consistent properties over time. According to NCDOT specifications (*54*), if a stockpile is to be replenished with a new source of RAP or RAS and used in an existing JMF, the binder content must be within specific tolerance limits. For RAP, the acceptable difference between the approved and new RAP sources is ± 0.4% for mixtures containing between 20 to 30% RAP and ± 0.3% for mixtures with more than 30% RAP. For RAS, the allowable difference is ±2.5%. The difference in binder content between the measured values obtained from the ignition oven and those listed in the JMF for all RAS materials falls within these limits. However, most RAP materials exceed the specified tolerance limits, typically showing higher measured asphalt content values than those listed in their respective JMFs, as indicated by the positive values in Table 5-2. NCDOT requires measurement of moisture content in RAP and RAS at the start of production and daily during production. Monitoring moisture is important because excess moisture requires additional heating and fuel consumption for evaporation, thus increasing production costs. For this reason, NCDOT recommends covering RAP and RAS stockpiles to keep them as dry as possible, although this practice is not commonly observed in North Carolina. While moisture content within stockpiles over time is generally consistent, it varies significantly across different plants, spanning from 1.7 to 5.4 percent.

The effective specific gravity (G_{se}) was back-calculated from G_{mm} measurements, using the measured binder content and assuming a binder specific gravity of 1.02. Despite the relatively long-time gap between samplings, the G_{se} values for the RAP materials were very consistent, with the largest within-plant difference being only 0.024 for Plant H. In contrast, notable differences were observed among the RAS samples from Plant K, suggesting potential changes in aggregate characteristics when the stockpile was replenished.

Table 5-2. Properties of the RAM Samples.

Mix	Recycled material	Binder content (%)	Binder content difference (%)	Moisture content (%)	G_{mm}	G_{se}
H-35/0-1	Coarse RAP	3.9	0.6	3.6	2.625	2.804
	Fine RAP	5.4	0.7	4.7	2.553	2.792
	Blend RAP	4.8	-	-	2.581	2.797
H-35/0-2	RAP	4.9	0.2	5.4	2.596	2.821
A-30/0-1	RAP	4.9	-0.1	3.8	2.538	2.748
A-30/0-2	RAP	5.0	0.0	4.0	2.527	2.739
K-30/3-1	RAP	5.3	0.8	1.7	2.499	2.720
	RAS	17.5	-0.5	2.6	2.135	2.780
K-30/3-2	RAP	5.0	0.5	1.9	2.503	2.710
	RAS	20.1	2.1	4.8	2.043	2.732
J-30/0-1	RAP	5.7	0.5	3.8	2.457	2.687
J-30/0-2	RAP	5.8	0.6	3.5	2.451	2.683

Note: Binder content difference = measured binder content minus the binder content listed in the JMF; G_{mm} = theoretical maximum specific gravity; G_{se} = effective specific gravity (back-calculated from G_{mm} and asphalt content measurements); Blend = blend of coarse and fine at the proportions used in the mixture.

5.4.2. Virgin and Recycled Binders Results

Figure 5-2 presents the AASHTO M 320 continuous grading high-temperatures (PGHs) of the (a) virgin, (b) recycled, and (c) estimates for the blended binders. The vertical error bars represent the maximum and minimum values from the test replicates.

Figure 5-2 (a) shows that the virgin binders PGH values comply with the specified high-temperature PGs listed in Table 5-1. The virgin binders from Plants H, A, and J have a PGH exceeding 64°C, while the binders from Plant K have a value that exceeds 58°C. The PGH values for the PG 64-22 virgin binders fall within a relatively narrow span of 67.5 to 69.8°C. The virgin binder results are even more consistent within a plant with a maximum difference in PGH between the two samples of 1.4°C.

Figure 5-2 (b) shows that the PGH values of the RAP binders are also generally consistent within a given plant with a maximum difference of 3.2°C. In contrast, the RAS binders from Plant K show a substantial difference between the first and second samples of nearly 20°C. Also, despite the consistency of the results of RAP binders within a given plant, there is a notable span in PGH values across plants of 94.3°C to 109.3°C with Plant K exhibiting the lowest value and Plant J showing the highest value. This 15°C difference could require different virgin binder grades to achieve an intended blended binder grade at a high RBR levels, which is not accounted for within current specifications that are agnostic to the specific RAP binder properties.

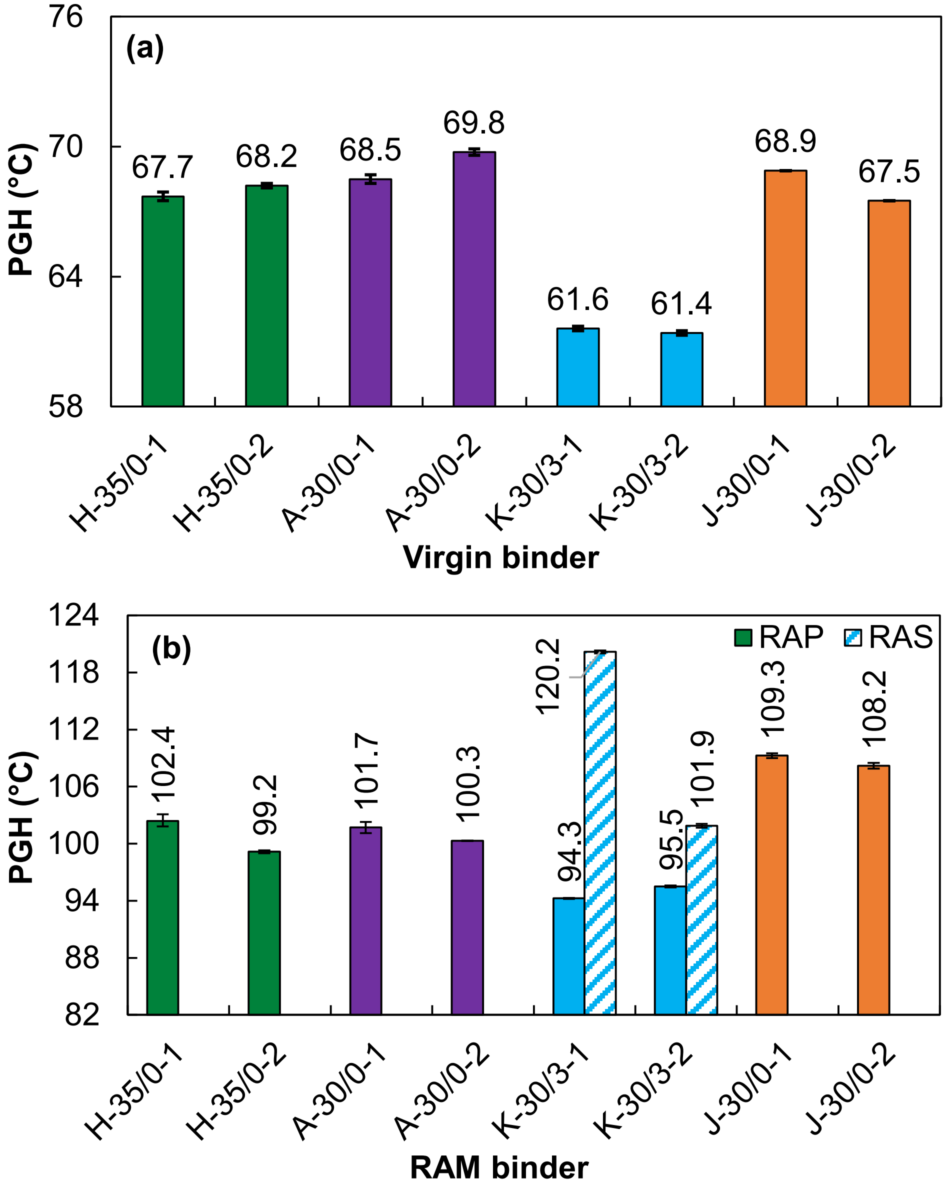

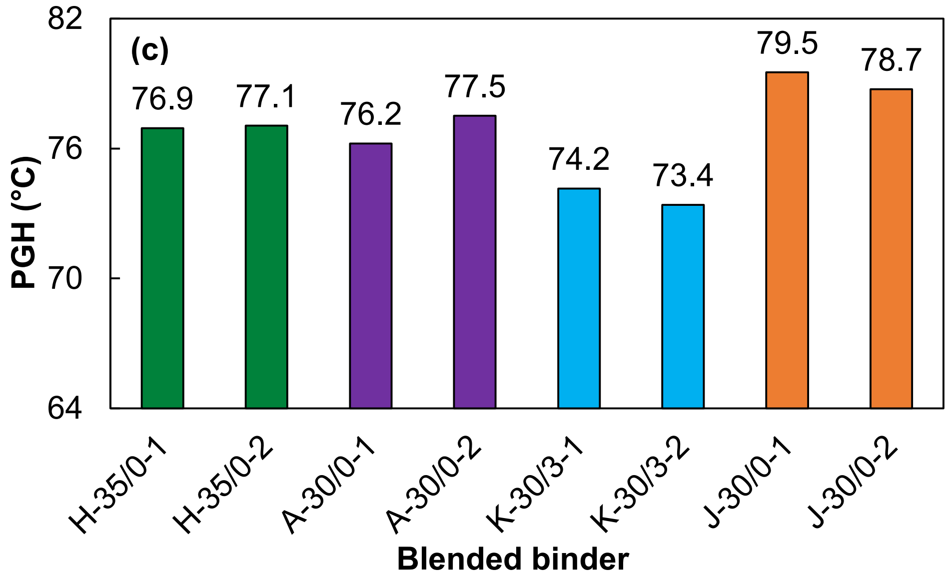

Figure 5-2. Continuous grading high-temperatures of the binders: (a) virgin, (b) RAM, and (c) estimated blended at RBR to match the respective mixture.

Figure 5-2 (c) shows the estimated blended binder PGH values, derived from the PGH values of virgin and RAM binders combined with the mixture RBR. All blended binder PGH values greatly exceed the critical climatic grade temperature of 64°C, indicating adequate rutting resistance is expected. For comparison, Figure 5-3 shows the estimated blended binder PGI values, which show that with the exception of Plant K, all blended binder grades exceed the climatic grade of 25°C, indicating potentially higher cracking susceptibility than intended.

The variation in blended binder PGH and PGI values between the two samples from a given plant is minimal, with a maximum difference of 2°C. However, a notable difference is observed when comparing across plants: the PGH and PGI values of the blended binders from Plant K are significantly lower than those from other plants. These lower values are attributed to several factors: (1) Plant K uses a PG 58-28 virgin binder whereas the other mixtures use a PG 64-22, (2) the RAP binders from Plant K have lower PGH values compared to those from the other plants, and (3) the RAS PGH values were relatively close to those of RAP binders from other plants. Previous research has shown that RAS binders from NC typically have higher PGH values, spanning 130°C to 194°C (*69*). The NCDOT specifies a PG 58-28 virgin binder when the RBR exceeds 0.30 for RAP mixtures or 0.20 for RAP/RAS mixtures (*54*). Consequently, despite having an RBR only marginally higher than the other mixtures, Plant K included a softer virgin binder. For mixtures with RAS binders with PGs that greatly exceed those of RAP binders, this may yield consistent blended binder characteristics across RAP and RAP/RAS mixtures. However, the Plant K RAP and RAS were both relatively soft, resulting in distinct characteristics. This finding underscores the potential impacts of variability in recycled binder properties that are not accounted for in the selection of virgin binder grades.

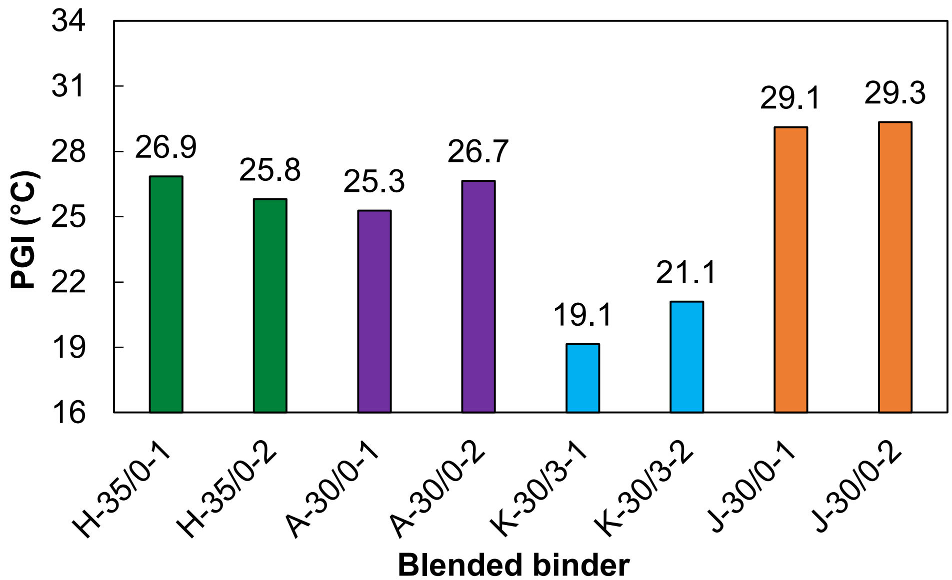

Figure 5-3. Continuous grading intermediate-temperatures grade estimated for the blended binders at RBR to match the respective mixture.

Figure 5-4 shows the G-R parameter results in terms of (a) estimated values for the blended binders and (b) virgin, RAP, and blends in a black space diagram. Trends in the results shown in Figure 5-4 (a) among the different plants generally align with those for PGI. Notably, the Plant K blended binders display low G-R values compared to the other plants, suggesting better expected cracking performance and aligning with the PGI results. The distinct G-R values of the Plant K blend are attributed to its softer virgin binder PG. The variability in the G-R results between the two samples from Plant H and Plant A is substantially higher than observed in the PGI results.

Figure 5-4 (b) shows the G-R results of the virgin, recycled, and blended binders in a black space diagram. The two curves in the black space diagram represent the thresholds for the onset of cracking and significant damage proposed by Anderson et al. (*61*). Furthermore, the two samples from a given plant are distinguished by the addition of a dash to the data points corresponding to second sample. Higher $|G^*|$ and lower δ values are associated with age-induced embrittlement and hence, greater cracking susceptibility (*61*).

Figure 5-4 (b) shows two distinct cluster of data points. One cluster is located at the top-left region of the plot and the other at the bottom-right region of the plot. The top-left cluster corresponds to the RAP binders, all of which fall within the block cracking zone. The RAP binders are highly oxidized and, therefore, have high $|G^*|$ and low δ values compared to the virgin binders and blends. The bottom-right cluster corresponds to the virgin and blended binders. These binders are less aged, with lower $|G^*|$ and higher δ values, which yield comparatively low G-R parameter values. This result aligns with previous studies, which have shown that as materials age, data points shift toward the top-left region of the plot due to increased $|G^*|$ and decreased δ values (*70*). None of the virgin binders crossed the threshold of 180 kPa for the onset of cracking. However, the blended binders are positioned between the virgin and RAP binders, with the blended binders from Plants J and A surpassing the 180 kPa threshold.

The black space diagram also explains the relatively low G-R values in the Plant K blends. The Plant K RAP binders display lower $|G^*|$ and higher δ values than the other RAP binders. The Plant K virgin binders also show lower $|G^*|$ values compared to the other virgin binders, owing to their lower PG. These factors led to comparatively low G-R values in the Plant K blends compared to the other cases. However, the δ values of the Plant K binders are not distinct from the other virgin binders, suggesting an inferior balance in modulus and relaxation characteristics, which can increase thermal cracking susceptibility (*61*).

In summary, although the overall trends in G-R values among the different plants generally correspond with the trends in PGI, the G-R parameter was more sensitive to differences between the two samples acquired from the same plant. Additionally, the black space diagram highlighted potentially inferior relaxation characteristics in the blend results in Plant K that were not evident when considering the PGI or G-R values alone.

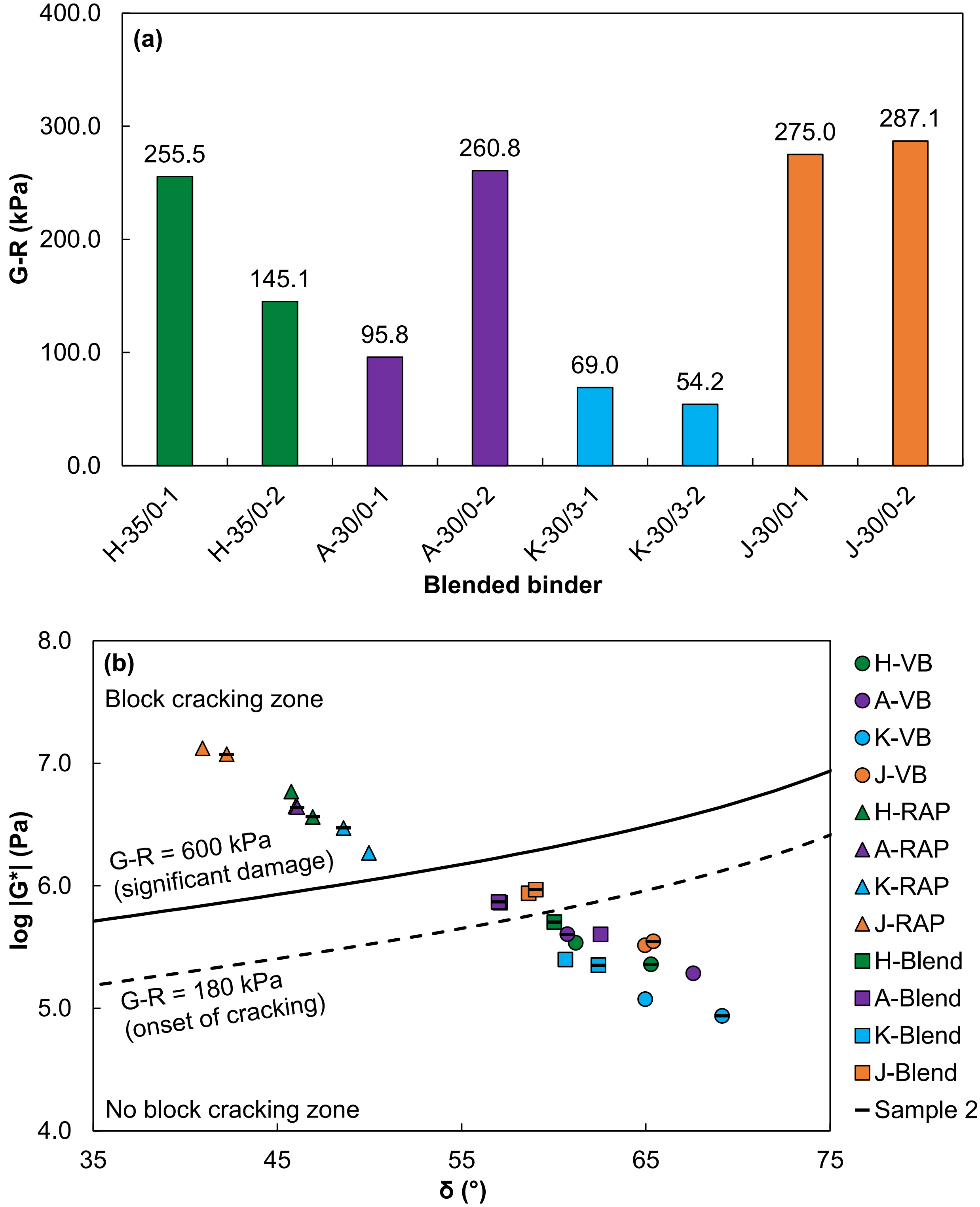

Figure 5-4. Glover-Rowe results: (a) G-R values, (b) black space diagram; VB = virgin binder.

5.4.3. Plant-produced Asphalt Mixtures Results

Figure 5-5 presents the extracted aggregate gradations for the plant-produced asphalt mixtures along with the reported gradations on the corresponding JMF. NCDOT specifications require that the difference between individual test results and the JMF must be within ±8.0 percent for the 2.36 mm sieve and ±2.5 percent for the 0.075 mm sieve. Only H-35/0-2 mixture failed these requirements, with a difference of 3.2 percent at the 0.075 mm sieve. Additionally, all type B mixtures, except for K-30/3-1, failed to meet the minimum control point of 60 percent at the 2.36 mm sieve. The H-35/0-2 also failed to meet the maximum control point of 8 percent passing at the 0.075 m sieve. For further comparison purposes, the collective extracted aggregate gradations are shown together in Figure 5-5(e), which reveal consistent gradations across all plants compared to the wide range permitted by the band specification limits. The largest differences in the percent passing a given sieve size among all curves is 10.6 percent, coinciding with the difference between J-30/0-1 and A-30/0-1 at the 0.3 mm sieve.

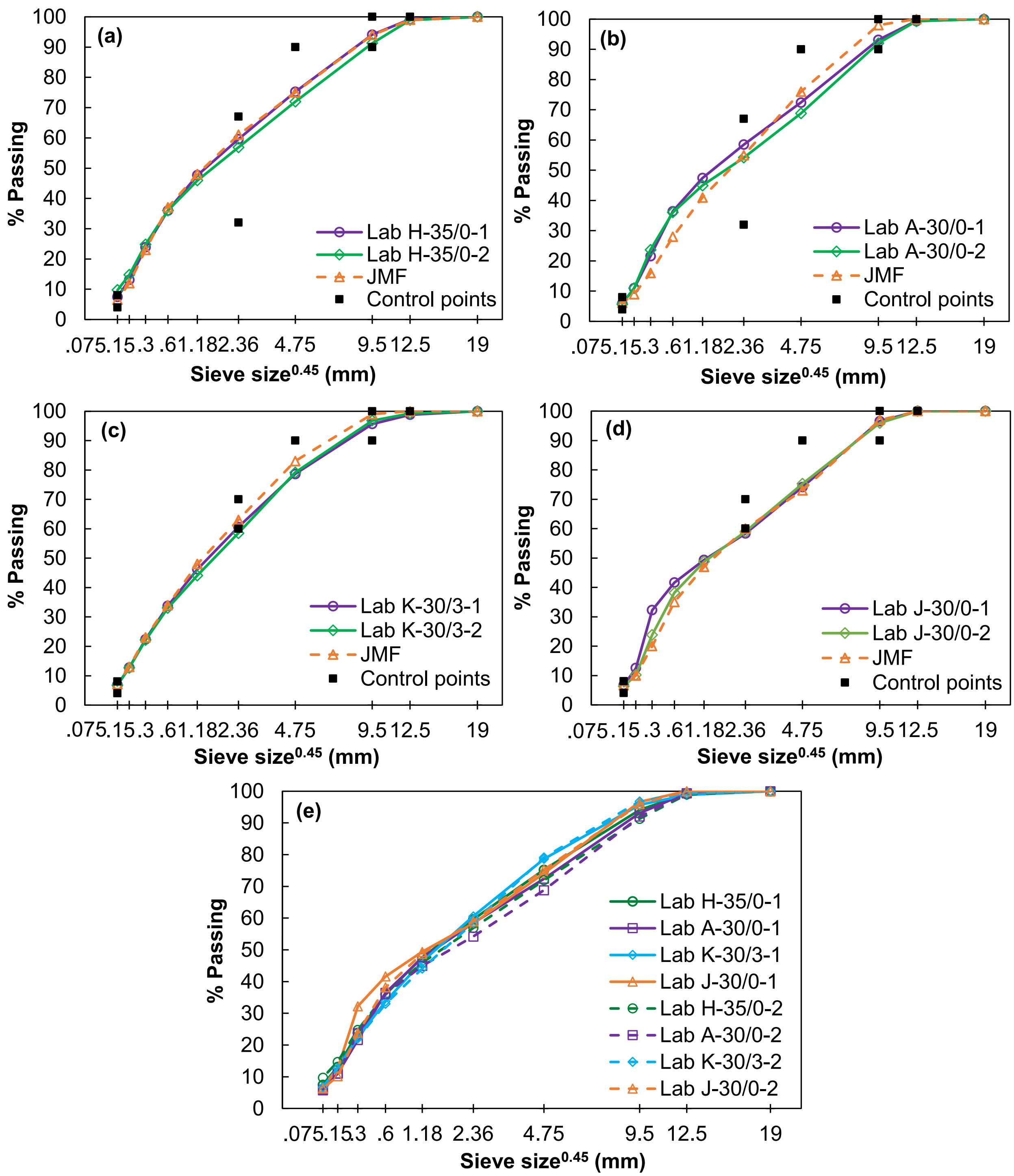

Figure 5-5. Extracted aggregate gradation of the plant-produced asphalt mixtures: (a) Plant H, (b) Plant A, (c) Plant K, (d) Plant J, (e) all plants.

Figure 5-6 shows the CT_{Index} results along with the asphalt contents of the plant-produced asphalt mixtures. The vertical error bars represent the standard deviation in the CT_{Index} among the test replicates. The NCDOT specification requires the difference in asphalt content between individual test results and the JMF fall within ±0.7 percent. All mixtures met this requirement. Despite the differences in asphalt content being deemed marginal based on NCDOT requirements, the CT_{Index} of the second sample was consistently lower than that of the first sample from the same plant mirroring trends in asphalt content. The percent difference in CT_{Index} between the two samples from a given plant spanned from 13.5 percent for Plant J to 35.3% in Plant A. These results align with past studies, which have shown that the CT_{Index} is highly sensitive to asphalt binder content, and reducing binder content leads to a decrease in CT_{Index} (*49*, *71*). A lower CT_{Index} represents poorer expected cracking performance. It is noteworthy that four mixtures (i.e., H-35/0-1, A-30/0-1, K-30/3-2, and J-30/0-2) all have the same binder content but the K-30/3-2 mixture has a visually distinct CT_{Index} result. This suggests that factors other than binder content may influence CT_{Index} values such as binder properties, gradation, and aggregate mineralogy. K-30/3-1 also displays a notably higher CT_{Index} than the mixtures from the other plants. The relatively high CT_{Index} results of the Plant K mixtures are attributed to their softer virgin binder grade of PG 58-28, which resulted in a softer blended matrix despite containing RAS. Previous studies have also shown that CT_{Index} is sensitive to asphalt binder grade (*71*).

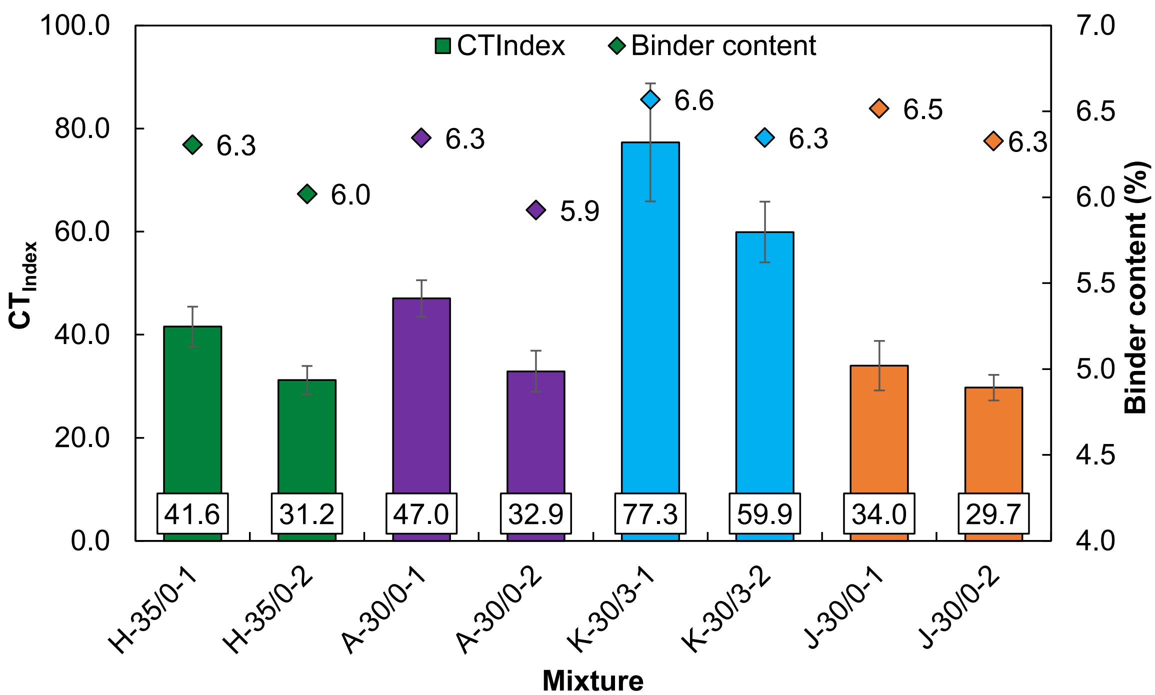

Figure 5-6. Cracking performance and asphalt content of the plant-produced asphalt mixtures.

In order to complement the visual inferences regarding the cracking performance, Figure 5-7 provides an interactive visual representation of statistical comparisons among the plant-produced mixture CT_{Index} based on the outcomes of the Tukey-Kramer test. On the left side of the plot, the black dots represent individual specimen CT_{Index} values for each mixture, the horizontal lines at the center of the green diamonds represent the mixture mean, and the vertical span represents the 95% confidence interval for the mixture mean. On the right side of the plot, the circles allow for visual comparisons of the mixtures by examining their intersections. The center of each circle aligns with the mean of a given mixture. Circles that do not intersect or only slightly intersect correspond to mixtures deemed significantly different. The Tukey-Kramer test results indicate that K-30/3-1 and K-30/3-2 are significantly different from all other mixtures. In contrast, the mixtures from all other plants show some degree of overlap, indicating relatively consistent performance across the RAP mixtures from the different plants. The only cases where statistically significant differences in CT_{Index} results exist between the first and second samples from a given plant are K-30/3-1 vs. K-30/3-2 and A-30/0-1 vs. A-30/0-2.

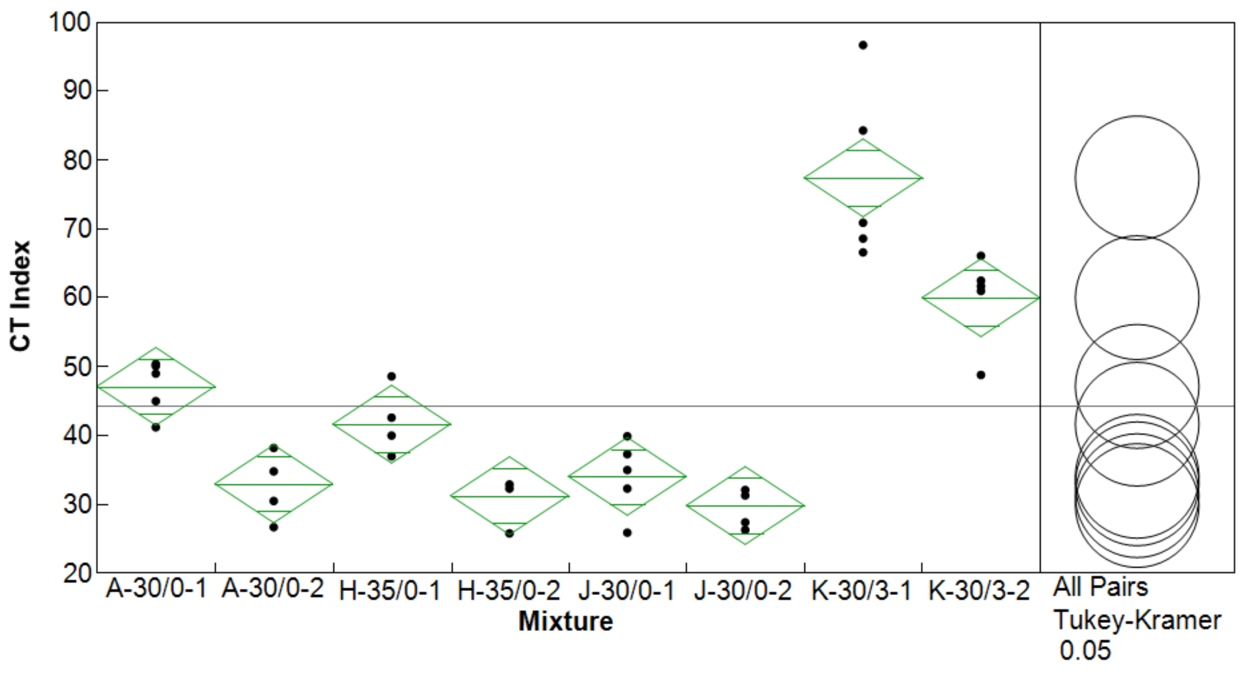

Figure 5-7. All pairs, Tukey-Kramer comparison circles for CT_{Index}.

Figure 5-8 presents the APA rut depth results for the plant-produced mixtures. Again, the asphalt contents are shown for comparison. A higher rut depth represents a poorer rutting performance. According to NCDOT specification (*54*), the maximum allowable rut depth at mix design is 6.5 mm for RS9.5C mixes and 9.5 mm for RS9.5B mixes. The rut depth values of all mixtures fall below these limits. The Plant K mixtures exhibit similar rut depths to the other mixtures despite having distinct CT_{Index} values, suggesting that characteristics of the blended binder had a smaller impact on rutting compared to cracking.

Upon comparing the IDEAL-CT and APA results from a given plant, a pattern is observed. The CT_{Index} values of the second samples were lower than those of the first samples from the same plant, indicating that the second samples had worse cracking resistance. On the other hand, the rut depth decreased from the first to second samples, indicating that the second samples exhibited better rutting resistance compared to their respective first sample. Thus, variability in the rut depth measurements between the first and second samples of a given mixture match trends in asphalt content, with higher asphalt contents corresponding to higher rut depths.

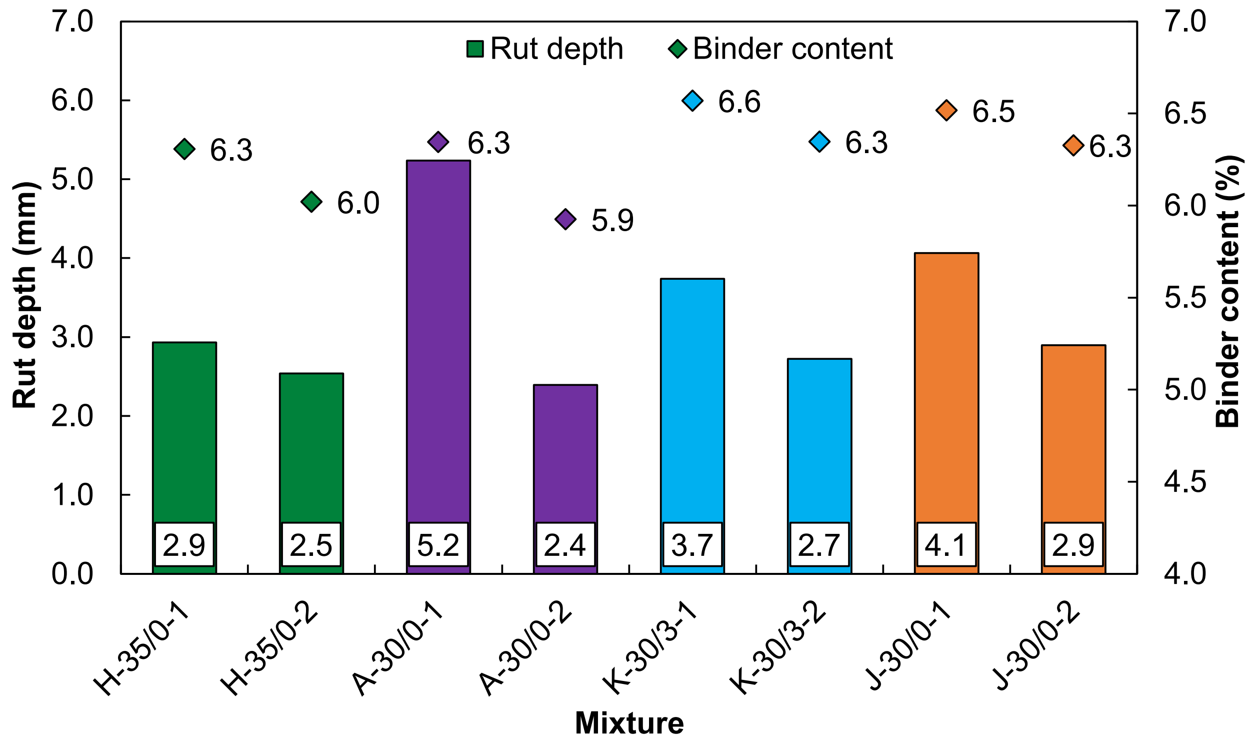

Figure 5-8. Rutting performance and asphalt content of the plant-produced asphalt mixtures.

Figure 5-9 shows the statistical comparisons among the plant-produced mixture rut depth results based on the outcomes of the Tukey-Kramer test. The results indicate that the rut depths of the mixtures do not differ significantly with a few exceptions. The similar gradation of all of the mixtures evaluated may have contributed to this finding. A-30/0-1 is the most distinct, differing significantly from A-30/0-2, H-35/0-1, H-35/0-2, K-30/3-2, and J-30/0-2. A-30/0-2 is also significantly different from J-30/0-1. The reason for the distinct rutting result of the A-30/0-1 mixture cannot be explained by trends in asphalt content or blended binder properties.

In summary, both visual observation and statistical analysis indicate that the Plant K mixtures exhibits superior cracking performance while showing comparable rutting performance to the other mixtures. With a few exceptions, the other mixtures displayed consistent performance. The distinct cracking performance of the Plant K mixtures is attributed to the properties of the recycled and virgin binders. As previously shown in Figure 5-2, the RAP binders from Plant K had the lowest continuous high-temperature values among all recycled binders. In addition, Plant K used a softer virgin binder, PG 58-28. The combination of a less oxidized RAP binder with a softer virgin binder resulted in the lowest blend PG and G-R parameter values among the study mixtures despite containing RAS, as shown in Figure 5-3 and Figure 5-4. Trends in the performance measures of the plant-produced mixtures corresponding to a given JMF closely followed trends in asphalt content, although in some cases the differences were deemed statistically insignificant.

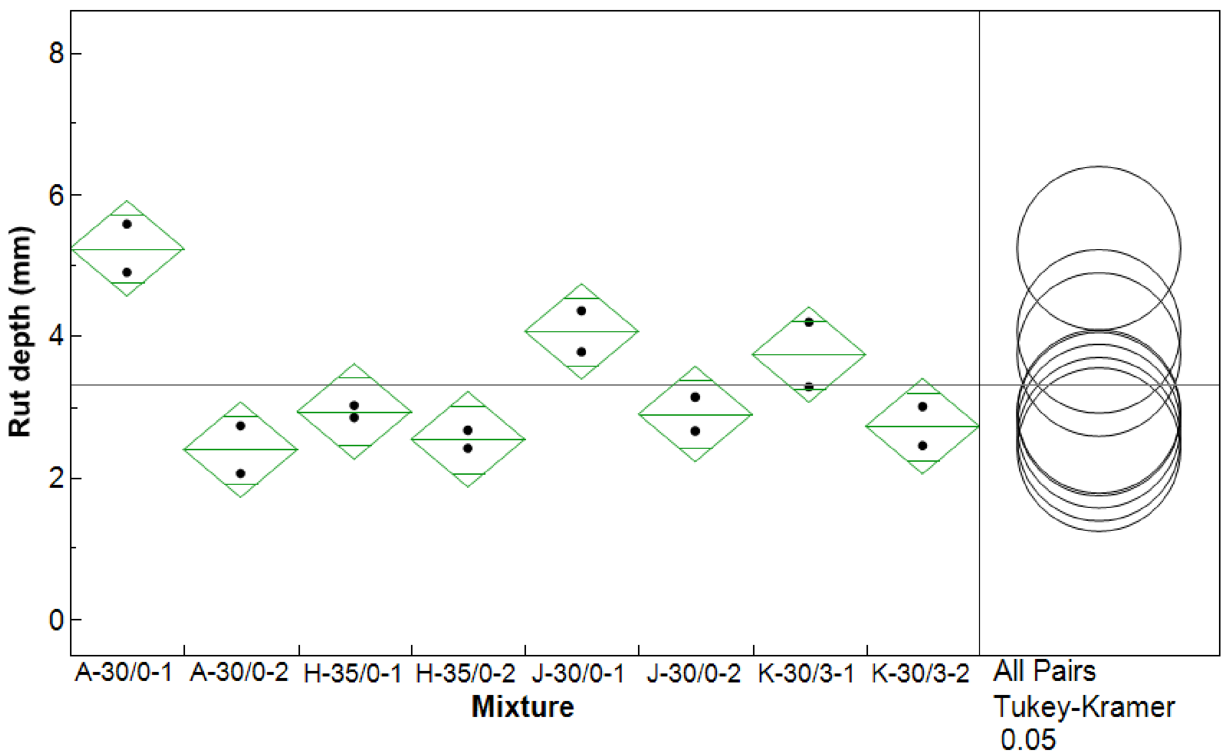

Figure 5-9. All pairs, Tukey-Kramer comparison circles for rut depth.

5.5. Conclusions and Recommendations

The conclusions and recommendations drawn from this study are:

- The properties of the RAP stockpiles varied across different plants within the state. Notably, the continuous high-temperature grades of the recovered binder spanned 15°C. The properties of a given RAP stockpile were relatively consistent over time. Despite the variation in RAP properties among the plants, the plant-produced RAP asphalt mixtures generally demonstrated similar cracking and rutting performance.
- The plant-produced asphalt mixture containing both RAP and RAS yielded significantly better cracking performance but comparable rutting performance to the RAP mixtures. This distinct cracking performance is attributed to the constituent binders. The RAP/RAS mixture included a softer virgin binder than the RAP mixtures and also had the softest RAP resulting in the softest blended binder matrix among the study mixtures despite containing RAS.
- The RAS stockpile evaluated demonstrated comparatively high variability over time with a nearly 20°C change in continuous high-temperature grade of the recovered binder and 2.6 percent change in asphalt content. Consequently, the corresponding mixture containing both RAP and RAS demonstrated greater variability in cracking performance over time than the RAP-only mixtures.
- Differences in the cracking and rutting performance of a given plant-produced mixture over time corresponded with changes in asphalt content. An increase in asphalt content improved cracking resistance but negatively affected rutting resistance. While these changes in performance were often statistically insignificant, there were instances where statistically significant performance changes occurred even when the variations in binder content were within acceptable limits.
- The findings of this study highlight the potential impacts of recycled binder properties on the cracking performance of asphalt mixtures. Since solvent extraction and recovery processes are impractical for routine use, incorporating performance measures into the mixture design and/or quality assurance process is crucial for ensuring consistent performance of high recycled content mixtures.
- Cracking and rutting performance measures were limited to the IDEAL-CT and APA tests, respectively. Future research should confirm the findings using mechanistic performance tests and pavement performance simulations.

6. Conclusions and Recommendations

6.1. Conclusions

- The probabilistic approach developed in this study demonstrates significant potential for optimizing RAP RBR thresholds while maintaining performance requirements. Analysis of NCDOT's current practices revealed that reducing the maximum RBR limit for PG 64-22 virgin binder in RAP mixtures from 0.30 to 0.20 substantially improves the probability of meeting intermediate- and low-temperature requirements (approximately 96%) while preserving compliance with high-temperature specifications. The current NCDOT maximum RBR limits of 0.40 and 0.45 provide adequate assurance (>90% probability) for meeting intermediate-temperature grading requirements.
- Notably, the research identified that different RBR levels can produce similar blended binder property distributions, with RBR = 0.2 yielding comparable high-temperature characteristics and RBR = 0.4 producing similar intermediate-temperature properties to PG 64-22 virgin binder. This finding suggests opportunities for flexible mixture design while maintaining performance standards.
- Using Zeng et al.'s approach without empirical calibration, both $S(60)$ and $m(60)$ achieved an R^2 of 0.83 relative to the line of equality, while the CPG yielded an R^2 of 0.82 with respect to the line of equality.
- The linear regression-based calibrations improved the DSR predictions of BBR test results for both $S(60)$ and $m(60)$, achieving an R^2 of 0.97 relative to the line of equality. The average absolute error in continuous low-grading temperature predictions was 0.7°C. The empirical calibration for $S(60)$ suggests that Poisson's ratio is approximately 0.40 for virgin binders and 0.23 for RAM binders at the BBR test conditions.
- RAP stockpile properties in North Carolina varied significantly across different plants, with continuous high-temperature grades spanning 15°C, yet individual stockpiles maintained relatively consistent properties over time. However, RAS stockpiles exhibited substantially higher variability over time, with nearly 20°C changes in continuous high-temperature grade and 2.6 percent variations in asphalt content, leading to greater performance variability in RAP/RAS mixtures compared to RAP mixtures.

6.2. Recommendations

- Quality assurance data collection should be extended to include low-temperature properties at -12°C for PG 58-28 binders and phase angle measurements at 25°C. These parameters could not be adequately evaluated in the current study but may provide important insights for comprehensive performance prediction.
- Future probabilistic analyses should incorporate blending chart uncertainty to provide more robust assessments of blended binder properties and associated confidence intervals.
- The proposed RBR thresholds require validation through comprehensive field performance evaluations to ensure practical applicability and long-term pavement performance.
- The calibrated equations for Zeng' et al.'s model should be validated using a broader data set and testing from other laboratories in the future. Notably, this study did not consider polymer-modified binders. In addition, given the relatively poorer prediction for ΔT_c using DSR test results compared to continuous performance grading ($R^2 = 0.63$ vs. $R^2 = 0.98$), research should identify and evaluate alternative parameters that could serve as more reliable predictors of low-temperature performance.

7. References

1. Khosla, N. P., S. Ramoju, and N. Prabu. *Determining Recycled Asphalt Binder Limits Contributed by Waste Materials*. Publication NCDOT Project 2012-04. North Carolina State University, Raleigh, NC, 2015.
2. Tavakol, M., and M. Hossain. *Minimum Virgin Binder Limits in Recycled Superpave Mixes in Kansas*. Publication K-TRAN: KSU-13-5. Kansas State University Transportation Center, Manhattan, Kansas, 2016.
3. Mogawer, W. S., A. J. Austerman, T. Pauli, S. Salmans, and J.-P. Planche. *Determination of the Binder Grade and Performance of High Percentage RAP-HMA Mixes*. Publication SPRII-15-57946. University of Massachusetts Dartmouth Highway Sustainability Research Center (HSRC), Boston, MA, 2016.
4. Stephens, J. E., J. Mahoney, and C. Dippold. *Determination of the PG Binder Grade to Use in a RAP Mix*. Publication JHR 00-278. University of Connecticut Connecticut Transportation Institute, Storrs, CT, 2001.
5. Roque, R., B. Park, J. Zou, and G. Lopp. *Enhanced Characterization of RAP for Cracking Performance*. Publication BDV31-977–70. University of Florida, Gainesville, FL, 2020.
6. Carret, J.-C., A. C. Falchetto, M. O. Marasteanu, H. Di Benedetto, M. P. Wistuba, and C. Sauzeat. Comparison of Rheological Parameters of Asphalt Binders Obtained from Bending Beam Rheometer and Dynamic Shear Rheometer at Low Temperatures. *Road Materials and Pavement Design*, Vol. 16, No. sup1, 2015, pp. 211–227. https://doi.org/10.1080/14680629.2015.1029696.
7. Sui, C., M. J. Farrar, P. M. Harnsberger, W. H. Tuminello, and T. F. Turner. New Low-Temperature Performance-Grading Method: Using 4-Mm Parallel Plates on a Dynamic Shear Rheometer. *Transportation Research Record: Journal of the Transportation Research Board*, Vol. 2207, No. 1, 2011, pp. 43–48. https://doi.org/10.3141/2207-06.
8. Lu, X., P. Uhlback, and H. Soenen. Investigation of Bitumen Low Temperature Properties Using a Dynamic Shear Rheometer with 4 Mm Parallel Plates. *International Journal of Pavement Research and Technology*, Vol. 10, No. 1, 2017, pp. 15–22. https://doi.org/10.1016/j.ijprt.2016.08.010.
9. Hajj, R., A. Filonzi, S. Rahman, and A. Bhasin. Considerations for Using the 4 Mm Plate Geometry in the Dynamic Shear Rheometer for Low Temperature Evaluation of Asphalt

Binders. *Transportation Research Record: Journal of the Transportation Research Board*, Vol. 2673, No. 11, 2019, pp. 649–659. https://doi.org/10.1177/0361198119855332.

10. Zeng, Z. 'Alan,' B. S. Underwood, and C. Castorena. Low-Temperature Performance Grade Characterisation of Asphalt Binder Using the Dynamic Shear Rheometer. *International Journal of Pavement Engineering*, Vol. 23, No. 3, 2022, pp. 811–823. https://doi.org/10.1080/10298436.2020.1774766.
11. AASHTO. Standard Specification for Superpave Volumetric Mix Design. Washington, DC, , 2022.
12. McDaniel, R., and R. M. Anderson. *Recommended Use of Reclaimed Asphalt Pavement in the Superpave Mix Design Method: Technician's Manual. NCHRP Report 452.* Washington, D.C., 2001.
13. West, R. C. *Best Practices for RAP and RAS Management. Report No. QIP 129*. Lanham, MD, 2015.
14. Khosla, N. P., and S. S. Ramoju. *Characterization of Different RAP Sources. Report No. FHWA/NC/2014-05*. Raleigh, North Carolina, 2017.
15. Aparicio Alvis, M. C. *Impacts of Material Variables on Recycled Binder Contribution and the Properties of Recycled Binder Blends.* North Carolina State University, Raleigh, NC., 2023.
16. Austerman, A. J., W. S. Mogawer, and K. D. Stuart. Variability of Reclaimed Asphalt Pavement (RAP) Properties within a State and Its Effects on RAP Specifications. *Transportation Research Record*, Vol. 2674, No. 6, 2020, pp. 73–84. https://doi.org/10.1177/0361198120917679.
17. Ninomiya, K., and J. D. Ferry. Some Approximate Equations Useful in the Phenomenological Treatment of Linear Viscoelastic Data. *Journal of Colloid Science*, Vol. 14, No. 1, 1959, pp. 36–48. https://doi.org/10.1016/0095-8522(59)90067-4.
18. Anderson, D. A., D. W. Christensen, H. U. Bahia, R. Dongre, M. Sharma, C. E. Antle, and J. Button. Binder Characterization and Evaluation, Volume 3: Physical Characterization. *Strategic Highway Research Program, National Research Council, Washington, DC*, 1994.
19. Farrar, M., C. Sui, S. Salmans, and Q. Qin. Determining the Low-Temperature Rheological Properties of Asphalt Binder Using a Dynamic Shear Rheometer (DSR). *Report 4FP*, Vol. 8, 2015, p. 20.

20. AASHTO. AASHTO Designation: T 164-22. Standard Method of Test for Quantitative Extraction of Asphalt Binder from Asphalt Mixtures.
21. ASTM International. ASTM D5404/D5404M-24 Standard Practice for Recovery of Asphalt Binder from Solution Using the Rotary Evaporator. Oct, 2024.
22. AASHTO. AASHTO Designation: T 240. Standard Method of Test for Effect of Heat and Air on a Moving Film of Asphalt Binder (Rolling Thin-Film Oven Test).
23. AASHTO. AASHTO Designation: T 315-22. Standard Method of Test for Determining the Rheological Properties of Asphalt Binder Using a Dynamic Shear Rheometer (DSR).
24. AASHTO. M 320-22 Standard Specification for Performance-Graded Asphalt Binder. Washington, D.C., , 2022.
25. Rice, J. A. *Mathematical Statistics and Data Analysis*. Thomson/Brooks/Cole Belmont, CA, 2007.
26. Shapiro, S. S., and M. B. Wilk. An Analysis of Variance Test for Normality (Complete Samples). *Biometrika*, Vol. 52, No. 3–4, 1965, pp. 591–611.
27. Fried, A., L. G. Xue, S. Gulzar, J. Preciado, B. S. Underwood, and C. Castorena. Evaluation of Recycling Agent and Extender Dosage Selection Procedures to Restore the High-Temperature Climatic Performance Grade. *Transportation Research Record*, Vol. 2676, No. 6, 2022, pp. 302–314. https://doi.org/10.1177/03611981221074361.
28. Castorena, C., A. Fried, J. Preciado, S. Gulzar, M. A. A. Alvis, and L. G. Xue. *Screening of Asphalt Extenders and Recycling Agents. Report No. FHWA/NC/2020-16*. Raleigh, North Carolina, 2023.
29. AASHTO. AASHTO Designation: R 28-22. Standard Practice for Accelerated Aging of Asphalt Binder Using a Pressurized Aging Vessel (PAV).
30. ASTM. Designation: D7643 − 16. Standard Practice for Determining the Continuous Grading Temperatures and Continuous Grades for PG Graded Asphalt Binders.
31. AASHTO. AASHTO Designation: PP 113-21 Standard Practice for Characterizing the Relaxation Behavior of Asphalt Binders Using the Delta Tc (ΔTc) Parameter. , 2021.
32. Benedetto, H. D., B. Delaporte, and C. Sauzéat. Three-Dimensional Linear Behavior of Bituminous Materials: Experiments and Modeling. *International Journal of Geomechanics*, Vol. 7, No. 2, 2007, pp. 149–157.

33. Kim, Y. S., J. R. Agudo, M. P. Wistuba, J. Büchner, and M. Schäffler. Determination of Complex Poisson’s Ratio of Asphalt Binders Using Torsion-Tension Tests in a Dynamic Shear Rheometer. *Road Materials and Pavement Design*, Vol. 26, No. 2, 2025, pp. 397–419.
34. Elwardany, M. D., J.-P. Planche, and G. King. Proposed Changes to Asphalt Binder Specifications to Address Binder Quality-Related Thermally Induced Surface Damage. *Transportation Research Record*, Vol. 2676, No. 5, 2022, pp. 176–191.
35. Preciado, J., S. Gulzar, A. Fried, C. Castorena, S. Underwood, J. Habbouche, and I. Boz. Low-Temperature Performance Evaluation of Recycled Binder Blends for Assessing Recycling Agents’ Acceptance. *Journal of Materials in Civil Engineering*, Vol. 36, No. 9, 2024, p. 04024257.
36. Xiao, F., N. Su, S. Yao, S. Amirkhanian, and J. Wang. Performance Grades, Environmental and Economic Investigations of Reclaimed Asphalt Pavement Materials. *Journal of Cleaner Production*, Vol. 211, 2019, pp. 1299–1312. https://doi.org/10.1016/j.jclepro.2018.11.126.
37. Copeland, A. *Reclaimed Asphalt Pavement in Asphalt Mixtures: State of the Practice. Report No. FHWA-HRT-11-021*. McLean, Virginia, 2011.
38. Hassan, M. M., A. Lodge, L. N. Mohammad, and W. “Bill” King. Variability and Characteristics of Recycled Asphalt Shingles Sampled from Different Sources. *Journal of Materials in Civil Engineering*, Vol. 26, No. 4, 2014, pp. 748–754. https://doi.org/10.1061/(ASCE)MT.1943-5533.0000876.
39. Zhou, F., H. Li, S. Hu, J. W. Button, and J. A. Epps. *Characterization and Best Use of Recycled Asphalt Shingles in Hot-Mix Asphalt. Report No. FHWA/TX-13/0-6614-2*. College Station, Texas, 2013.
40. Hand, A. J. T., and T. B. Aschenbrener. *Successful Use of Reclaimed Asphalt Pavement in Asphalt Mixtures. Report No. WRSC-TR-21-10*. Reno, Nevada, 2021.
41. Hand, A. J. T., T. Aschenbrener, and S. Cooper. *A Field Review: Successful Practices and Lessons Learned When Using Reclaimed Asphalt Shingles in Asphalt Mixtures. Report No. WRSC-TR-20-01*. Reno, Nevada, 2020.
42. Zaumanis, M., J. Oga, and V. Haritonovs. How to Reduce Reclaimed Asphalt Variability: A Full-Scale Study. *Construction and Building Materials*, Vol. 188, 2018, pp. 546–554. https://doi.org/10.1016/j.conbuildmat.2018.08.137.

43. Hajj, E. Y., P. E. Sebaaly, and R. Shrestha. Laboratory Evaluation of Mixes Containing Recycled Asphalt Pavement (RAP). *Road Materials and Pavement Design*, Vol. 10, No. 3, 2009, pp. 495–517. https://doi.org/10.3166/rmpd.10.495-517.
44. Bonaquist, R. *Effect of Recovered Binders from Recycled Shingles and Increased RAP Percentages on Resultant Binder PG. Report No. WHRP 11-13*. Sterling, VA, 2011.
45. National Center for Asphalt Technology. Moving Towards Balanced Mix Design for Asphalt Mixtures. Asphalt Technology News, 29, 1, , 2017, pp. 1–5.
46. Yazdipanah, F., M. Khedmati, and H. F. Haghshenas. *Nebraska Balanced Mix Design - Phase I. Report No. SPR-FY22(002)*. 2023.
47. Newcomb, D., and P. Investigator. *Balanced Design of Asphalt Mixtures. Report No. MN/RC 2018-22*.
48. West, R., F. Yin, C. Rodezno, and A. Taylor. *Balanced Mixture Design Implementation Support*. Auburn, Alabama, 2021.
49. Bowers, B. F., T. Lynn, F. Yin, N. Moore, S. Diefenderfer, and I. Boz. *Impact of Production Variability on Balanced Mix Designs in Virginia. Report No. FHWA/VTRC 23-R20*. 2023.
50. Mogawer, W. S., K. D. Stuart, A. J. Austerman, F. Zhou, and P. Romero. Balanced Mix Design Sensitivity to Production Tolerance Limits and Binder Source. *Journal of the Association of Asphalt Paving Technologists*, Vol. 88, 2019.
51. Austerman, A. J., W. S. Mogawer, and K. D. Stuart. Influence of Production Considerations on Balanced Mixture Designs. *Transportation Research Record*, Vol. 2672, No. 28, 2018, pp. 426–437. https://doi.org/10.1177/0361198118786826.
52. Rahman, M., J. Harvey, J. Buscheck, J. Brotschi, A. Mateos, D. Jones, and S. Pourtahmasb. Laboratory Performance and Construction Challenges for Plant Produced Asphalt Mixes Containing RAP and RAS. *Construction and Building Materials*, Vol. 403, No. August, 2023, p. 133082. https://doi.org/10.1016/j.conbuildmat.2023.133082.
53. North Carolina Department of Transportation. Standard Specifications for Roads and Structures.
54. North Carolina Department of Transportation. Asphalt Quality Management System.
55. AASHTO. AASHTO Designation: T 308-21. Standard Method of Test for Determining the Asphalt Binder Content of Asphalt Mixtures by the Ignition Method.

56. ASTM. Designation: D6857/D6857M - 23. Standard Test Method for Maximum Specific Gravity and Density of Asphalt Mixtures Using Automatic Vacuum Sealing Method.
57. AASHTO. AASHTO T 315 Standard Method of Test for Determining the Rheological Properties of Asphalt Binder Using a Dynamic Shear Rheometer (DSR). Washington, D.C., , 2020.
58. Alvis, M. A., S. Pape, L. G. Xue, and C. Castorena. Effects of Asphalt Mixture Constituents on the Recycled Binder Contribution. *Transportation Research Record*, Vol. 2677, No. 11, 2023, pp. 192–204. https://doi.org/10.1177/03611981231165021.
59. Fried, A., and C. Castorena. Practical Methods to Construct Asphalt Binder Master Curves and Calculate Christensen – Anderson Model Parameters. *Transportation Research Record: Journal of the Transportation Research Board*, Vol. 2677, No. 12, 2023, pp. 647–660. https://doi.org/10.1177/03611981231169274.
60. Rowe. Evaluation of the Relationship Between Asphalt Binder Properties and Non-Load Related Cracking. *Journal of the Association of Asphalt Paving Technologists, Prepared Discussion*, Vol. 80, 2011, pp. 615–664.
61. Anderson, R. M., G. N. King, D. I. Hanson, and P. B. Blankenship. Evaluation of the Relationship between Asphalt Binder Properties and Non-Load Related Cracking. *Journal of the Association of Asphalt Paving Technologists*, Vol. 80, 2011, pp. 615–664.
62. Glover, C. J., R. R. Davison, C. H. Domke, Y. Ruan, P. Juristyarini, D. B. Knorr, and S. H. Jung. *Development of a New Method for Assessing Asphalt Binder Durability with Field Validation. Report No. FHWA/TX-05/1872-2*. College Station, Texas, 2005.
63. Elkashef, M., S. S. Hung, J. T. Harvey, and D. Jones. Assessing the Use of Blending Charts to Estimate the Allowable Reclaimed Asphalt Pavement (RAP) Binder Content for Mixes Containing Rap from Different Sources. *Journal of Testing and Evaluation*, Vol. 49, No. 5, 2020, pp. 3132–3147. https://doi.org/10.1520/JTE20200106.
64. AASHTO. AASHTO Designation: T 30-21. Standard Method of Test for Mechanical Analysis of Extracted Aggregate.
65. AASHTO. AASHTO Designation: T 209-20. Standard Method of Test for Theoretical Maximum Specific Gravity (Gmm) and Density of Asphalt Mixtures.
66. AASHTO. AASHTO Designation: T 340-23. Standard Method of Test for Determining Rutting Susceptibility of Asphalt Mixtures Using the Asphalt Pavement Analyzer (APA).

67. AST. Designation: D8225 - 19. Standard Test Method for Determination of Cracking Tolerance Index of Asphalt Mixture Using the Indirect Tensile Cracking Test at Intermediate Temperature.

68. LaCroix, A. T. *Performance Prediction of the NCAT Test Track Pavements Using Mechanistic Models*. North Carolina State University, 2013.

69. Castorena, C., S. Pape, G. L. Xue, D. Mocelin, M. C. A. Alvis, and M. Ravichandran. *Improving the Design of RAP and RAS Mixtures. Report No. FHWA/NC/2019-21*. Raleigh, North Carolina, 2022.

70. Duarte, G. M., and A. L. Faxina. Low-Temperature and Fatigue Properties of Asphalt Binders Modified with Crumb Rubber from Discarded Tires and Recycled Low-Density Polyethylene. *Journal of Materials in Civil Engineering*, Vol. 34, No. 9, 2022. https://doi.org/10.1061/(asce)mt.1943-5533.0004365.

71. Zhou, F. *Development of an IDEAL Cracking Test for Asphalt Mix Design, Quality Control and Quality Assurance. NCHRP IDEA Project 195*. 2019.